EFFECT OF NANOFLUID-BASED ABSORBERS ON DIRECT SOLAR COLLECTOR

THAM CHI MENG

RESEARCH PROJECT SUBMITTED IN PARTIAL FULFILMENT OF THE REQUIREMENTS FOR THE DEGREE OF MASTER OF ENGINEERING

FACULTY OF ENGINEERING
UNIVERSITY OF MALAYA
KUALA LUMPUR

2011

ABSTRACT

As conventional energy like fossil fuels is getting rare, cost of energy production has been increasingly higher. The concern of environmental pollution caused by burning of hydrocarbon fuels has also been raised among developed and developing nations. These make clean renewable energy a major research topic in recent decades. Among them, solar energy, as the most vastly available energy and also supremely effective in terms of energy conversion has been the most sought after. The most common solar thermal collector utilizes black surface as radiant absorber but the efficiency is limited to the effectiveness of the black surface and the transfer of thermal energy from the black surface to the working fluid. Direct Solar Collector, has come to be an innovative measure to this is by using nanofluids as volumetric absorber. Nanofluids are expected to provide excellent optical properties and enhanced thermal transfer. The aim of this study is to analyze the effect of nanofluid as working fluid for Direct Solar Collector. With aluminium nanoparticles as additive material and pure water as base fluid, the extinction coefficient of nanofluid is evaluated with nanoparticle size and volume fraction as parameters. The particle sizes and volume fraction studied are 1 nm to 10 nm and 0.1% to 8.0% respectively. The particle size shows minimal influence to the optical properties of nanofluid while the extinction coefficient is linearly proportionate to volume fraction. The transmissivity of light is compared between pure water (base fluid) and nanofluid. The improvement is promising and with only 1.0% volume fraction, the nanofluid is already almost opaque to light wave.

ABSTRAK

Kos pengeluaran tenaga konvensional seperti bahan api fosil telah menjadi semakin tinggi kerana tenaga tersebut sudah menjadi semakin jarang. Kebimbangan pencemaran alam sekitar yang disebabkan oleh pembakaran bahan api hidrokarbon juga telah dibangkitkan di kalangan negara-negara maju dan membangun. Tenaga boleh diperbaharui yang bersih telah menjadi topik penyelidikan utama dalam beberapa dekad kebelakangan ini. Antaranya, tenaga suria yang dikenali sebagai tenaga yang paling luas tersedia dan juga paling berkesan dari segi penukaran tenaga telah menjadi tenaga yang terbaik. Pemungut tenaga suria yang paling umum menggunakan permukaan hitam sebagai penyerap sinaran tetapi kecekapan itu adalah terhad kepada kecekapan permukaan hitam dan kecekapan pemindahan tenaga haba dari permukaan hitam kepada bendalir pemindahan. Pemungut Suria secara langsung telah menjadi langkah inovatif dengan menggunakan "nanofluids" sebagai penyerap. "Nanofluids" dijangka untuk menyediakan ciri-ciri optik yang baik dan boleh meningkatkan kecekapan pemindahan haba. Tujuan kajian ini adalah untuk menganalisis kesan "nanofluid" sebagai bendalir pemindahan untuk Pemungut Suria secara Langsung. Ciri-ciri optik "nanofluid" dinilaikan dengan partikel aluminium digunakan sebagai bahan penambah dan air tulen sebagai bendalir asas. Saiz nanopartikel dan pecahan isi padu dijadikan sebagai parameter dalam pengajian ini. Saiz zarah yang dikajikan adalah 1 nm dan 10 nm manakala pecahan isi padu adalah 0.1% kepada 8.0%. Saiz zarah menunjukkan pengaruh yang minimum kepada sifat-sifat optik nanofluid manakala pekali kepupusan adalah berkadar secara linear kepada pecahan isi padu. Keterusan cahaya antara air tulen (bendalir asas) dan nanofluid dibandingkan. Peningkatan tersebut amat memberangsangkan dan dengan hanya 1.0% pecahan isipadu, "nanofluid" sudah menjadi hampir legap kepada gelombang cahaya.

ACKNOWLEDGEMENT

First of all, I would like to use this opportunity to thank my supervisor, Dr. Saidur Rahman for giving me guidance and advices throughout the completion of this thesis. Further to this, I would like to give my appreciation to my fellow course mate, Mr Ler Cherk Yong for the help and assist during the preparation of the thesis.

TABLE OF CONTENTS

ABSTRACT ……... II

ACKNOWLEDGEMENT III

TABLE OF CONTENTS IV

LIST OF FIGURES VI

LIST OF TABLES IX

NOMENCLATURE X

LIST OF APPENDICES XII

CHAPTER 1: INTRODUCTION 1

1.0 BACKGROUND 1

1.1 RENEWABLE ENERGIES 5

1.1.1 Solar Energy 8

1.2 OBJECTIVE 13

1.3 THESIS ORGANIZATION 13

CHAPTER 2: LITERATURE REVIEW 15

2.0 INTRODUCTION 15

2.1 PROPERTIES OF LIGHT 15

2.1.1 Light Scattering 20

2.1.1.1 Rayleigh Scattering 22

2.1.1.2 Mie Scattering 23

2.1.2 Light Absorption 25

2.1.3 Light Extinction 26

2.2 SOLAR COLLECTORS 28

2.2.1 Classification of Solar Collectors 32

2.2.2 Concentrating Solar Collectors 34

2.2.3 Non-Concentrating Solar Collectors 37

2.2.3.1 Flat Plate Solar Collector (FPC) 37

2.2.3.2 Evacuated Tube Solar Collectors (ETC) 44

2.3 NANOFLUID 46

2.3.1 Optical Properties of Nanofluid 49

CHAPTER 3: METHODOLOGY 52

3.0 INTRODUCTION 52

3.1 DIRECT ABSORPTION COLLECTOR (DAC) 52

3.2 RADIATIVE PROPERTIES OF NANOFLUID 57

3.2.1 Radiative Properties of Base Fluid 57

3.2.2 Radiative Properties of Nanoparticles 62

CHAPTER 4: RESULTS AND DISCUSSIONS 69

4.0 INTRODUCTION 69

4.1 TRANSMISSIVITY OF BASE FLUID (PURE WATER) 70

4.2 OPTICAL PROPERTIES OF NANOPARTICLES 71

4.3 TRANSMISSIVITY OF NANOFLUID 79

CHAPTER 5: CONCLUSION AND FUTURE RECOMMENDATION 83

BIBLIOGRAPHY 85

APPENDIX 1 94

LIST OF FIGURES

Figure	Content	Page
1.1	Growth in world electric power generation and total energy consumption, 1990-2035, Derived from EIA, International Energy Statistics database (as of November 2009) (U.S. DOE, 2010a)	2
1.2	World net electricity generation by fuel, 2007-2035, Derived from EIA, International Energy Statistics database (as of November 2009) (U.S. DOE, 2010b)	3
1.3	Renewable energy Share of Global final energy Consumption, 2009 (REN 21, 2011)	7
1.4	Renewable energy Share of Global electricity Production, 2010	8
1.5	Solar energy distribution (Four Peaks Technologies, 2010)	9
1.6	Yearly sum of global irradiance (Meteonorm, 2008)	11
1.7	A Solarimeter, also refer to as a “Pyranometer”	12
2.1	Linear visible light spectrum.	16
2.2	Electromagnetic spectrum	17
2.3	Spectral characteristics of: incident solar radiation (red) with varying concentration levels (C); black body radiation (black); and emissive properties of a selective surface (green) (Lenert, 2010).	19
2.4	Solar Radiation Spectrum of incident solar radiant	20
2.5	Angular dependence of the scattered light with polarization parallel and perpendicular to the plane of observation for spherical gold particles. A: the limiting case of infinitely small particles. B: particles with a diameter of 160 nm. C: particles with a diameter of 180 nm (Horvath, 2009, p.793).	24
2.6	Light Absorption	25
2.7	Attenuation coefficient of gold suspensions with different particle sizes. (Horvath, 2009)	27
2.8	Solar heating existing Capacity, Top 12 Countries, 2009 (Weiss and Mauthner, 2011)	30

Figure	Content	Page
2.9	Total capacity of newly installed collectors in the 10 leading countries in 2009 (Weiss and Mauthner, 2011)	31
2.10	Distribution of the total installed capacity in operation by collector type in 2009 (Weiss and Mauthner, 2011)	32
2.11	Concentration of sunlight using (a) parabolic trough collector (b) linear Fresnel collector (c) central receiver system with dish collector and (d) central receiver system with distributed reflectors	36
2.12	Typical set up of Flat Plate Collector (FPC)	38
2.13	Thermosyphon Solar water heater	39
2.14	Pictorial view of a flat plate collector (Kalogirou, 2004, p.241)	40
2.15	Exploded view of a flat plate collector (Kalogirou, 2004, p.241)	41
2.16	Schematic diagram of an evacuated tube collector (Kalogirou, 2004).	45
2.17	Working principle of heat pipe in evacuated tube collector.	45
2.18	Length scale and some examples related (Serrano, et al., 2009)	47
3.1	Power loss due to re-radiation as a function of temperature: from a black body (black), and a selective surface (green) (Lenert, 2010).	53
3.2	Difference between surface-based and volumetric solar absorbers (Lenert, 2010).	54
3.3	Schematic of the nanofluid-based direct absorption solar collector (DAC)	55
3.4	Transmittance spectra of water and glycol-based nanofluids with the same SWCNH concentrations (0.005 g/L for G1 and A1 and 0.05 g/L for G4 and A4). Spectra of the pure base fluids are shown for comparison (G0 and A0) (Mercatelli, 2011).	59
3.5	Absorption Coefficient for water (Chaplin, 2011).	60
3.6	Calculated and published values of Refractive Index, n of water (Otanicar et al., 2009)	61

Figure	Content	Page
3.7	Calculated and published values of Extinction Index, n of water (Otanicar et al., 2009)	61
3.8	Collector efficiency as a function of the particle size, D (fv = 0.8%)	67
4.1	Transmissivity and Absorption Coefficient, kaλ of Base Fluid (Pure Water) at Various Light Path Length	70
4.2	The Effect of Nanoparticle Sizes towards Absorption Coefficient, kaλ	71
4.3	The Effect of Nanoparticle Sizes towards Scattering Coefficient, ksλ	72
4.4	The Effect of Nanoparticle Sizes towards Extinction Coefficient, keλ	72
4.5	The Effect of Nanoparticle Volume Fraction, fv (0.1% - 2.5%) towards Absorption Coefficient, kaλ	75
4.6	The Effect of Nanoparticle Volume Fraction, fv (1.0% - 8.0%) towards Absorption Coefficient, kaλ	75
4.7	The Effect of Nanoparticle Volume Fractions, fv (0.1% - 2.5%) towards Scattering Coefficient, ksλ	76
4.8	The Effect of Nanoparticle Volume Fractions, fv (2.0% - 8.0%) towards Scattering Coefficient, ksλ	77
4.9	The Effect of Nanoparticle Volume Fractions, fv (1.0% - 8.0%) towards Extinction Coefficient, keλ	78
4.10	The Extinction Coefficient and Transmissivity of Nanofluid (fv = 0.1%)	80
4.11	The Extinction Coefficient and Transmissivity of Nanofluid (fv = 0.5%)	80
4.12	The Extinction Coefficient and Transmissivity of Nanofluid (fv = 1.0%)	81

LIST OF TABLES

Table	Content	Page
2.1	Colour spectrum and its frequency and wavelength (Bruno and Paris, 2005 cited in Wikipedia, 2011c)	16
2.2	Types of solar energy collectors (Kalogirou, 2003)	33
2.3	Optical properties of commonly used glazing materials (Everett, 2004, p.27)	42

NOMENCLATURE

c_o	Speed of light in vacuum, c = 2.9979 x 10^8 m/s
d	Diameter of the particle
E	Energy Content
ETC	Evacuated Tube Solar Collector
FPC	Flat Panel Solar Collector
f_v	Volume fraction [%]
h	Planck's constant, h = 6.62606957 x 10^{-34} J.s or 4.135667516 x 10^{-15} eV.s
h_c	Convective heat transfer coefficient
I	Transmitted light intensity
I_λ	Total incident light intensity
k	Absorption index of the particle
$K_{a\lambda}$	Spectral absorption coefficient
k_B	Boltzmann constant, k_B = 1.38 x 10^{-23} J/K
$K_{e\lambda}$	Spectral extinction coefficient
$K_{s\lambda}$	Spectral scattering coefficient
m	Normalized refractive index of the particle to the fluid
$m_{particle}$	Complex refractive index of the particle
n	Refractive index of the particle
q	Heat transfer
$Q_{a\lambda}$	Absorption coefficient
$Q_{e\lambda}$	Extinction coefficient
$Q_{s\lambda}$	Scattering coefficient
R	Distance between the particle and the observer
T_{solar}	Solar surface temperature, T_{solar} = 5800 K

ΔT	Temperature difference
v	Frequency of photon associated electromagnetic wave
y	Length of light path

Greek symbols

α	Size parameter
θ	Scattering angle
λ	Wavelength [μm]

LIST OF APPENDICES

Appendix 1

Calculated Data for Optical Properties of Base Fluid (Pure Water), Nanoparticles (Aluminium Nanoparticles) and Nanofluid

Chapter 1: Introduction

1.0 Background

Fire marked a leap in human civilization history and is used directly or indirectly in every day's life. It is used to cook, sterilize, provide heating during cold seasons and at night, "landscape management" in agriculture industry in many developing countries and most importantly, provide thermal energy in power plants to generate electricity. The hominid fossil record suggests that cooked food may have appeared as early as 1.9 Ma (Wrangham, et al., 1999) although reliable evidence for controlled fire use does not appear in the archaeological record until after 400,000 years ago, with evidence of regular use much later (Karkanas, et al., 2007). The routine domestic use of fire is believed to begin around 50,000 to 100,000 years ago (Bar-Yosef, 2002).

Conventional electricity generation is an energy conversion process of turning fire, or more scientifically, heat or thermal energy into kinetic energy by boiling water to create steam that turns turbines in power plants and eventually turning kinetic energy into electric energy. The electricity consumed by the world is increasing year by year and electricity generation has become ever more important to the world. According to the United States Energy Information Administration, world net electricity generation increases by an average of 2.3 per cent per year from 2007 to 2035 in the International Energy Outlook (IEO) 2010 Reference case. Electricity supplies an increasing share of the world's total energy demand and grows faster than liquid fuels, natural gas, and coal in all end-use sectors except transportation. From 1990 to 2007, growth in net electricity generation outpaced the growth in total energy consumption (1.9 per cent per year and 1.3 per cent per year, respectively), and the growth in demand for electricity continues to outpace growth in total energy use throughout the projection period (U.S. DOE,

2010a). This is further illustrated in Figure 1.1 below where net energy generation and total energy consumption on year 1990 is served as 1.

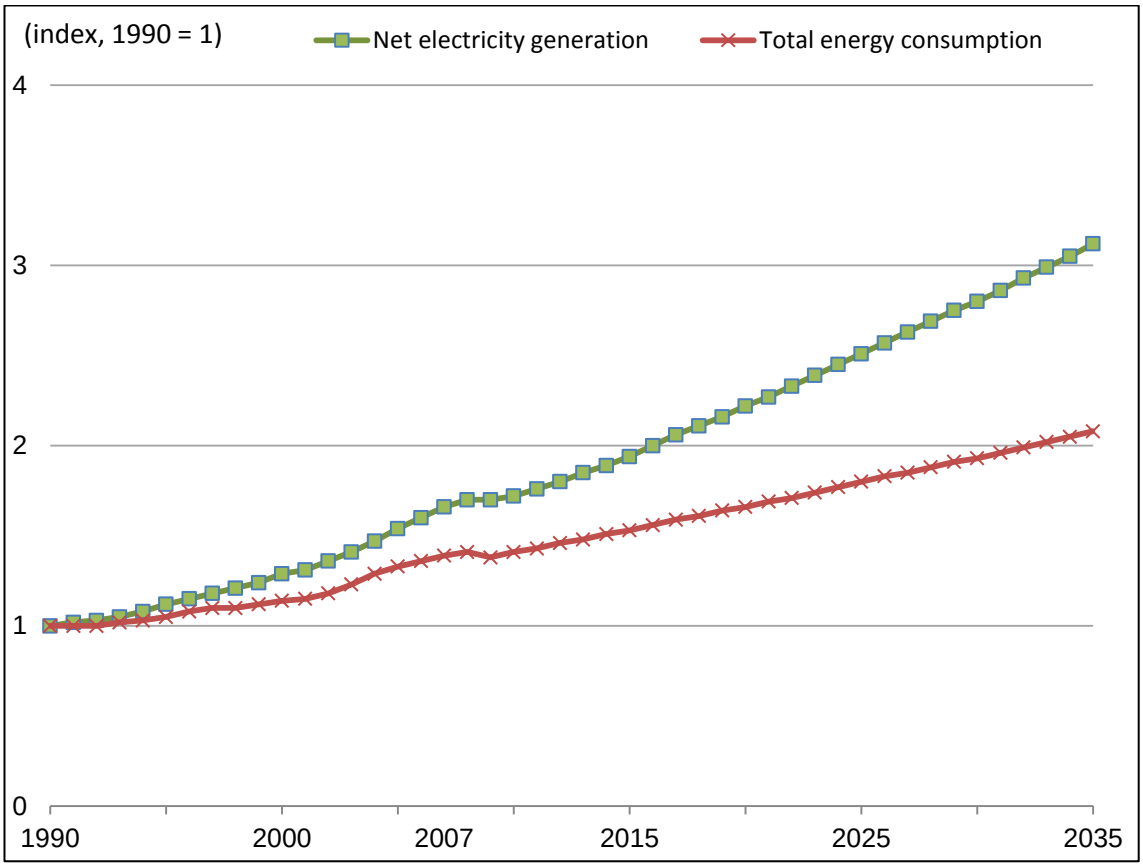

Figure 1.1 : Growth in world electric power generation and total energy consumption, 1990-2035, Derived from EIA, International Energy Statistics database (as of November 2009) (U.S. DOE, 2010a)

As the most vastly used and relatively well developed energy system, fossil fuels can say to be the most vital energy form to human modern civilization. Fossil fuels such as coal, petroleum and natural gas are used for steam generation in boilers in electric power plants and these plants stand a majority stack in the electricity power plant in the whole world. Thousands and millions tons of fossil fuels are burn every day to create enough energy to support human's quest for energy. Figure 1.2 shows the composition of types of fuel used in electricity generation.

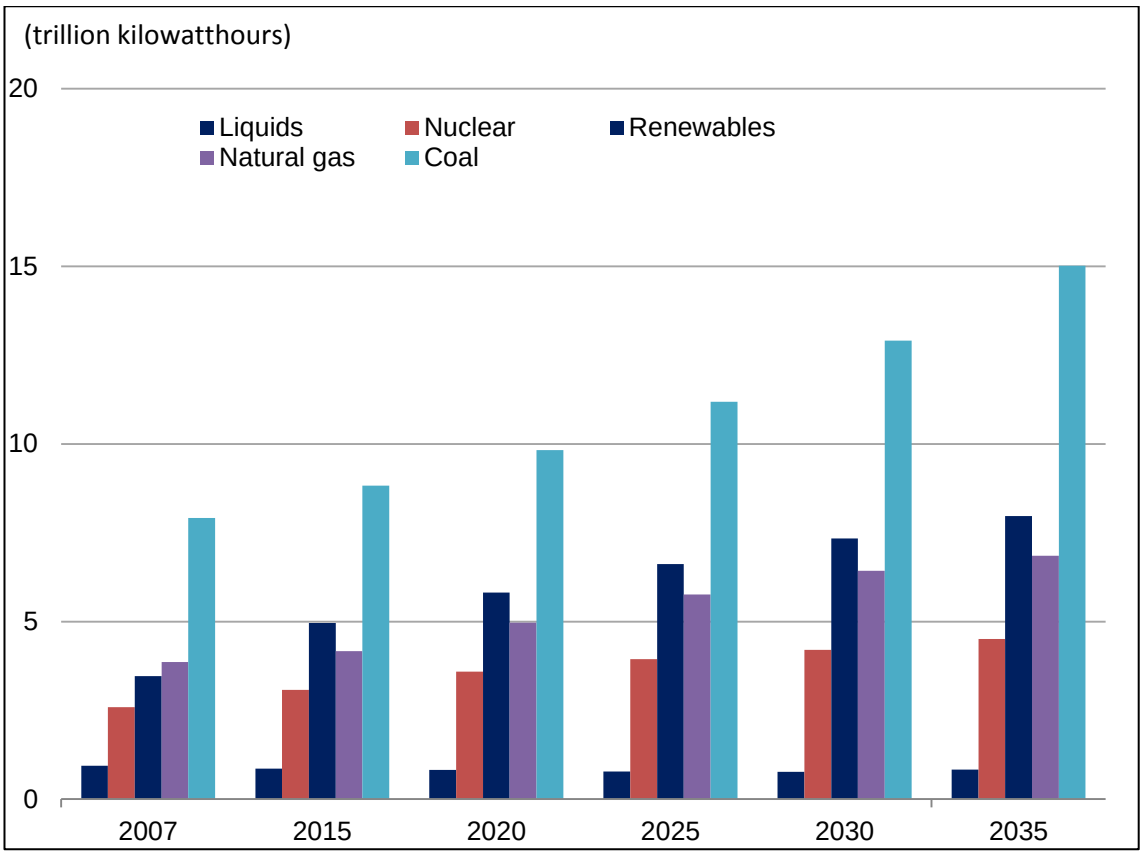

Figure 1.2 : World net electricity generation by fuel, 2007-2035, Derived from EIA, International Energy Statistics database (as of November 2009) (U.S. DOE, 2010b)

It can be clearly seen that the usage of liquid fuels for example petroleum to produce electricity is in the decline trend while natural gas, as the new member in the game has gained its pace in becoming a dominant player in the world electricity generation sector. On the other hand, coal, as one of the oldest member in the history of human usage of solid fossil fuel, is projected to increase its importance due mainly to its massive reserve. From the chart and prediction above, fossil fuels are yet still, the obvious major source of energy in the field.

Although technology breakthrough over the years has made fossil fuels a steady energy source, there are always two sides of a coin. Despite the development in this system for the past few decades, the problems in using fossil fuels extensively are still significant. For instances, fossil fuels are getting scarcer. No matter how advance in

technology we are in recovering oil wells or digging coal, the truth of using up all fossil fuels on earth crust one day is inevitable. Production cost is increasing over the years because of this. Such a scenario is outlined by the Hubbert curve (Tester, et al., 2005), which projects the production rate of petroleum as a function of time. According to this projection, it is expected that due to the limited amount of petroleum resources, its rate of production would peak after a certain amount of time, followed by an increase in its cost. Moreover the peak is expected to be followed by a sharp drop, which would provide very little time to develop and switch to alternative technologies once the peak is reached.

Further to that, air pollution due to burning of fossil fuels has always been a headache to governments, investors, environmentalists and researchers. Our dependency on fossil fuels has been damaging our environment irreversibly. Over the past decades, greenhouse effect has become one of the most talk-about topics relating to energy. As ozone level depreciating and climate changes are becoming more and more serious, this issue has to be addressed. The Kyoto Protocol is a protocol to the United Nations Framework Convention on Climate Change (UNFCCC or FCCC), aimed at combating global warming. The objective of the Kyoto climate change conference was to establish a legally binding international agreement, whereby all the participating nations commit themselves to tackling the issue of global warming and greenhouse gas emissions (Wikipedia, 2011a). It has been recognized that the carbon dioxide (CO_2) is the highest contributor in the greenhouse effects among the other gases such as sulphur dioxide (SO_2), nitrogen oxide (NO_x), and carbon monoxide (CO). CO is colourless and odourless. Exposure to CO reduces the blood's ability to carry oxygen. It might cause death if one is continuously exposed to high concentration of CO. NO_x is a generic term for mono-nitrogen oxides (NO and NO_2). These oxides are produced during combustion, especially at high temperatures. When NO_x and volatile organic compounds (VOCs)

react in the presence of sunlight, they form photochemical smog, a significant form of air pollution, especially in the summer. Children, people with lung diseases such as asthma, and people who work or exercise outside are susceptible to adverse effects of smog such as damage to lung tissue and reduction in lung function (US EPA, 2011a). SO_2 is the component of greatest concern and is used as the indicator for the larger group of gaseous sulphur oxides (SO_x). SO_x can react with other compounds in the atmosphere to form small particles. These particles penetrate deeply into sensitive parts of the lungs and can cause or worsen respiratory disease, such as emphysema and bronchitis, and can aggravate existing heart disease, leading to increased hospital admissions and premature death (US EPA, 2011b).

In view the running out of availability, rising cost of production and environmental impact caused by using fossil fuels to create energy and electricity, renewable energy is a promising counter measure to the above problems.

1.1 Renewable Energies

Renewable energy can be defined as “energy obtained from the continuous or repetitive currents of energy recurring in the natural environment” (Twidell and Weir, 2006) or as “energy flows which are replenished at the same rate as they are used” (Sørenson, 2011). The definitions for renewable energy above both emphasized on energy “recurring” and “replenishing”, which suggested that this uprising star of energy sector will not diminish or reduce in its reserve unlike conventional non-renewable energy. Continuing concerns about the “sustainability” of both fossil fuels and nuclear energy have been a major spur in bringing renewable energy back into the limelight in recent decades. By self “recurring” and “replenishing”, renewable energy can tackle all

cost related problems from the root as production cost will only become lower when technologies to harvest this energy are getting more mature.

Renewable energy can also help to reduce poverty through improved basic energy access like lightings, communications, water pumping, heating and cooling at some rural areas which are severely underserved with electricity. These will generate economy growth and gives a start to eliminate extreme poverty. PV household systems, wind turbines, micro-hydro powered or hybrid mini-grids, biomass-based systems or solar pumps, and other renewable technologies are being employed in homes, schools, hospitals, agriculture, and small industry in rural and off-grid areas of the developing world.

Above and beyond this, one of the key attractiveness of renewable energy is its environmental friendliness. Despite the fact that renewable energy release close-to-zero emission when it generates power, there are some arguments saying that the raw material required for manufacturing of the parts of renewable energy source, such as in a solar collector, may still lead to some carbon footprint. But however, Masruroh et al. (2006) demonstrated in a life cycle analysis showing a clear reduction of up to 50% in carbon footprint by using solar thermal system instead of natural gas or oil for heating purposes.

Renewable energy consists of Solar Energy, Wind Energy, Wave Energy, Hydro Energy, Nuclear Energy, Tidal Energy, Geothermal Energy and last but not least Biomass Energy. Renewable energy, which experienced no downturn in 2009, continued to grow strongly in all end-use sectors – power, heat and transport – and supplied an estimated 16% of global final energy consumption (REN21, 2011). These are further explained with Figure 1.3 and Figure 1.4 below.

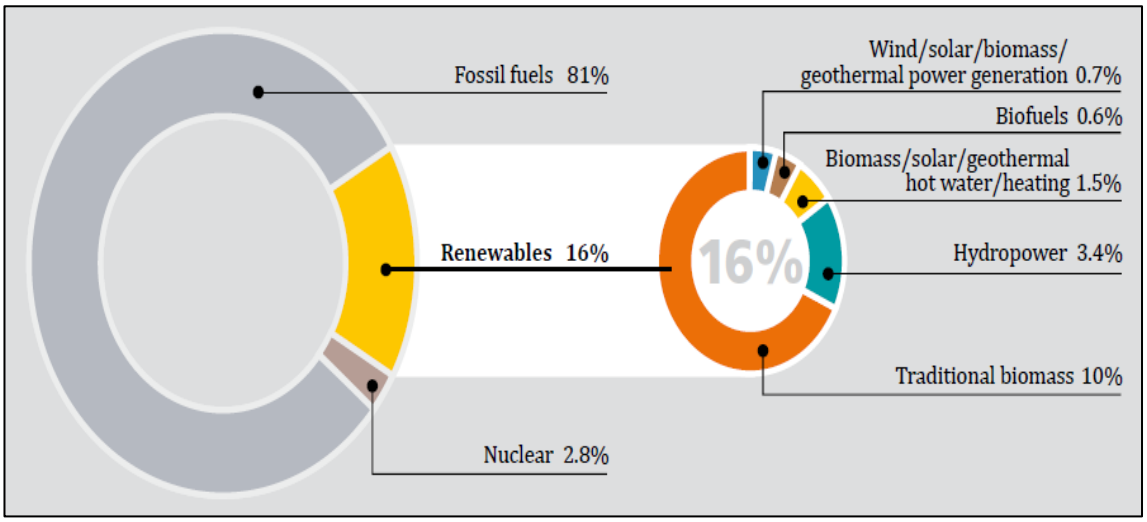

Figure 1.3 : Renewable energy Share of Global final energy Consumption, 2009 (REN 21, 2011)

Renewable energy accounted for approximately half of the estimated 194 gigawatts (GW) of new electric capacity added globally during the year. Renewables delivered close to 20% of global electricity supply in 2010, and by early 2011 they comprised one quarter of global power capacity from all sources. Existing renewable power capacity worldwide reached an estimated 1,320 gigawatts (GW) in 2010, up almost 8% from 2009. Renewable capacity now comprises about a quarter of total global power generating capacity (estimated at 4,950 GW in 2010) and supplies close to 20% of global electricity, with most of this provided by hydropower (REN21, 2011). This is showed in Figure 1.4 below.

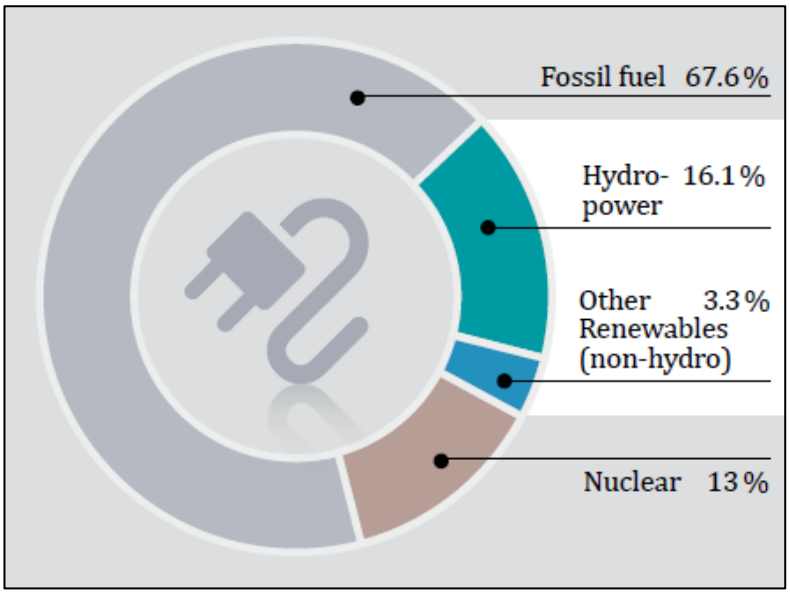

Figure 1.4 : Renewable energy Share of Global electricity Production, 2010

The facts and figures above demonstrated the importance of renewable energy to many nations and the potential of it to increase its stake in global energy contribution. It is believed that with the improving technologies and increasing interest showed by the governments, renewable energy is in fact the possible main energy source for the coming century.

1.1.1 Solar Energy

Among renewable energies, solar energy shows various advantages and relatively easier integration to existing power system. A brief introduction of solar energy and its upper hands are described below. The sun is a sphere of intensely hot gaseous matter with a diameter of 1.39 x 10^9 m. The solar energy strikes our planet a mere 8 min and 20s after leaving the giant furnace, the sun which is 1.5 x 10^{11} m away. The sun has an effective blackbody temperature of 5762 K (Kreith and Kreider, 1978). The temperature in the central region is much higher and it is estimated at 8 x 10^6 to 40 x 10^6 K. In effect the sun is a continuous fusion reactor in which hydrogen is turned into

helium. The sun's total energy output is 3.8 x 10^{20} MW which is equal to 63 MW/m^2 of the sun's surface. This energy radiates outwards in all directions. Only a tiny fraction, 1.7 x 10^{14} kW, of the total radiation emitted is intercepted by the earth (Kreith and Kreider, 1978). However, even with this small fraction it is estimated that 30 min of solar radiation falling on earth is equal to the world energy demand for one year. Figure 1.5 below illustrates the portion of solar power that are absorbed and reflected by earth, cloud and atmosphere.

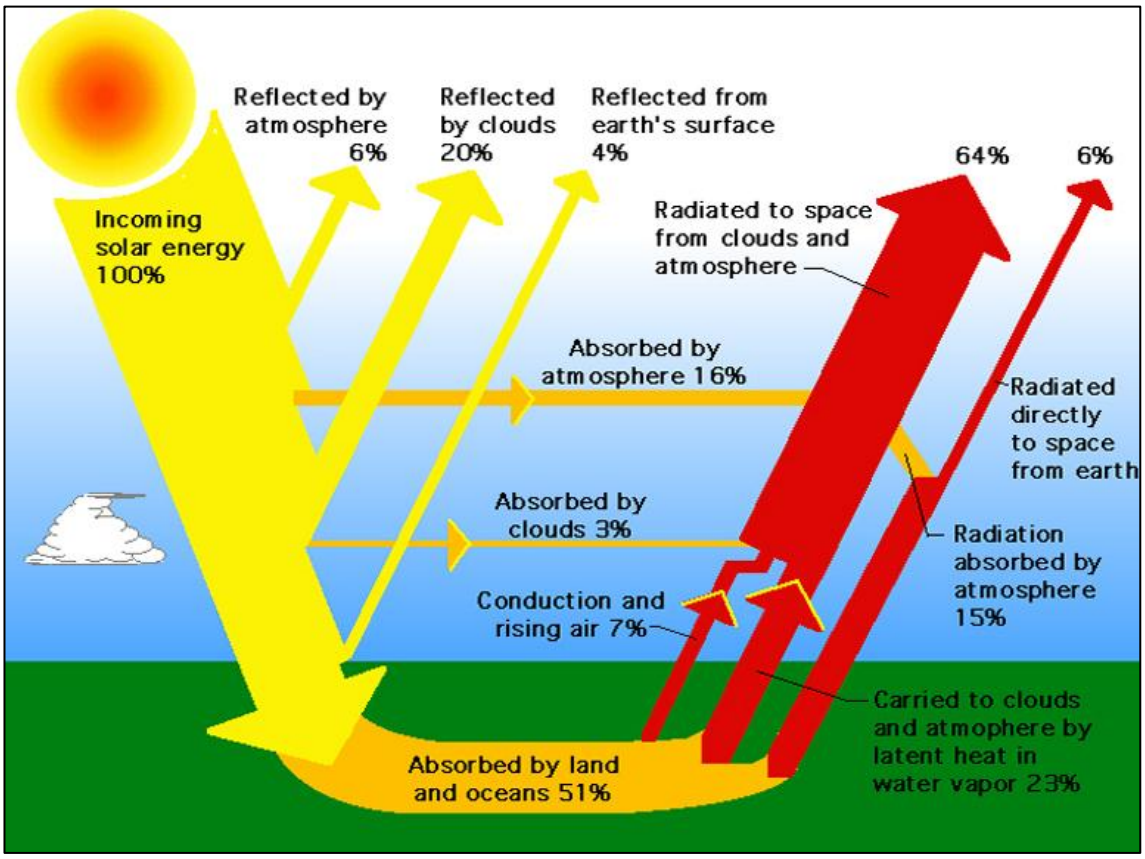

Figure 1.5 : Solar energy distribution (Four Peaks Technologies, 2010)

From Figure 1.5, the average amount of the sun's radiation of 0.70 kilo-watts per square meter that penetrates the atmosphere and reaches the earth is 51% of the total incoming energy as illustrated above. Of the 49% that does not reach the earth, 30% is reflected back into space and 19% is absorbed by the atmosphere and clouds. In 2005,

the earth's energy use by mankind was approximately 500 exajoules. This was about 0.01% of the total energy coming from the sun. Putting this in another way, the earth absorbs more energy in one hour than the world uses in one year according to physicist Steven Chu, Director of Lawrence Berkeley National Laboratory (Four Peaks Technologies, 2010). Among the 30% reflected radiant, 4% is reflected by earth's surface which means it can be further reap as well. This means that the total available portion of solar power to earth to be harvested will equal 55% and most importantly, this huge source of energy is free and clean to use. All these facts and figures show a hopeful energy source waiting for mankind to ripe.

As a matter of fact, solar energy is seen to be the highest form of energy by some researchers. The International Energy Agency (2002) explains: "Renewable energy is derived from natural processes that are replenished constantly. In its various forms, it derives directly from the sun, or from heat generated deep within the earth. Included in the definition is electricity and heat generated from solar, wind, ocean, hydropower, biomass, geothermal resources, and biofuels and hydrogen derived from renewable resources". The above statement gives an idea of two main direct sources of renewable energies, which are solar power and geothermal power, while other renewable energies are derivatives of them. In this derivatives form, solar energy goes through at least one level of energy conversion state. Fossil fuel for example, a form of energy converted from dead animals compressed in the earth crust millions of years ago, is another form of solar energy conversion. According to the first law of thermodynamic, energy cannot be created or destroyed but it may be converted from one form to another. However, in the second law of thermodynamic, energy conversion might involve irreversible physical process and the "usable" energy or exergy will decrease. Thus, we can easily confirm that solar energy is the highest form of energy among renewables energies. It can be argues that engineers should be able to tailor power generation

systems for direct utilization of solar radiation with efficiencies exceeding other multi-step energy conversion cycles that rely on the earth to modify solar energy into higher quality and more readily usable energy source.

Solar energy is also a relatively "fair" form of renewable energy. Most renewable energies are highly geometrically dependent. For instances, wind energy works well offshore or near shore but weaken abruptly when we move towards inland; hydro energy needs rivers and dams at preferably higher level to have good potential energy. While on the other hand, solar energy is best readied near the equator but through careful system design, it is available even in winter of seasonal countries. Interest in solar energy has prompted the accurate measurement and mapping of solar energy resources over the globe. The yearly sum of global irradiance is displayed in Figure 1.6 below. It can be seen that most part of the earth receive more or less the same total amount of radiant per annum. Solar power gradually decrease with greater latitude but in most developed nations, the power exposed is still promising.

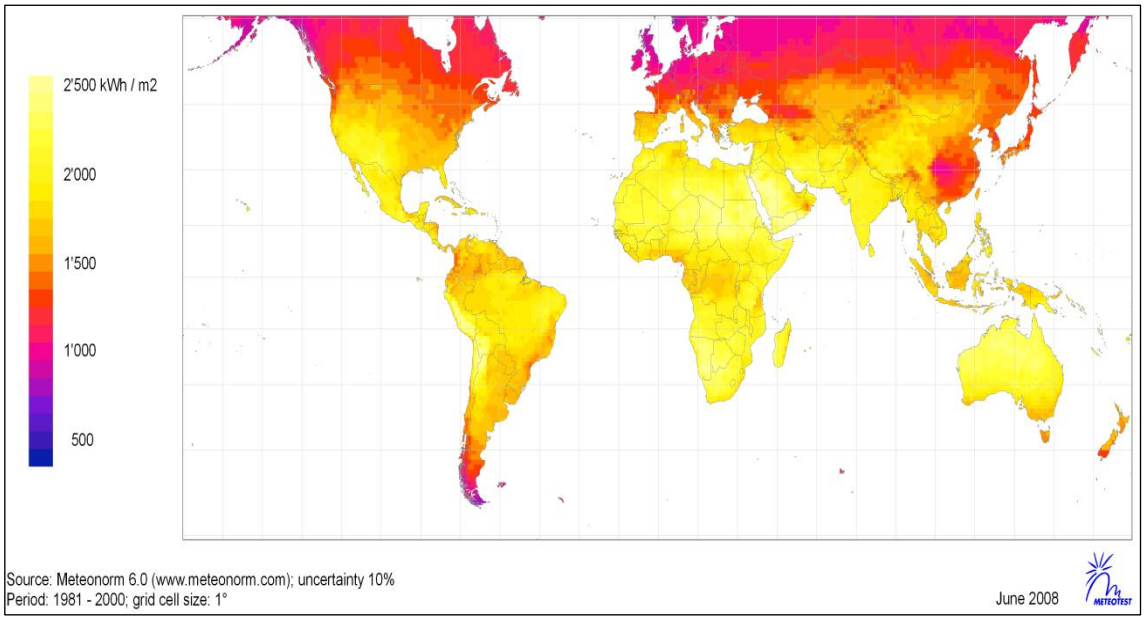

Figure 1.6 : Yearly sum of global irradiance (Meteonorm, 2008)

This is normally done using solarimeters as illustrated in Figure 1.7. These contain carefully calibrated thermoelectric elements fitted under a glass cover, which is open to the whole vault of the sky. A voltage proportional to the total incident light energy is produced and then recorded electronically (Everett, 2004)

Figure 1.7 : A Solarimeter, also refer to as a “Pyranometer”

With the higher energy form and availability of solar power, it is favoured to researchers in further developing it. Nonetheless, certain limits on the efficiency of direct solar power generation exist; current solar thermal technologies are not functioning close to these limits which leave room for enhancement for future solar thermal systems. The efficiency of a solar thermal collector relies on the effectiveness of absorbing solar radiant power and heat transfer from the absorber to the carrier, which is normally fluid. The conversion of highly concentrated sunlight into thermal energy suffers from relatively low efficiencies of 50% to 60% (Pacheco, 2001). Furthermore, current solar thermal power plants offer limited energy storage in order to

buffer the diurnal nature of the solar radiation. The overall efficiency of generating power in these plants is approximately 15% (Pacheco, 2001), whereas fossil power plants have reached efficiencies exceeding 50% in combined cycle plants. By way of higher improving the receivers and heat transfer mechanisms, direct solar collector can work closer to its limit. This thesis contributes in making solar thermal power generation more ubiquitous in the future.

1.2 Objective

The objectives of this thesis are the following:

1. To investigate the suitability of nanofluid to be used as a volumetric absorber.
2. To explore the radiative properties of the two components of nanofluid, namely the base fluid and the nanoparticles.
3. To propose nanoparticle sizes and volume fractions for nanofluid.
4. To compares the transmissivity of light through base fluid and nanofluid.

1.3 Thesis Organization

This thesis begins with the introduction to the current energy crisis, the environmental issues faced and the possible of overcoming them by utilizing renewable energy. Chapter 2 includes the literature reviews that describe the basic light properties and equations, the working principles of solar collector, particularly Flat Plate Solar Collector (FPC) and Evacuated Tube Solar Collector (ETC) and the current studies of nanofluid in terms of optical properties and the proposal of using it as volumetric absorber. FPC and ETC are introduced these two types of collectors have similar

working principle with Direct Absorption Solar Collector (DAC). With the change of working fluid to nanofluid as volumetric absorber, FPC and ETC will become a DAC. Chapter 3 discusses the methodology of this thesis. The governing equations to calculate the optical properties of base fluid and nanoparticles are discussed in detail in this chapter. The results obtained with the equations and the discussions are presented in Chapter 4 while the last chapter, Chapter 5, concludes the study and gives future recommendations to the researchers.

Chapter 2: Literature Review

2.0 Introduction

The literature review for this thesis will includes mainly three parts. In the first part, the properties of light and some important terminologies are discussed. The second section will give description to solar collector and the last section will review the current studies of nanofluid in terms of optical properties and the incorporation into solar collectors.

2.1 Properties of Light

Before the description of solar collectors, it is crucial that the basic or primary properties of light and some key terminology are explained to give a better understanding to the further part of the discussion.

Light or visible light is electromagnetic radiation that is visible to the human eye, and is responsible for the sense of sight. Everything we see and the beautiful colours from the blue sky and green mountains are merely the reflection and scattering of light. Visible light has wavelength in a range from about 380 nanometres to about 740 nm, with a frequency range of about 405 THz to 790 THz. The visible range extends from the extreme violet at about 400 nm to the extreme red at about 700 nm according to Smith (2006). From short to long wavelengths, the colours across the visible spectrum are: violet, indigo, blue, cyan (blue-green), green, yellow, orange and red. Figure 2.1 below shows light spectrum with their respective wavelength while table 2.1 gives more detail to each specific colour and its particular range of frequency and wavelength.

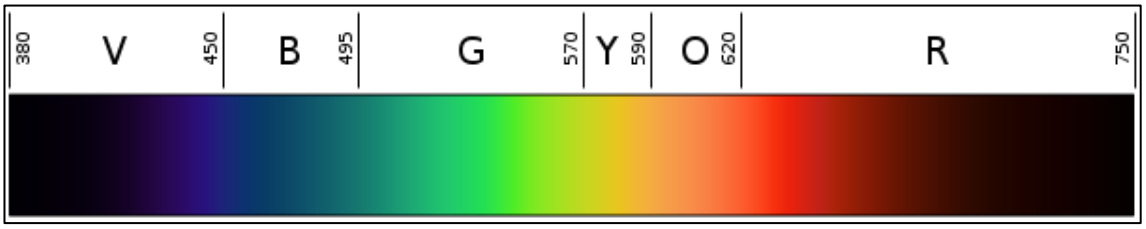

Figure 2.1 : Linear visible light spectrum.

Table 2.1 : Colour spectrum and its frequency and wavelength (Bruno and Paris, 2005 cited in Wikipedia, 2011c)

Colour	**Frequency**	**Wavelength**
violet	668–789 THz	380–450 nm
blue	631–668 THz	450–475 nm
cyan	606–630 THz	476–495 nm
green	526–606 THz	495–570 nm
yellow	508–526 THz	570–590 nm
orange	484–508 THz	590–620 nm
red	400–484 THz	620–750 nm

The spectrum does not, however, contain all the colors that the human eyes and brain can distinguish. Unsaturated colors such as pink, or purple variations such as magenta, are absent, for example, because they can only be made by a mix of multiple wavelengths (Wikipedia, 2011b). White light is a mixture of all colours.

In physics, the term “light” sometimes refers to electromagnetic radiation of any wavelength, whether visible or not (Kumar, 2008). It is a form of electromagnetic wave. The range of all possible frequency of electromagnetic radiation is called

electromagnetic spectrum. The electromagnetic spectrum extends from low frequencies used for modern radio to gamma radiation at the short-wavelength end, covering wavelengths from thousands of kilometers down to a fraction of the size of an atom. The long wavelength limit is the size of the universe itself, while it is thought that the short wavelength limit is in the vicinity of the Planck length, although in principle the spectrum is infinite and continuous. Based on a figure from NASA, figure 2.2 illustrates the relationship between the wavelength and frequency of electromagnetic wave and also gives an idea to the scale of the wavelength. Some radiations are marked as "N" for "no" in the diagram to show that they cannot penetrate the atmosphere, although extremely minimally of such radiations do still penetrate the atmosphere.

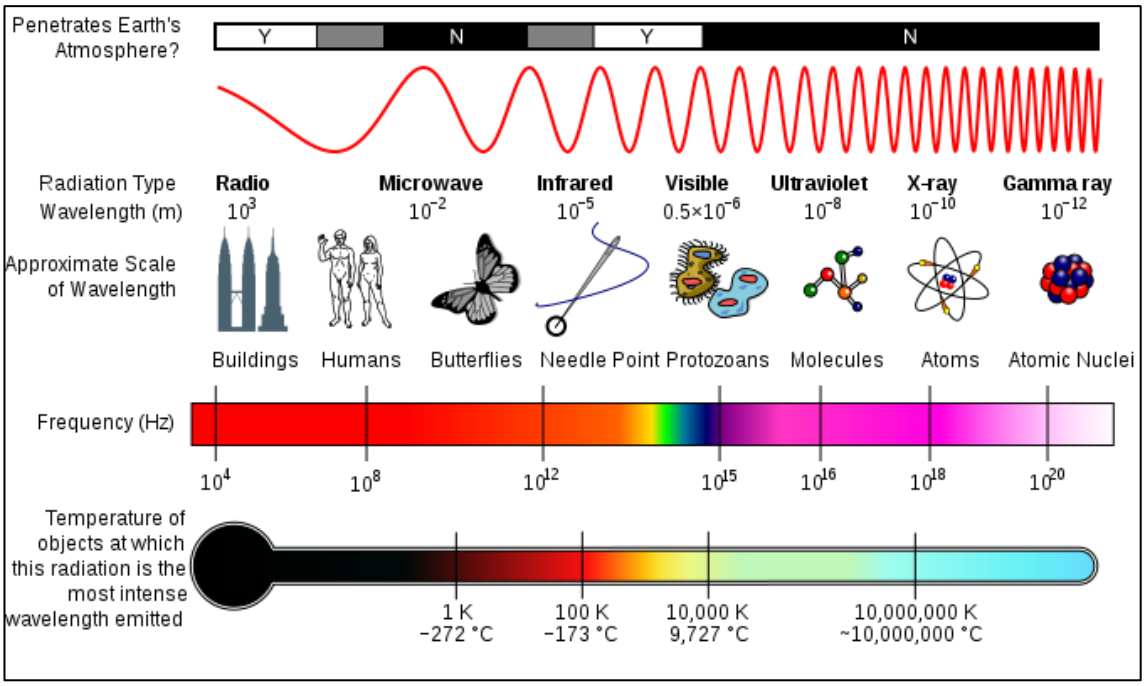

Figure 2.2 : Electromagnetic spectrum

In electromagnetic (EM) wave, the wavelength is inversely proportional to the frequency. Gamma ray may have the shortest wavelength but it has the highest frequency in EM wave. The relationship between energy content and frequency of EM wave is called the Planck relation or the Planck–Einstein equation:

$$E = hv \tag{2.1}$$

where **h** is the Planck's constant and is equal to 6.62606957 x 10^{-34} J.s or 4.135667516 x 10^{-15} eV.s (Mohr, et al., 2011) and $\boldsymbol{v}$ is the frequency of photon associated electromagnetic wave and is related to speed of light in vacuum, $\mathbf{c_o}$, by $\boldsymbol{\lambda v} = \mathbf{c_o}$. This gives the Planck relation to become:

$$E = \frac{hc_o}{\lambda} \tag{2.2}$$

This relation demonstrates that the wavelength is inversely proportional to energy. As so, gamma ray has the highest energy while radio wave has the lowest.

Although EM wave has higher energy when the wavelength is shorter, the solar radiation has a characteristic peak at a wavelength of 500 nm and approximately 95% of its overall power below 2,000 nm (Lenert, 2010). Figure 2.3 shows the spectral distribution of the incident solar radiation as approximated by a black body spectrum at a temperature of 5787 K (illustrated in red). As the solar radiation is concentrated, the intensity scales with the concentration level (C). An ideal receiver will absorb the concentrated solar radiation, convert that incident solar radiation into heat and transfer the heat to the heat transfer fluid.

Figure 2.4 displays the solar radiation spectrum for direct light at both the top of the Earth's atmosphere and at sea level. The sun produces light with a distribution similar to what would be expected from a 5525 K (5250 ℃) blackbody, which is approximately the sun's surface temperature. As light passes through the atmosphere, some is absorbed by gases with specific absorption bands. Additional light is redistributed by Rayleigh scattering, which is responsible for the atmosphere's blue color. In the atmosphere, gases filter some wavelengths from incoming solar energy.

The yellow field shows the wavelengths of energy that reach the top of the atmosphere. The red field shows the wavelengths that reach sea level. The amount of radiation is reduced overall as different gases filter out different wavelengths. Ozone filters out the shortest wavelength ultraviolet and oxygen filters out most infrared, at about 750 nm (Wikibooks, 2011). These curves are based on the American Society for Testing and Materials (ASTM) Terrestrial Reference Spectra (2003) which are standards adopted by the photovoltaic industry to ensure consistent test conditions and are similar to the light that could be expected in North America. Regions for ultraviolet, visible and infrared light are indicated.

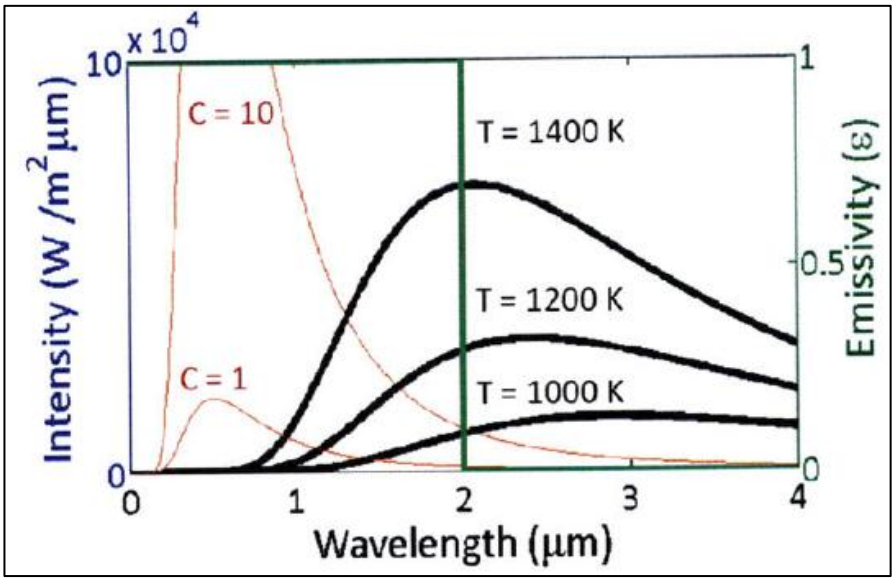

Figure 2.3 : Spectral characteristics of: incident solar radiation (red) with varying concentration levels (C); black body radiation (black); and emissive properties of a selective surface (green) (Lenert, 2010).

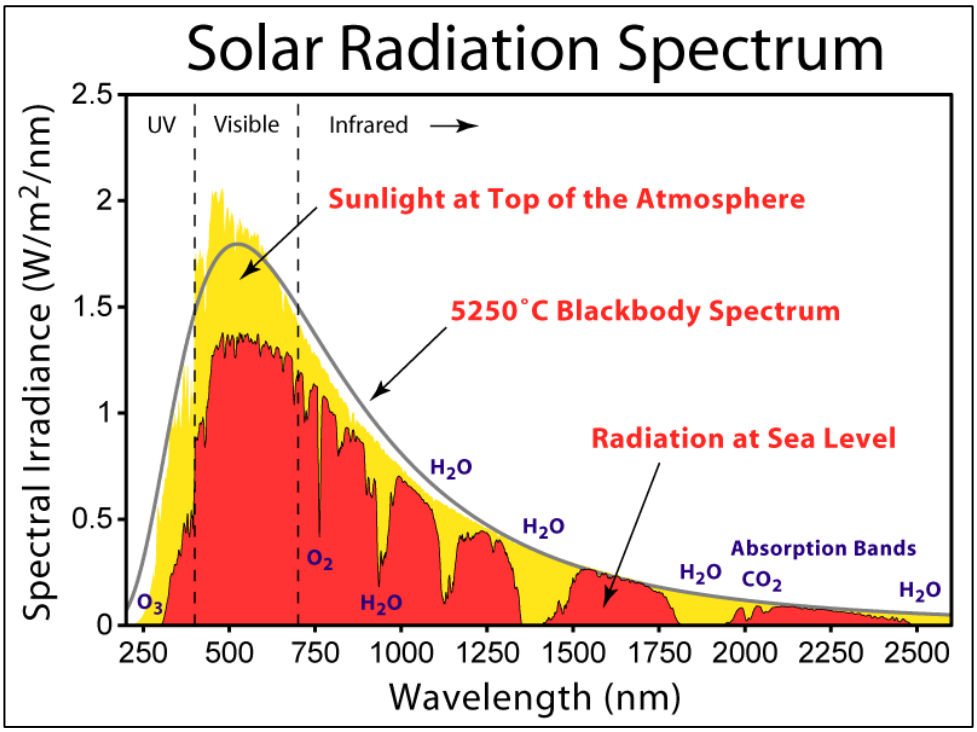

Figure 2.4 : Solar Radiation Spectrum of incident solar radiant

Besides light properties like wavelength and frequency, there are few phenomenon in determining the efficiency of absorbing incident radiant. They are further discussed below.

2.1.1 Light Scattering

Light is hardly observed directly from its source. Most of the light we see reaches our eyes in an indirect way. Looking at a tree, or a house, we see diffusely reflected sunlight. Looking at a cloud, or at the sky, we see scattered sunlight (van de Hulst, 1981).

Light scattering is a form of scattering in which light is the form of propagating energy which is scattered. Light scattering can be thought of as the deflection of a ray from a straight path, for example by irregularities in the propagation medium, particles, or in the interface between two media. Deviations from the law of reflection due to

irregularities on a surface are also usually considered to be a form of scattering (Wikipedia, 2011d). Most objects that one sees are visible due to light scattering from their surfaces. Indeed, this is our primary mechanism of physical observation (Kerker, 1909 cited in Wikipedia, 2011d; Mandelstam, 1926, cited in Wikipedia, 2011d). Scattering of light depends on the wavelength or frequency of the light being scattered. Since visible light has wavelength on the order of a micron, objects much smaller than this cannot be seen, even with the aid of a microscope. Colloidal particles as small as 1 μm have been observed directly in aqueous suspension (van de Hulst, 1981)

Light will not scatter when it traverses across homogeneous medium. In fact, any material medium has inhomogeneity as it consists of molecules, each of which acts as a scattering center, but it depends on the arrangement of these molecules whether the scattering will be very effective. In a perfect crystal at zero absolute temperature, the molecules are arranged in a very regular way, and the waves scattered by each molecule interfere in such a way as to cause no scattering at all but just a change in the overall velocity of propagation (van de Hulst, 1981). In a gas, or fluid, on the other hand, statistical fluctuations in the arrangement of the molecules cause a real scattering, sometimes may be appreciable, which in this study, will be refer to the study of nanofluid.

There are a handful types of light scattering phenomenon discovered or explained so far by scientists, for instance Mie scattering, Rayleigh scattering, Raman scattering, Tyndall scattering and Brillouin scattering. Among these, Rayleigh scattering and Mie scattering are the two most commonly used and important theories to explain the light scattering phenomenon.

2.1.1.1 Rayleigh Scattering

Rayleigh scattering, named after the British physicist Lord Rayleigh, is defined by a mathematical formula that requires the light-scattering particles to be far smaller than the wavelength of the light. For a dispersion of particles to qualify for the Rayleigh formula, the particle sizes need to be below roughly 40 nanometers; and the particles may be individual molecules. Rayleigh scattering gives blue scattered light and explains the origin of the blue sky in 1899 (Rayleigh and Strutt, 1909 cited in Horvath, 2009, p.790; Lilienfeld, 2004). In Rayleigh scattering, the intensity of the scattered radiation is given by:

$$I = I_o \frac{1 + cos^2\theta}{2R^2} \left(\frac{2\pi}{\lambda}\right)^4 \left(\frac{n^2 - 1}{n^2 + 1}\right)^2 \left(\frac{d}{2}\right)^6 \quad (2.3)$$

where **R** is the distance between the particle and the observer,

θ is the scattering angle,

n is the refractive index of the particle, and

d is the diameter of the particle.

It can be seen from the above equation that Rayleigh scattering is strongly dependent upon the size of the particle and the wavelengths. The intensity of the Rayleigh scattered radiation increases rapidly as the ratio of particle size to wavelength increases. The Rayleigh scattering model breaks down when the particle size becomes larger than around 10% of the wavelength of the incident radiation. In the case of particles with dimensions greater than this, Mie's scattering model can be used to find

the intensity of the scattered radiation. Thus, scattering by particles similar to or larger than the wavelength of light is typically treated by the Mie theory.

2.1.1.2 Mie Scattering

Mie scattering or Mie theory was named after German professor of physics Gustav Mie (1868 – 1957). His work was a rigorous treatment of the interaction of light with a particle smaller than or comparable to the wavelength of light and combined theory with applications to a real practical case: the scattering and absorption of light, its polarization, and colour phenomena observed for gold colloids (Horvath, 2009).

Mie scattering can use to calculate the spectrum of the scattered light. For particles with sizes between 20 and 140 nm, almost independently of size, the scattered light is green to yellow, the largest amount of light is scattered by particles sized between 100 and 140 nm. Particles with sizes between 140 and 180 nm predominantly scatter orange to red light. Both theoretical findings are in agreement with observations (Horvath, 2009).

Mie scattering also explains the polarization of light particles. It is stated that if particles are illuminated by unpolarized light, the scattered light is usually partly polarized. For particles smaller than 100 nm (Rayleigh scattering) the light scattered at 90 ºis completely polarized, which is also true for gold particles. For particles with sizes between 100 and 180 nm the degree of polarization diminishes rapidly with increasing particle size, again in agreement with the observations (Horvath, 2009). Three diagrams taken from Mie's publication are shown in Figure 2.5 for a wavelength of 550 nm.

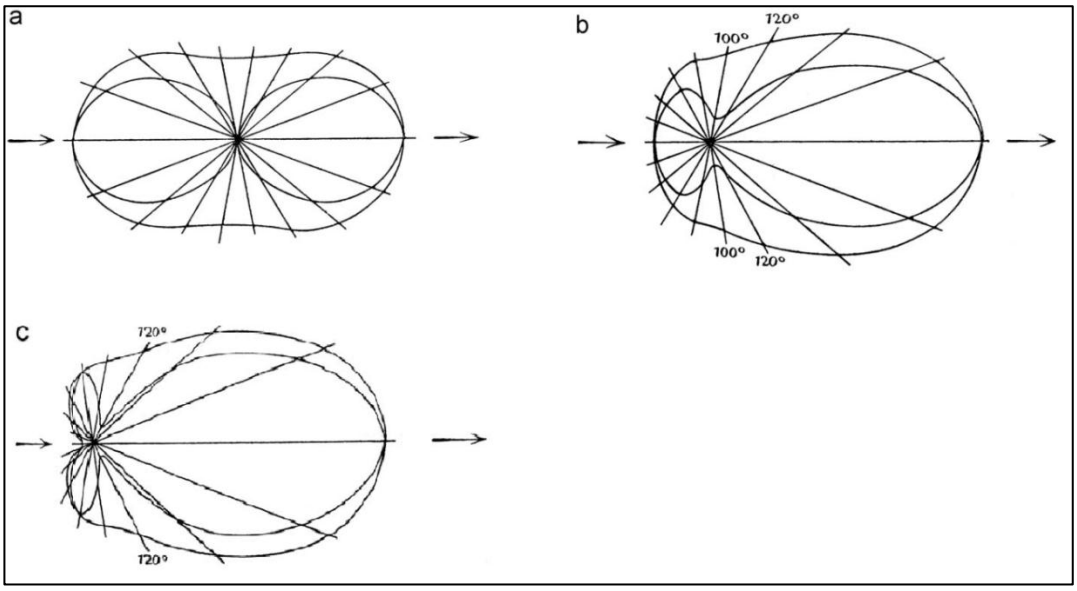

Figure 2.5 : Angular dependence of the scattered light with polarization parallel and perpendicular to the plane of observation for spherical gold particles. A: the limiting case of infinitely small particles. B: particles with a diameter of 160 nm. C: particles with a diameter of 180 nm (Horvath, 2009, p.793).

Mie pointed out that with increasing particles size the forward scattering rapidly increases in comparison to the backscattering. He also noted that the proper choice of the refractive index is absolutely critical. The polar diagram also makes possible to determine the degree of polarization. It is immediately evident, that complete polarization of the scattered light for particles below a diameter of 180 nm is not possible outside of the Rayleigh range no matter at what angle. Maximum polarization outside the Rayleigh range is attained for scattering angles between 110 ºand 120 º.

In short, Mie scattering is a broader class of scattering of light by spherical particles of any diameter compare to Rayleigh scattering. The scattering intensity is generally not strongly dependent on the wavelength, but is sensitive to the particle size.

2.1.2 Light Absorption

Scattering is often accompanied by absorption. A leaf of a tree looks green because it scatters green light more effectively than red light. The red light incident on the leaf is absorbed; this means that its energy is converted into some other form and is no longer present as red light. Absorption is preponderant in materials such as coal and black smoke and is nearly absent in clouds (van de Hulst, 1981). Figure 2.6 below illustrates the process of light absorption and the change of energy of particles when absorption happens.

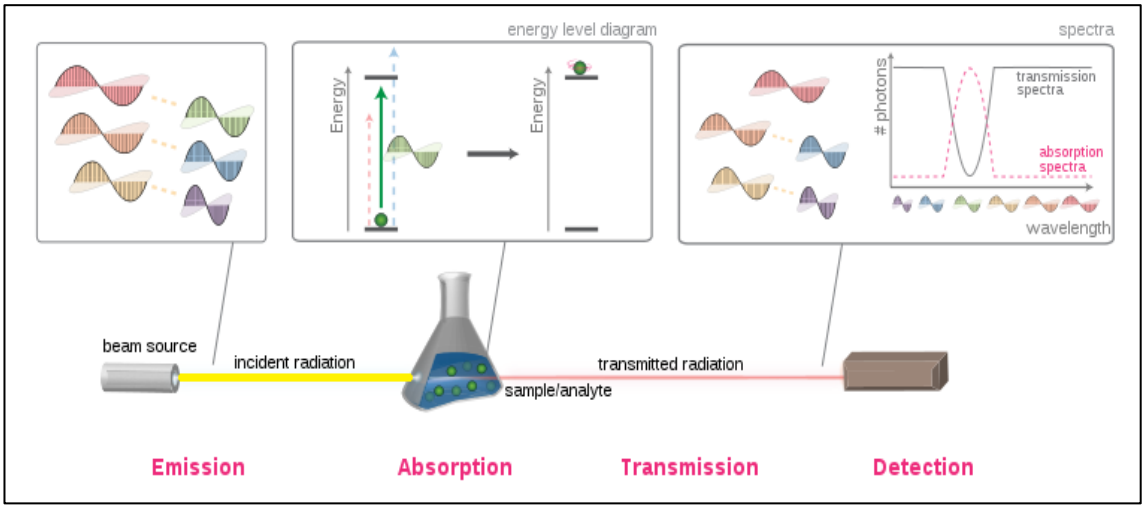

Figure 2.6 : Light Absorption

From Figure 2.6, light source, normally white light, comprising continuous wavelength of visible region (400-700nm) is emitted towards a sample or analyte. Here the discrete colors are arranged in descending wavelength (i.e., increasing energy) to simplify the representation of white light. Polarization does not affect absorption and is not represented; complementary colors are denoted with yellow lines. The “Beam source” generally indicates a broad spectrum light, e.g., from black-body radiation and

laser beam is not within this scope as they are monochromatic (single wavelength). Light in the visible region induces electronic excitation and it will rearrange the electron clouds. This applies only for visible light - the removal of a colour results in beam appearing as its complementary color. Here, the removal of green within the red-green pair gives the transmitted beam a red color when light beam traverses through the sample. Molecules have quantized energy levels, and photons have quantized energy. If the incoming photon has exactly the matching energy for the promotion of the molecule, the molecule would absorb the photon, and changes state from the ground state to an excited state. The specific physical change depends on the radiation. A spectra is effectively a continuous histogram describing the composition of light. By comparing the attenuation of the transmitted light with the incident, absorption spectra can be obtained. Absorption spectra is represented as a transmission spectra, which is shown in gray in Figure 2.5, where the y-axis shows the photon count of transmitted light, or an absorption spectra (magenta) where the attenuation is plotted. The former is commonly used in infrared/microwave spectroscopy, and the latter in UV-Vis and NMR.

2.1.3 Light Extinction

Both scattering and absorption remove energy from a beam of light traversing the medium. The beam is then attenuated. This attenuation, which is called extinction, is seen when we look directly at the light source. The sun, for instance, is fainter and redder at the sunset than at noon. This indicates extinction in the long air path, which is strong in all colours but even stronger in blue light than in red light. Extinction can be defines as scattering plus absorption (van de Hulst, 1981).

$$Extinction = Scattering + Absorption \tag{2.4}$$

In Mie study, light passing through a gold colloid loses energy both due to scattering of the light and absorption inside the particles. The maximum attenuation is at 525 nm, the minimal one is in the red, and thus the colloid appears ruby red in transmission. For particle sizes between 20 and 100 nm the maximum of the attenuation slightly shifts to longer wavelengths, which still produces a red colour in transmission. A graph of Mie's data of the light extinction (attenuation) coefficient, which is called ''absorption'' by Mie, is shown in Figure 2.7.

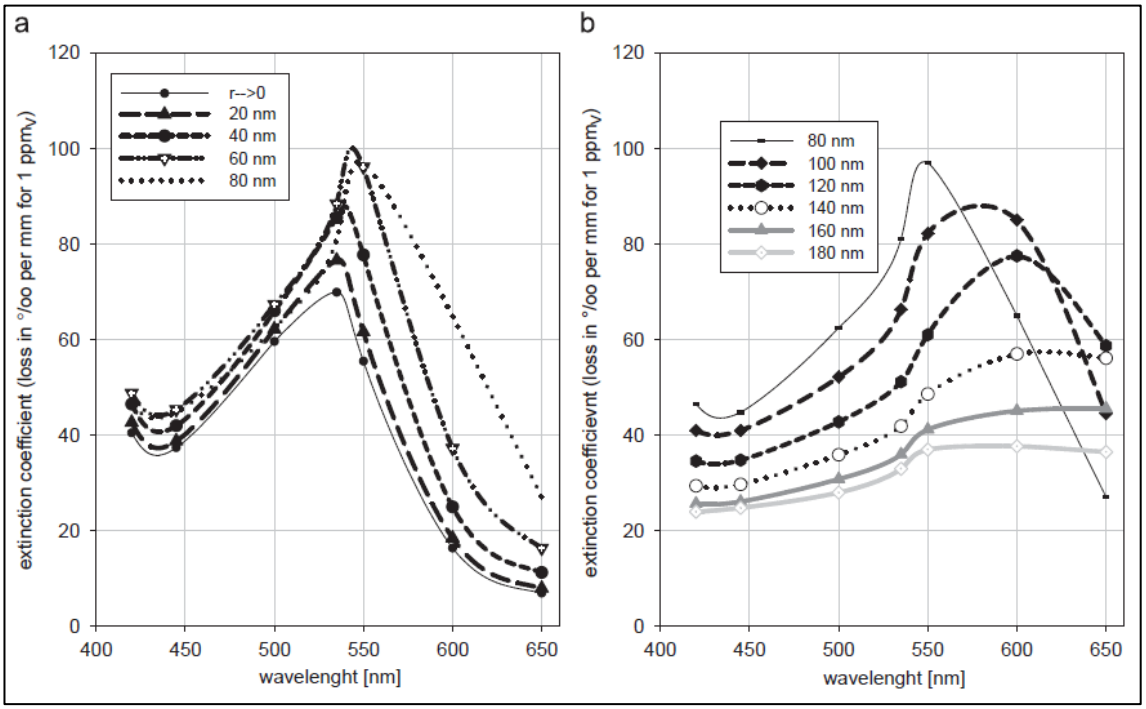

Figure 2.7 : Attenuation coefficient of gold suspensions with different particle sizes. (Horvath, 2009)

For sizes above 100 nm the wavelength-dependent attenuation changes significantly. The absorption maximum shifts towards longer wavelengths and the

weakest attenuation is between 400 and 450 nm, causing the colloid to appear violet in transmission for particle sizes ~100nm, deep blue for ~120 nm, indigo for ~160 nm, and green–blue for ~180 nm. These results give an important guide in choosing the size of nanoparticles to be used in nanofluid for Direct Solar Absorber. The nanoparticles size is suggested to be smaller than 100 nm as the solar radiant has peak concentration around the wavelength of 500 nm (Lenert, 2010) as discussed in section 2.1.

2.2 Solar Collectors

As explained in the previous chapter, solar energy can perceive to be a higher level of energy. Basically, all the forms of energy in the world as we know it are solar in origin. Oil, coal, natural gas and woods were originally produced by photosynthetic processes, followed by complex chemical reactions in which decaying vegetation was subjected to very high temperatures and pressures over a long period of time (Kreith and Kreider, 1978). Even the wind and tide energy have a solar origin since they are caused by differences in temperature in various regions of the earth. In such, harvesting energy directly from solar can avoid losses in the process of converting energy from one form to the other. Besides, the lesser processes or steps it is to convert solar energy into electrical power or any usable energy form to us may help to reduce carbon footprint.

The idea of using solar energy collectors to harness the sun's power is recorded from the prehistoric times when at 212 BC the Greek scientist/physician Archimedes devised a method to burn the Roman fleet. Archimedes reputedly set the attacking Roman fleet afire by means of concave metallic mirror in the form of hundreds of polished shields; all reflecting on the same ship (Anderson, 1977). There were many developments in methods of solar harvesting ever since Archimedes (Meinel and Meinel, 1976; Kreider and Kreith, 1977).

In water and space heating sector, the hot water and house heating appeared in the mid-1930s, but gained interest in the last half of the 40s. Until then millions of houses were heated by coal burn boilers. The idea was to heat water and fed it to the radiator system that was already installed (Kalogirou, 2004). Currently in freezing climates, solar water heating costs US$0.11–0.12/kWh, while in mild or "sunbelt" climates, solar water heating costs about US$0.08–0.10/kWh. In some countries such as China, solar water heating systems are already competitive with conventional systems in certain climates (EGRE, 2005).

In 2010, existing solar water and space heating capacity increased by an estimated 25 gigawatts-thermal (GW_{th}), or about 16%, to reach approximately 185 GW_{th}, excluding unglazed swimming pool heating. China added an estimated 17.5 GW_{th} (25 million m^2 of collectors) for a total of just under 118 GW_{th} (168 million m^2) (Weiss and Mauthner, 2011). Figure 2.8 demonstrate the solar heating existing capacity of the top 12 countries, and respectively. From Figure 2.8, we can see that China has become the biggest installer of solar collector in the world followed by Germany. The existing capacity of solar collector installed in China consist more than half of the world capacity.

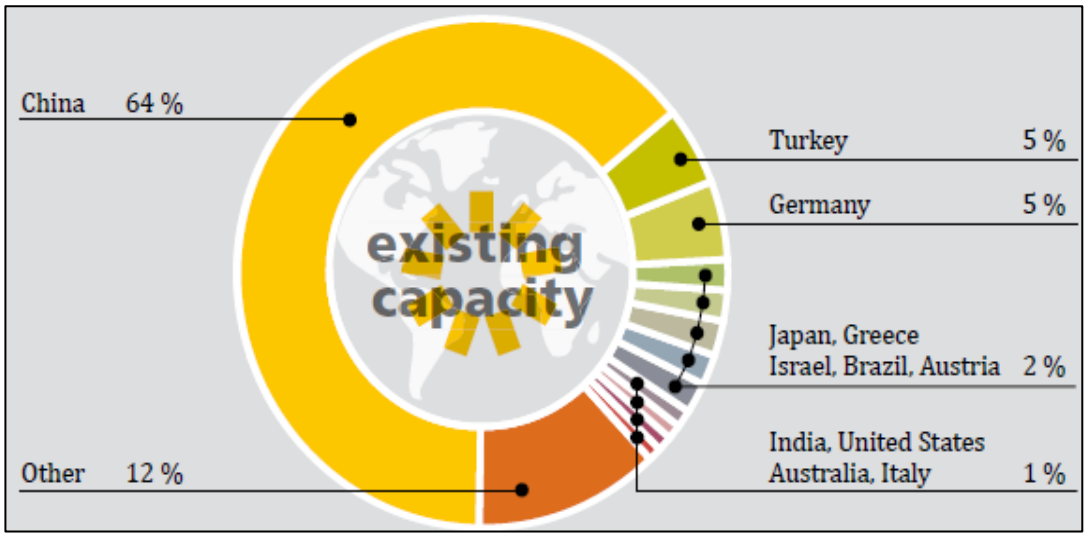

Figure 2.8 : Solar heating existing Capacity, Top 12 Countries, 2009 (Weiss and Mauthner, 2011)

Besides having the most solar collectors installed, figure 2.9 which shows the total capacity of newly installed glazed and unglazed water collectors in the 10 leading countries also indicates that China is growing in the fastest pace in 2009 as the European Union and major western markets had been hit hard by economy meltdown. The leading market in Europe, Germany, underwent a downturn of 23.1% in its newly installed capacity of glazed water collectors compared with 2008 (Weiss and Mauthner, 2011). In general, market development had been affected by lower fossil fuel prices and declining end-user investments.

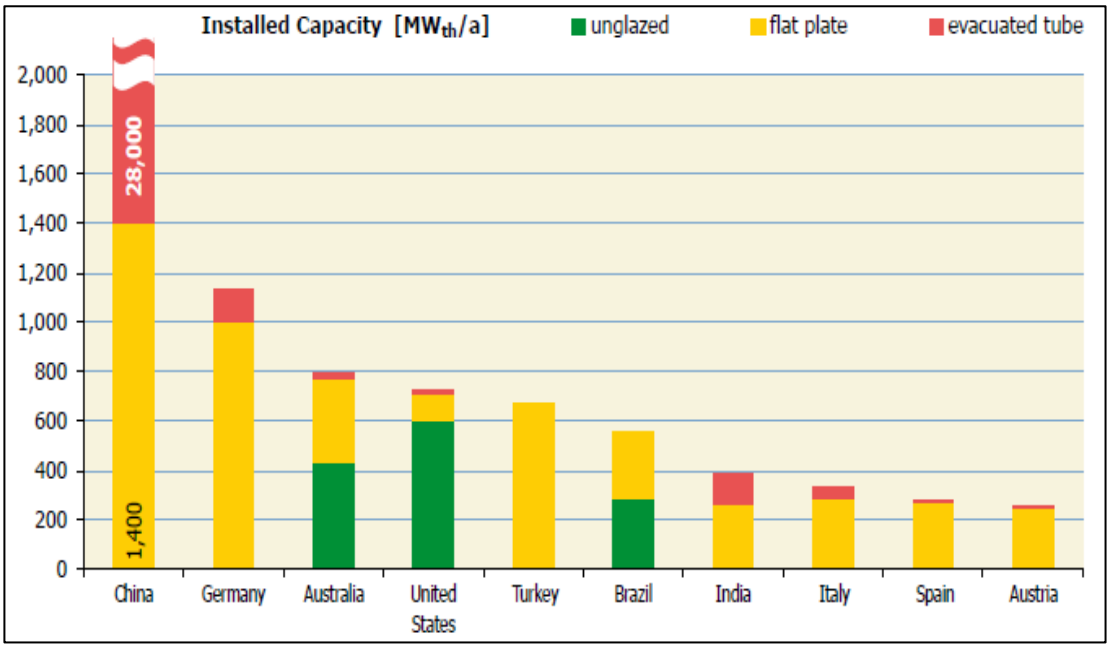

Figure 2.9 : Total capacity of newly installed collectors in the 10 leading countries in 2009 (Weiss and Mauthner, 2011)

However, with compare to the European Union, the second largest solar collector installer community, China is installed mainly with more expensive evacuated tube collector which gives more superior efficiency compare to conventional flat plate collector. It has been reported that more than 95% of the newly installed systems were equipped with this collector type. Consequently, the growth rates by type of glazed water collector in 2009 are high for vacuum tubes (+ 34.5%) and almost stagnating (+ 2.4%) for flat plate collectors (Weiss and Mauthner, 2011). This is showed in Figure 2.9 and also gives explanation to the large portion of evacuated tube collector in the market share which is showed in Figure 2.10 that illustrates the distribution of the total installed capacity in operation by collector type. All these figures are extracted from the Solar and Heat Worldwide 2011: Markets and Contribution to the Energy Supply 2009 report by Weiss and Mauthner (2011).

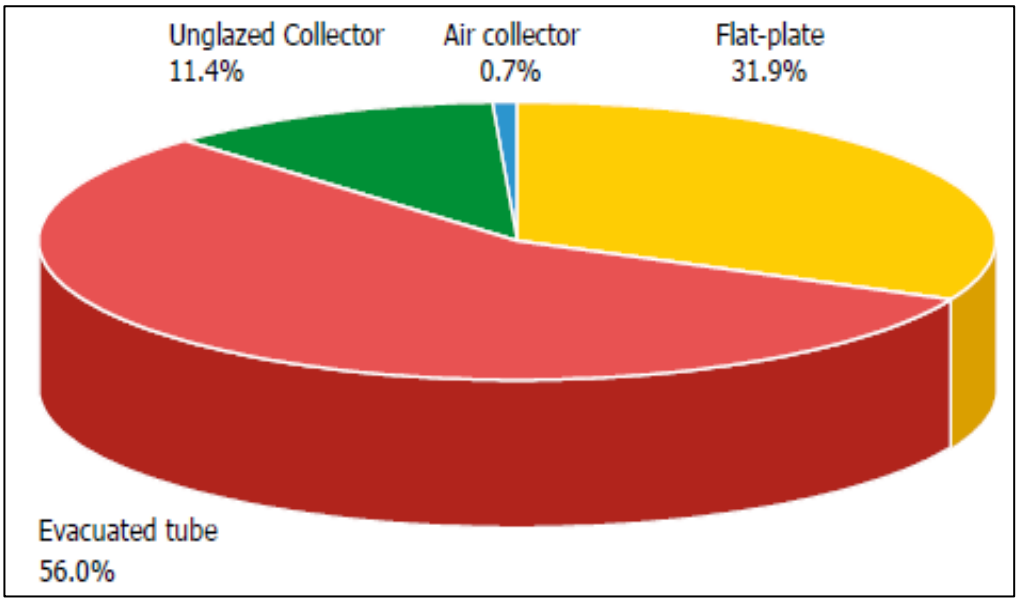

Figure 2.10 : Distribution of the total installed capacity in operation by collector type in 2009 (Weiss and Mauthner, 2011)

2.2.1 Classification of Solar Collectors

Solar energy collectors are special kind of heat exchangers that transform solar radiation energy to internal energy of the transport medium. The major component of any solar system is the solar collector. This is a device which absorbs the incoming solar radiation, converts it into heat, and transfers this heat to a fluid (usually air, water, or oil) flowing through the collector. The solar energy thus collected is carried from the circulating fluid either directly to the hot water or space conditioning equipment or to a thermal energy storage tank from which can be drawn for use at night and/or cloudy days (Kalogirou, 2004).

There are basically two types of solar collectors: non-concentrating or stationary and concentrating. A non-concentrating collector has the same area for intercepting and for absorbing solar radiation, whereas a sun-tracking concentrating solar collector usually has concave reflecting surfaces to intercept and focus the sun's

beam radiation to a smaller receiving area, thereby increasing the radiation flux (Kalogirou, 2003). During the past 50 years many variations were designed and constructed using focusing collectors as a means of heating the transfer or working fluid which powered mechanical equipment. With such, a large number of solar collectors are available in the market. A comprehensive list is shown in Table 2.2.

Table 2.2 : Types of solar energy collectors (Kalogirou, 2003)

Motion	Collector type	Absorber type	Concentration ratio	Indicative temperature range (℃)
Stationary	Flat plate collector (FPC)	Flat	1	30 – 80
	Evacuated tube collector (ETC)	Flat	1	50 – 200
	Compound parabolic collector (CPC)	Tubular	1 – 5	60 – 240
Single-axis tracking			5 – 15	60 – 300
	Linear Fresnel reflector (LFR)	Tubular	10 – 40	60 – 250
	Parabolic trough collector (PTC)	Tubular	15 – 45	60 – 300
	Cylindrical trough collector (CTC)	Tubular	10 – 50	60 – 300

Table 2.2, continued.

Two-axes tracking	Parabolic dish reflector (PDR)	Point	100 – 1000	100 – 500
	Heliostat field collector (HFC)	Point	150 – 2000	150 – 2000

2.2.2 Concentrating Solar Collectors

Energy delivery temperatures can be increased by decreasing the area from which the heat losses occur. Temperatures far above those attainable by non-concentrating solar collectors can be reached if a large amount of solar radiation is concentrated on a relatively small collection area. This is done by interposing an optical device between the source of radiation and the energy absorbing surface. Concentrating collectors exhibit certain advantages as compared with the conventional flat-plate type or non-concentrating collectors (Kalogirou, Eleftheriou, Lloyd & Ward, 1994). The main ones are:

1. The working fluid can achieve higher temperatures in a concentrator system when compared to a flat-plate system of the same solar energy collecting surface. This means that a higher thermodynamic efficiency can be achieved.

2. It is possible with a concentrator system, to achieve a thermodynamic match between temperature level and task. The task may be to operate thermionic, thermodynamic, or other higher temperature devices.

3. The thermal efficiency is greater because of the small heat loss area relative to the receiver area.

4. Reflecting surfaces require less material and are structurally simpler than FPC. For a concentrating collector the cost per unit area of the solar collecting surface is therefore less than that of a FPC.

5. Owing to the relatively small area of receiver per unit of collected solar energy, selective surface treatment and vacuum insulation to reduce heat losses and improve the collector efficiency are economically viable.

Their disadvantages are:

1. Concentrator systems collect little diffuse radiation depending on the concentration ratio.

2. Some form of tracking system is required so as to enable the collector to follow the sun.

3. Solar reflecting surfaces may lose their reflectance with time and may require periodic cleaning and refurbishing.

The two primary solar technologies used for concentrating collectors are the central receivers and the distributed receivers employing various point and line-focus optics to concentrate sunlight. Central receiver systems use fields of heliostats (two-axis tracking mirrors) to focus the sun's radiant energy onto a single tower-mounted receiver (SERI, 1987 cited in Kalogirou, 2004, p.238). Distributed receiver technology includes parabolic dishes, Fresnel lenses, parabolic troughs, and special bowls. Parabolic dishes track the sun in two axes and use mirrors to focus radiant energy onto a point-focus receiver. Troughs and bowls are line-focus tracking reflectors that concentrate sunlight onto receiver tubes along their focal lines. Receiver temperatures range from 100 ℃ in low-temperature troughs to close 1500 ℃ in dish and central receiver systems (SERI, 1987 cited in Kalogirou, 2004, p.238). Concentration ratios, i.e. the ratio of aperture to

absorber areas, can vary over several orders of magnitude, from as low as unity to high values of the order of 10,000 (Kalogirou, 2004). Obviously, increased ratios mean increased temperatures at which energy can be delivered but consequently these collectors have increased requirements for precision in optical quality and positioning of the optical system. Figure 2.11 gives a clearer illustration to the above mentioned solar collectors.

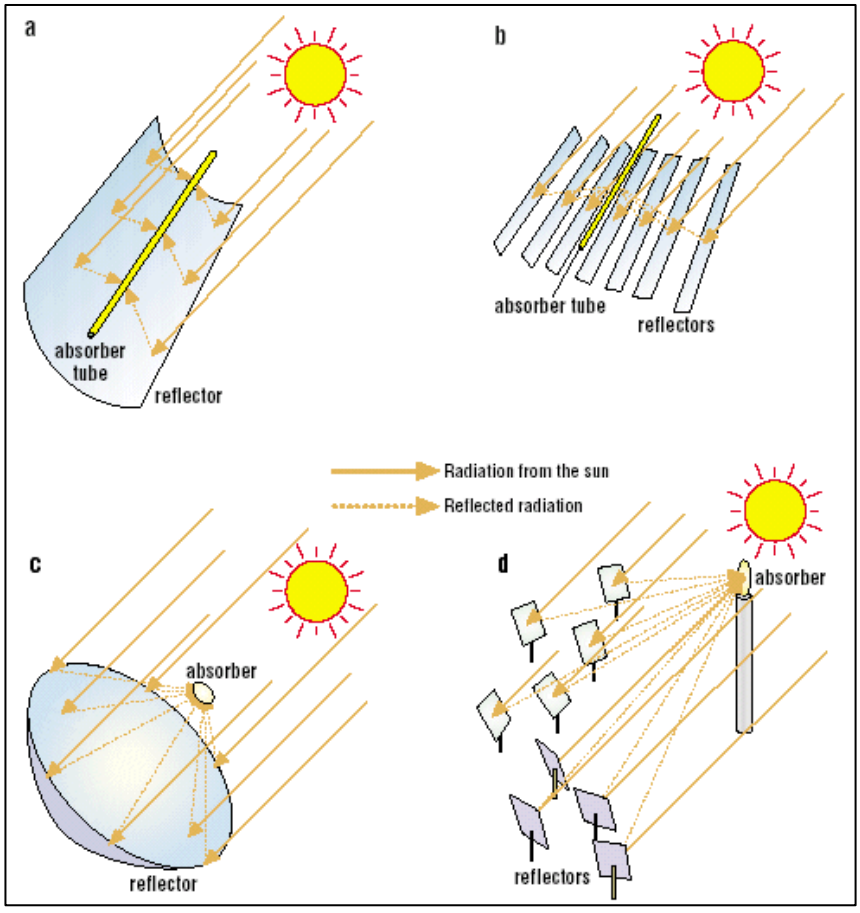

Figure 2.11 : Concentration of sunlight using (a) parabolic trough collector (b) linear Fresnel collector (c) central receiver system with dish collector and (d) central receiver system with distributed reflectors

2.2.3 Non-Concentrating Solar Collectors

For non-concentrating collectors, hot water heating system is an important field as mentioned in the previous section. The hot water heating system uses mainly stationary solar collector which are permanently fixed in position and do not track the sun. These collectors consist of flat plate collector (FPC) (glazed or unglazed), evacuated tube collector (ETC) and stationary compound parabolic collector (CPC). The passive thermosiphon system is the most common type of solar water heating system worldwide. Simple flat plate collectors made of copper absorbers, aluminum enclosures, and glass cover plates were the predominant technology for this system for the last few decades (EGRE, 2005). However, evacuated tube collectors have recently dominated the world market because of the development of water-in-glass evacuated tube systems in China.

Being the major market player and also the system in which the effect of nanofluid as thermal transfer fluid is studied in this thesis, the flat plate collector and evacuated tube collector are briefly discussed and elucidated.

2.2.3.1 Flat Plate Solar Collector (FPC)

The most commonly used systems in water heating system are the flat-plate, black-surface absorbers, which absorb solar energy through a solid surface (Okujagu & Adjepong 1989). Figure 2.12 below shows a typical flat plate collector set up used in water heating. The solar collector is installed at the roof of the building with certain designed tilt angle to maximize the incident solar radiant. A close loop circuit with water or heat transfer fluid flows through the solar collector with the help of a pump. The fluid is heated up when it passes by the collector and the heat is ejected or released

to a water storage tank. The water in the storage tank is now heated and ready to be used. A boiler, either gas or electric powered, is normally supplied in the system to serve as a standby power source in the time of insufficient solar energy.

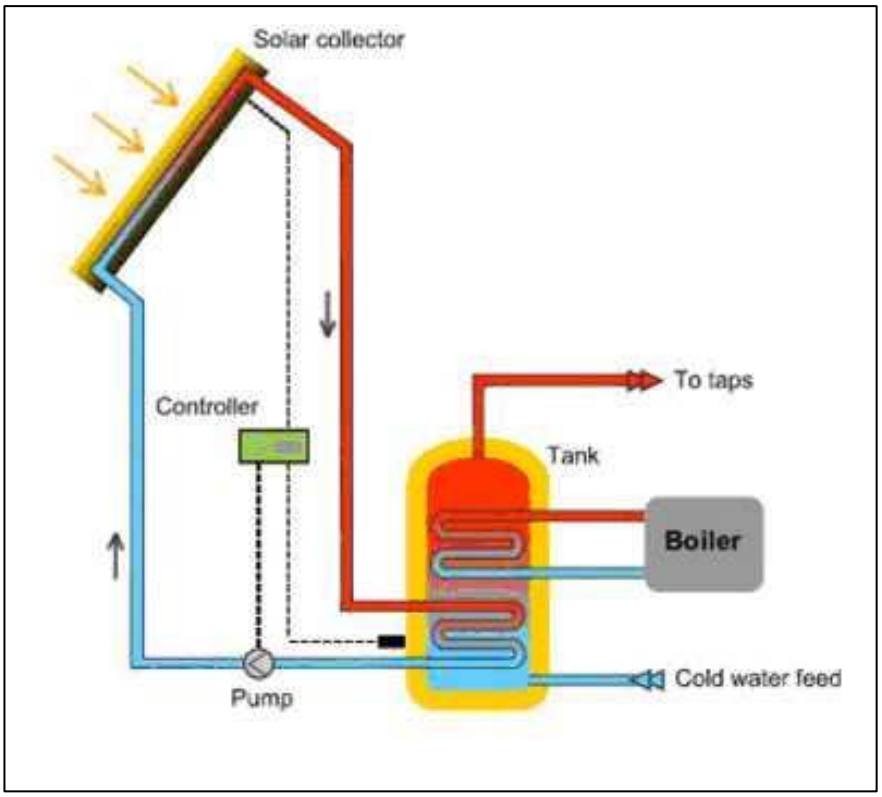

Figure 2.12 : Typical set up of Flat Plate Collector (FPC)

Besides this set up, there is another similar arrangement commonly used in the market called Thermosyphon solar water heater. Figure 2.13 below displays this type of arrangement.

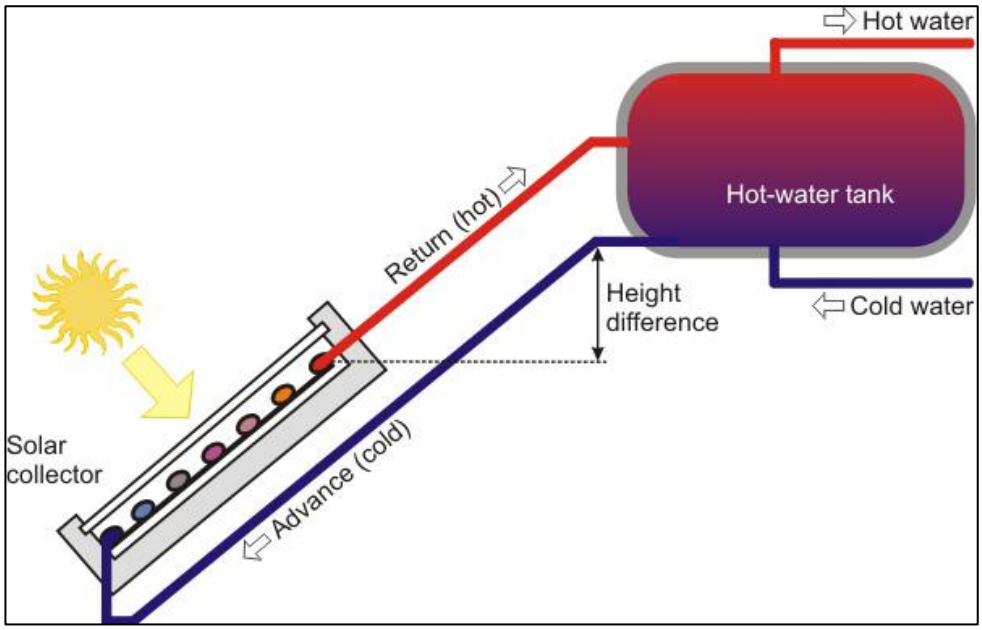

Figure 2.13 : Thermosyphon Solar water heater

Thermosyphon solar water heater works with exactly the same concept and pattern as the typical set up except it does not have a pump installed in the system. The advantage of this arrangement is that it can save space and cost by omitting the pump. The need of maintenance to the system become close to nil as there is basically no moving parts. These advantages make it a more favourable system in today's property development as living space has become a major limitation in big cities. However, this system has its restriction. The water tank has to be located above the solar collector within certain height and distance (about 30cm) to allow the heat transfer fluid to flow naturally from the collector to the water tank with the help of natural convection and to prevent backflow of cooler storage water to the collector in the case when the collector is colder than the water stored. The water in the collector expands becoming less dense as the sun heats it and rises through the collector into the top of the storage tank. There it is replaced by the cooler water that has sunk to the bottom of the tank, from which it flows down the collector. At night, or whenever the collector is cooler than the water in the tank the direction of the thermosyphon flow will reverse, thus cooling the stored water.

Disregard of which system been used, the flat plate solar collector is the same. FPC has been built in a wide variety of designs and from many different materials. They have been used to heat fluids such as water, water plus antifreeze additive, or air. Their major purpose is to collect as much solar energy as possible at the lower possible total cost. The collector should also have a long effective life, despite the adverse effects of the sun's ultraviolet radiation, corrosion and clogging because of acidity, alkalinity or hardness of the heat transfer fluid, freezing of water, or deposition of dust or moisture on the glazing, and breakage of the glazing because of thermal expansion, hail, vandalism or other causes. These causes can be minimized by the use of tempered glass. A typical flat plate solar collector is shown in figure 2.14 and 2.15 in pictorial and exploded view respectively.

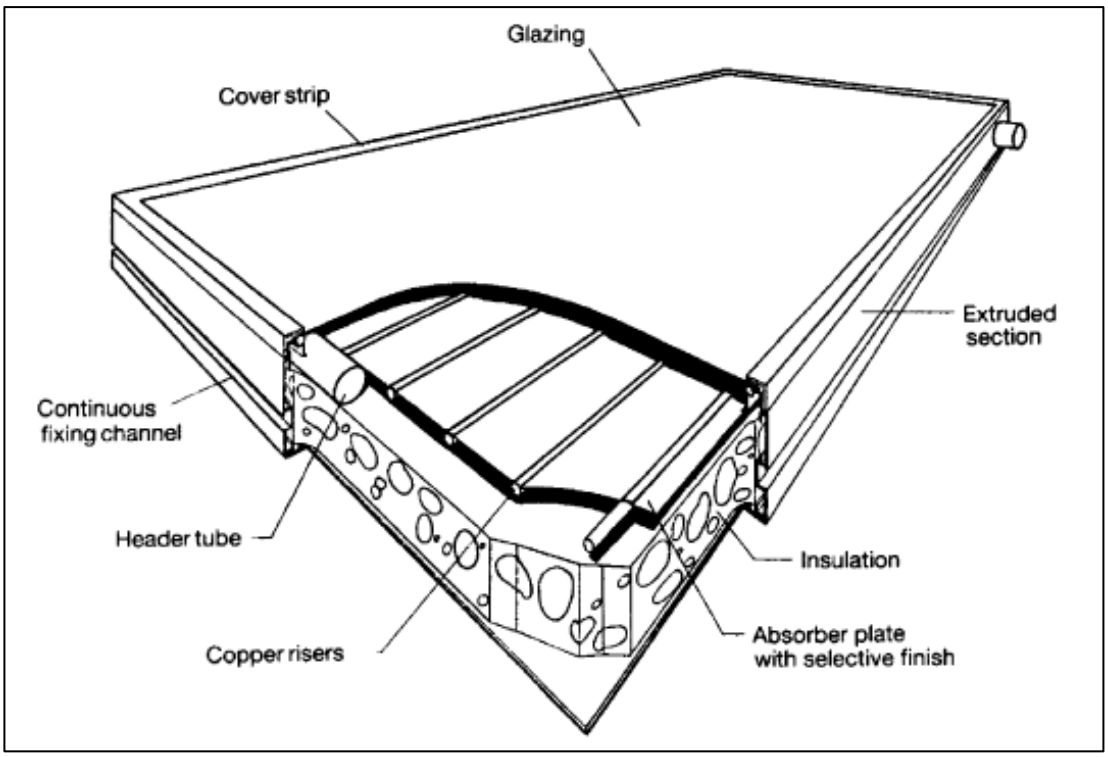

Figure 2.14 : Pictorial view of a flat plate collector (Kalogirou, 2004, p.241)

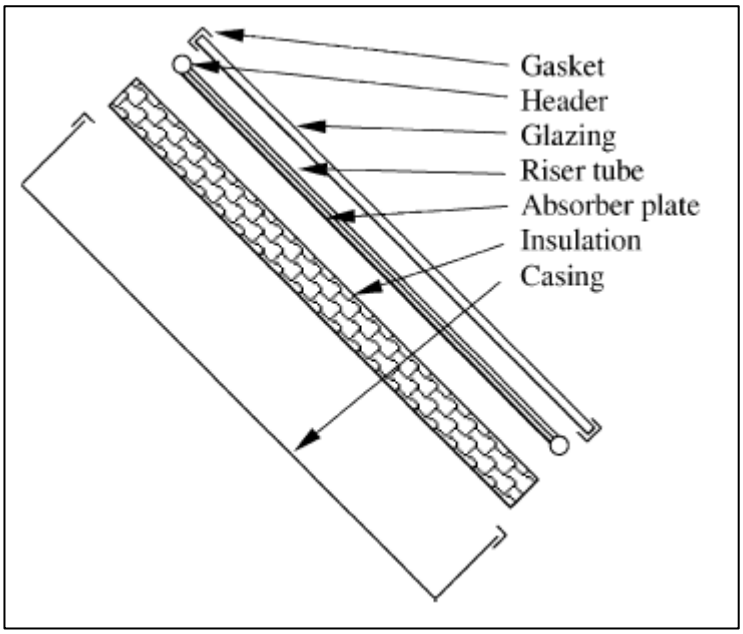

Figure 2.15 : Exploded view of a flat plate collector (Kalogirou, 2004, p.241)

When solar radiation passes through a transparent cover and impinges on the blackened absorber surface of high absorptivity, a large portion of this energy is absorbed by the plate and then transferred to the transport medium in the fluid tubes to be carried away for storage or use. The underside of the absorber plate and the side of casing are well insulated to reduce conduction losses. The liquid tubes can be welded to the absorbing plate, or they can be an integral part of the plate. The liquid tubes are connected at both ends by large diameter header tubes. The transparent cover is used to reduce convection losses from the absorber plate through the restraint of the stagnant air layer between the absorber plate and the glass. It also reduces radiation losses from the collector as the glass is transparent to the short wave radiation received by the sun but it is nearly opaque to long-wave thermal radiation emitted by the absorber plate (greenhouse effect).

Every part shown in the figures above has its own function. The glazing may have one or more sheets of glass or other diathermanous material for light transmitting.

The glazing should admit as much solar irradiation as possible and reduce the upward loss of heat as much as possible. Table 2.3 below shows the optical properties of commonly used glazing materials. The solar transmittance is high (close to 1.0) while the long-wave infra-red transmittance is very low by comparison (Everett, 2004). Although glass is virtually opaque to the long wave radiation emitted by collector plates, absorption of that radiation causes an increase in the glass temperature and a loss of heat to the surrounding atmosphere by radiation and convection.

Table 2.3 : Optical properties of commonly used glazing materials (Everett, 2004, p.27)

Material	Thickness (mm)	Solar Transmittance	Love-wave infrared transmittance
Float glass (normal window glass)	3.9	0.83	0.02
Low-iron glass	3.2	0.90	0.02
Perspex	3.1	0.82	0.02
Poly vinyl fluoride (tedlar)	0.1	0.92	0.22
Polyester (mylar)	0.1	0.87	0.18

The tubes, fins or passages, whichever they are called by manufacturers, are used to conduct or direct the heat transfer fluid from the inlet to the outlet. Absorber plates are flat, corrugated or grooved, which the tubes, fins or passages are attached. The plate may be integral with the tubes in some designs. The collector plate need to absorb as much of the irradiation as possible through the glazing, while losing as little heat as possible upward to the atmosphere and downward through the back of the casing. The collector plates transfer the retained heat to the transport fluid. The absorptivity of

the collector surface for shortwave solar radiation depends on the nature and colour of the coating and on the incident angle. The design and material selection of the plate are the most essential items as it directly affects the efficiency of solar energy being converted to thermal energy in the fluid. Essentially, typical selective surfaces consist of a thin upper layer, which is highly absorbent to shortwave solar radiation but relatively transparent to long wave thermal radiation, deposited on a surface that has a high reflectance and a low emissivity for long wave radiation. Selective surfaces are particularly important when the collector surface temperature is much higher than the ambient air temperature. For fluid-heating collectors, passages must be integral with or firmly bonded to the absorber plate. A major problem is obtaining a good thermal bond between tubes and absorber plates without incurring excessive costs for labour or materials. Material most frequently used for collector plates are copper, aluminium, and stainless steel. However, even the best design will still implies certain degree of thermal losses through conduction or convection. Reduction of heat loss from the absorber can be accomplished either by a selective surface to reduce radiative heat transfer or by suppressing convection. Francia (1961) and Hollands (1965) showed that a honeycomb made of transparent material, placed in the airspace between the glazing and the absorber, was beneficial.

The headers or manifolds are to admit and discharges the fluid while the insulation to minimize the heat loss from the back and sides of the collector. Last but not least, the container or casing is important as well to surround the aforementioned components and keep them free from dust, moisture, etc.

FPC are usually employed for low temperature applications up to 100 ℃, although some new types of collectors employing vacuum insulation and/or TI can achieve slightly higher values (Benz, Hasler, Hetfleish, Tratzky & Klein, 1998 cited in Kalougirou, 2004, p.243).

Another category of collectors is the uncovered or unglazed solar collector (Soltau, 1992). These collectors are usually cheaper solution but still offer effective solar thermal energy in applications such as water preheating for domestic or industrial use, heating of swimming pools (Molineaux, Lachal & Gusian, 1994; Winter, 1994), space heating and air heating for industrial or agricultural applications.

As one of the most common and vastly used solar thermal collector, surface absorption type panel has its limitations. These limitations are the need of large solar receiving area, efficiency of the surface absorber, thermal transfer loss from the black surface absorber to the inner tube containing the fluid carrier and the surface absorber losses to the environment due to convection and reflection. Volumetric absorber has thus been view as a possible enhancement to the conventional surface absorption solar collector.

2.2.3.2 Evacuated Tube Solar Collectors (ETC)

Conventional simple flat-plate solar collectors were developed for use in sunny and warm climates. However, their performance is greatly shrunk when conditions become unfavourable during cold, cloudy and windy days. Furthermore, weathering influences such as condensation and moisture will cause early deterioration of internal materials resulting in reduced performance and system failure (Kalogirou, 2004). Evacuated heat pipe solar collectors (tubes) operate differently than the other collectors available on the market. These solar collectors consist of a heat pipe inside a vacuum-sealed tube, as shown in figure 2.16 and 2.17.

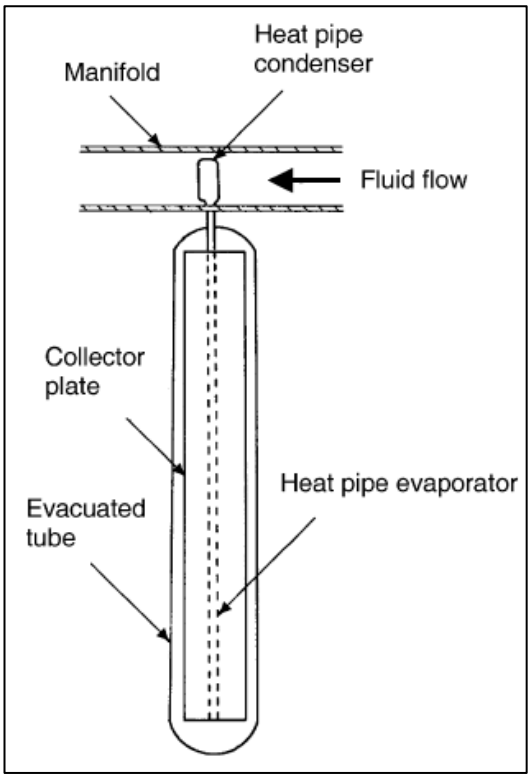

Figure 2.16 : Schematic diagram of an evacuated tube collector (Kalogirou, 2004).

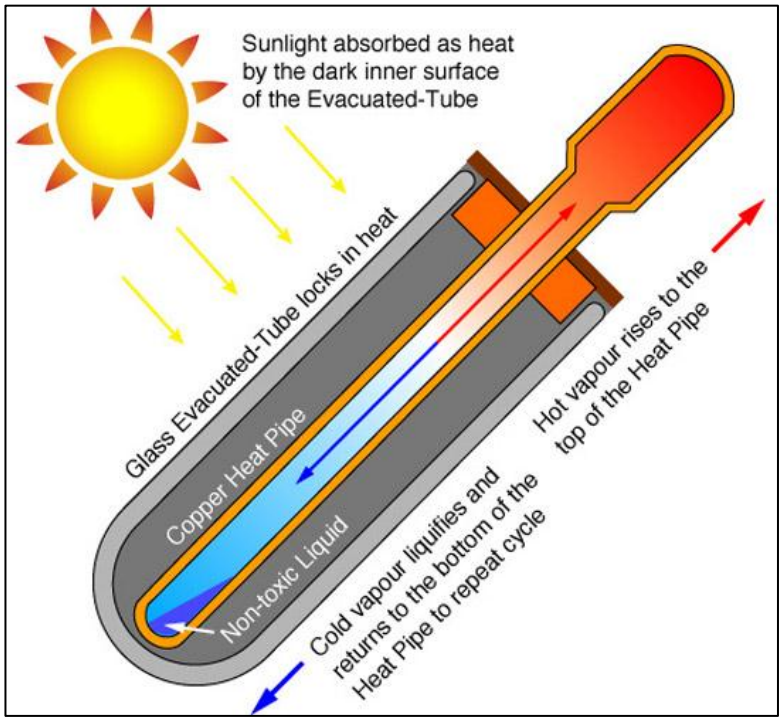

Figure 2.17 : Working principle of heat pipe in evacuated tube collector.

Heat pipes are highly efficient thermal conductors with simple working principle. It generally exploits the occurrence of natural convection in fluid when temperature gradient arises. The pipe is a sealed copper pipe and is attached to a black copper fin that fills the absorber plate. The top of each heat pipe is a metal tip attached to the sealed header which serves as a condenser. The heat pipe contains a small amount of fluid that undergoes an evaporating-condensing cycle. In this cycle, solar heat evaporates the liquid, and the vapour travels to the heat sink region where it condenses and releases its latent heat. The condensed fluid return back to the solar collector and the process is repeated. Water, or glycol, flows through the manifold and picks up the heat from the tubes. The heated liquid circulates through another heat exchanger and gives off its heat to a process or to water that is stored in a solar storage tank.

ETC offers superior performance at high temperature compare to FPC as the vacuum envelope reduces convection and conduction losses. ETC, similar to FPC, collect both direct and diffuse radiation but provide higher efficiency at low incident angles. Besides, as no evaporation or condensation above the phase-change temperature is possible, the heat pipe offers inherent protection from freezing and overheating. This self-limiting temperature control is a unique feature of the evacuated heat pipe collector. These effects give ETC a higher hand compare to FPC and make it a more favourable choice in recent years. As presented in the earlier section, the new installation of ETC outpaced conventional FPC by far.

2.3 Nanofluid

Nanofluids, as a relatively new class of fluids, consist of a base fluid with nano-sized particles (1–100nm) suspended within them (Saidur, et al., 2011). It is first termed by Choi (1995) as a mixture of base fluid with a very small amount of

nanoparticles, dispersed uniformly and suspended stably, which can provide impressive improvements in the thermal properties of the base fluid. A length scale of nano-size objects is exemplified in figure 2.18.

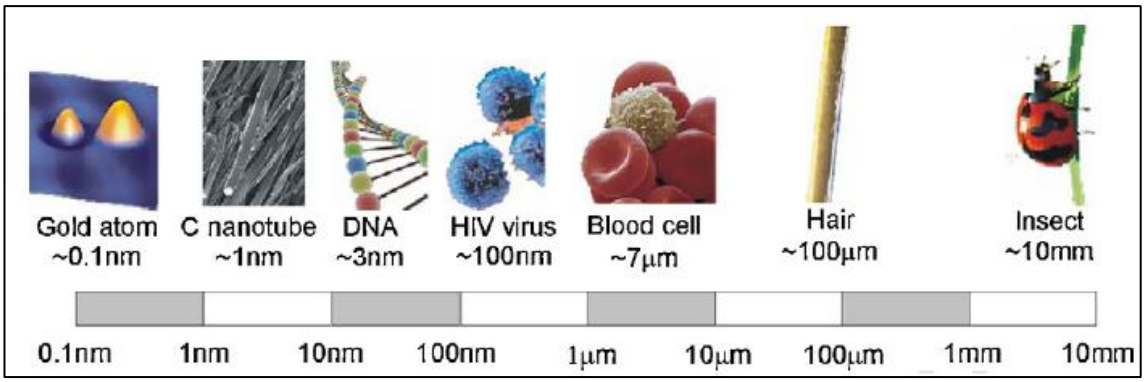

Figure 2.18 : Length scale and some examples related (Serrano, et al., 2009)

Most things on earth comply with the saying “Size does matter”; however, even nanoparticles are smaller than DNA, it provides a great leap forward in technology for scientists in creating material with desired properties. These nanometers-grain-sized materials have been found to have unique optical, electrical and chemical properties (Gleiter, 1989). It specifically implies not only the miniaturization but also the precise manipulation of atoms and molecules to design and control the properties of the nanomaterials/nanosystems. These properties are completely different than those possessed by the bulk materials, which helps in constructing custom-made devices with capabilities not found in bulk materials or in nature, or even to replicate some natural processes that have not been currently achieved through synthetic materials (Serrano, et al., 2009).

The idea of volumetric absorption using small particles has been proposed long before the ability to controllably synthesize nanoparticles was developed. In the 1970s,

large temperature differences at the interface between the absorber and the heat transfer fluid were identified, and particle-based volumetric absorbers for solar central-receivers were proposed by Hunt (1978) and Abdelrahman (1979). Attempts of using black liquids, for instance water soluble dyes, as the absorbing medium were brought up by Minardi and Chunag (1975). Tyagi et al. (2009) investigated the feasibility of using a non-concentrating direct absorption solar collector (DAC) and compares its performance with that of a typical flat-plate collector. He used a mixture of water and aluminium nanoparticles as the nanofluid and found that with the presence of nanoparticles, the absorption of incident radiation is increased by nine times over that of pure water. The efficiency of DAC using nanofluid as the working fluid is found to be up to 10% higher (on an absolute basis) than that of a flat-plate collector. This shows a promising improvement to conventional heat collector and further study and research are encouraged.

The technology of nanofluid has been implemented in parabolic trough solar collectors for years. However, without the mirrors used to reflect and concentrate solar radiant in the parabolic trough solar collectors, the fluid used for volumetric direct solar collectors is ought to possess excellent optical properties beside conventional requirement of good thermal transfer properties. Researches on thermal behavior of nanofluids have been done extensively over the pass decades and many correlations had been set-up and confirmed with experiments. However, the research on optical properties of nanofluid has shown slower progress. The numerous parameters such as physical and optical properties of base fluid and nanoparticles and the concentration of nanoparticles used have been some major investigation topics or obstacles for researchers to understand the solar absorption behavior of nanofluid.

2.3.1 Optical Properties of Nanofluid

In order to properly design a nanofluid-based solar collector it is important to develop a basic understanding of the radiative properties of nanofluids. Nanofluid consists of two main components which are the nanoparticles and the base fluid. Nanoparticles are added into water or refrigerant to improve and alter the optical properties of the fluid to become more solar favourable. In the base fluid point of view, a study of solar-weighted absorption coefficient for fluid's baseline capacity for absorbing solar energy by Otanicar, et al. (2009) suggested that water is the best absorber among the four tested liquids namely water, ethylene glycol, propylene glycol and therminol VP-1. However, it is still a weak absorber, only absorbing 13% of the energy.

On the other hand, the addition of small particles causes scattering of the incident radiation allowing higher levels of absorption within the fluid, and hence an enhancement in collector efficiency (Tyagi, 2008). The optical properties of the effective fluid are highly dependent on the shape and size of the particle, and the optical properties of the base fluid and particles themselves (Khlebtsov et al., 2005). The radiation absorption characteristics of a Ni nanoparticle suspension were investigated by spectroscopic transmission measurement by Kameya and Hanamura (2011). It was demonstrated that the absorption coefficient of the nanoparticle suspension is much higher than that of the base liquid for visible to near-infrared wavelengths. Radiation characteristics predicted by the Mie theory showed good agreement with the increase of absorption coefficient in wavelengths where the base liquid is transparent. Recently, carbon nanohorns (CNHs), as the latest to be discovered in the family of carbon-based nanostructured materials (Iijima, 1999), with large surface area and large number of cavities (Fan, 2007), were used as nanoparticles to improve optical properties of direct solar absorbers. The studies showed promising improvement of absorption and

scattering properties for carbon nanohorns-based nanofluid with compare to water and glycol as base fluid (Sani, et al., 2010; Mercatelli, et al., 2011).

The temperature difference between the absorbing particles and the fluid has been shown to be negligible owing to the particles' large surface to volume ratio (Minardi and Chunag, 1975; Miller, F. J., and Koenigsdorff, R. W., 2000). The temperature dependence of the optical/spectroscopic properties of metallic nanoparticles (in particular nanoshells) including absorption, scattering, and enhanced-Raman scattering for admolecules is studied via theoretical modelling by Chen et al. (2008). It is suggested that these properties in general have optimal values at a certain temperature specific to the shell configuration except for relatively thin shells.

The optical absorption of nanofluid also depends on the concentration or volume/weight fraction of nanoparticles added to the base fluid. Both researches published by Mishra et al. on year 2008 and 2009 showed a shift of absorption spectra towards longer wavelength in nanofluid with higher concentration. Carbon nanotubes, graphite, and silver were used as nanoparticles and by utilizing nanofluids as the absorption mechanism in solar thermal collectors; it was demonstrated efficiency improvements of up to 5% (Otanicar, et al., 2010). In addition, their experimental data were compared with a numerical model of a solar collector with direct absorption nanofluids. The experimental and numerical results demonstrated an initial rapid increase in efficiency with volume fraction, followed by a leveling off in efficiency as volume fraction continues to increase.

Further to optical properties, the addition of nanoparticles to a base fluid has been shown to improve thermal conductivity. Studies suggested that the thermal conductivity is enhanced due to dispersion of nanoparticles (Pak and Cho, 1998; Xuan and Li, 2000), intensification of turbulence (Xuan and Li, 2000), Brownian motion

(Keblinski et al., 2002; Koo and Kleinstreuer, 2005), thermophoresis and diffusiophoresis (Buongiorno, 2006). The application of nanofluids as a working medium for solar collectors is a relatively new concept. Further study on the physical properties in help of enhancing direct solar collectors has to be carried out.

In this thesis, the optical properties of nanofluid are studied and the transmissivity of base fluid and nanofluid is compared. From section 2.1, we can determine that the nanoparticles proposed for this study should be of size lesser than 10% of the incident wavelength as Rayleigh scattering will not be valid anymore if the size of nanoparticles exceeded this size. This limits the size of nanoparticles to be around 20 nm. Adding to the above, since ETC provides good solar to thermal energy conversion efficiency, the use of nanofluid in replacing the working fluid in the heat pipes may be considered. However, as the fundamental working principle of a heat pipe is by natural convection and no mechanical force is added, the volume fraction of nanoparticles in the nanofluid should not be too much. This is to avoid clogging of working fluid in heat pipes and eventually reduce their effectiveness.

Chapter 3: Methodology

3.0 Introduction

This chapter is divided into two components. The first component or section describes the working principle and some equations to calculate the incident solar intensity and transmissivity of Direct Absorption Collector (DAC).The second section in this chapter will explain and demonstrate the governing equations used for nanofluid to develop its optical properties.

3.1 Direct Absorption Collector (DAC)

Solar water heating technologies are becoming widespread and contribute significantly to hot water production in several countries. China, Germany, Turkey, India, and Australia led the market for newly installed capacity during 2009, with China, Turkey, Germany, Japan, and Greece taking the top spots for total installations by the end of that year (REN 21, 2011). Although with such popularity, these types of solar collectors exhibit several shortcomings, such as limitations on incident flux density, relatively high losses, and corrosion effect. In order to overcome these drawbacks, the idea of using volumetric direct solar collectors is raised.

Direct Absorption Solar Collector (DAC) has a few advantages compare to conventional surface absorption collector. Besides larger solar absorption area and actual installation surface area ratio due to the contribution of nanoparticle surface area, DAC can avoid surface heat losses due to excessive temperature on surface absorption collector. For a black body receiver, the radiative losses scale as the fourth power of the temperature, as seen in figure 3.1. For surface solar absorber, the efficiency sharply drops with increasing temperature. To suppress radiative heat loss from the receiver,

selective surfaces are manufactured to have low emissivity at the longer wavelengths which correspond to thermal radiation. However, the performance of a receiver at high temperatures is limited by the Kirchoff's Law, which states that the spectral absorptivity must equal the spectral emissivity. In other words, since an absorber is absorptive for wavelength in the solar spectrum, it consequently emits in those same wavelengths which leads to a lower absorber efficiency. Figure 3.1 illustrates how the power losses from an ideal selective surface exhibit the same forth order dependence on the absorber temperature as a black body except the trend is shifted to higher temperature (Lenert, 2010).

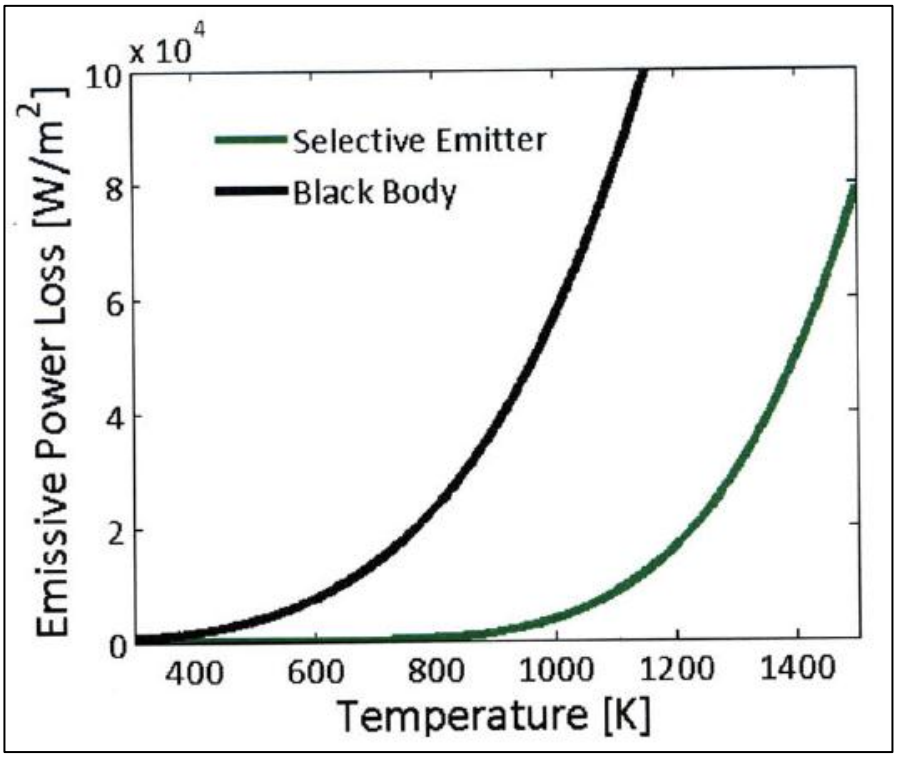

Figure 3.1 : Power loss due to re-radiation as a function of temperature: from a black body (black), and a selective surface (green) (Lenert, 2010).

The convection losses to the ambient air also become significant as the temperature difference between the absorber surface and ambient air become larger. This is a simple demonstration of heat transfer by convection with equation of :

$$q = h_c \Delta T$$

By using nanofluid as volumetric absorber, the drawbacks of surface emission and convection heat loss can be eliminated. A schematic of the difference of surface absorber versus volumetric receiver utilizing nanofluid to absorb solar radiation is illustrated in Figure 3.2.

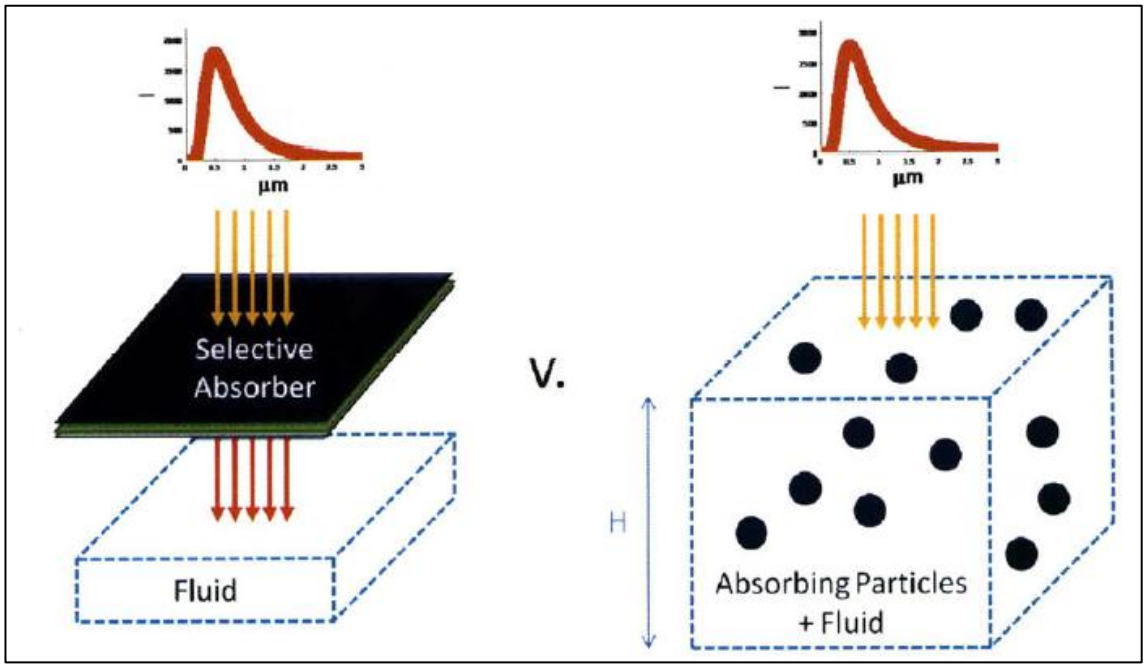

Figure 3.2 : Difference between surface-based and volumetric solar absorbers (Lenert, 2010).

The schematic of the nanofluid-based Direct Absorption Solar Collector (DAC) is shown in Figure 3.3. The fluid is contained within the enclosed space of the DAC. The bottom wall is considered to be adiabatic, i.e. no heat flux is allowed to pass through it, except for transmitted radiation. This assumption is based on the case when the bottom surface is highly insulating and transparent. The fluid is enclosed at the top

by a glass surface which allows most of the incident solar flux to pass through. This top surface is assumed to be exposed to the ambient atmosphere and thus loses heat by convection. In order to model the heat transfer characteristics of this surface it is assumed that it loses heat to the ambient through convection. The incident radiation is considered to be the incoming solar radiation. For the study of the principal behavior of the nanofluid-based DAC, atmospheric absorption was neglected in these calculations. Hence, the incident solar intensity is calculated using the blackbody relation given by Eq. (3.1), where the value of $\mathbf{T_{solar}}$ is taken as 5800 K (Tyagi, 2008; Tyagi, Phelan & Prasher, 2009).

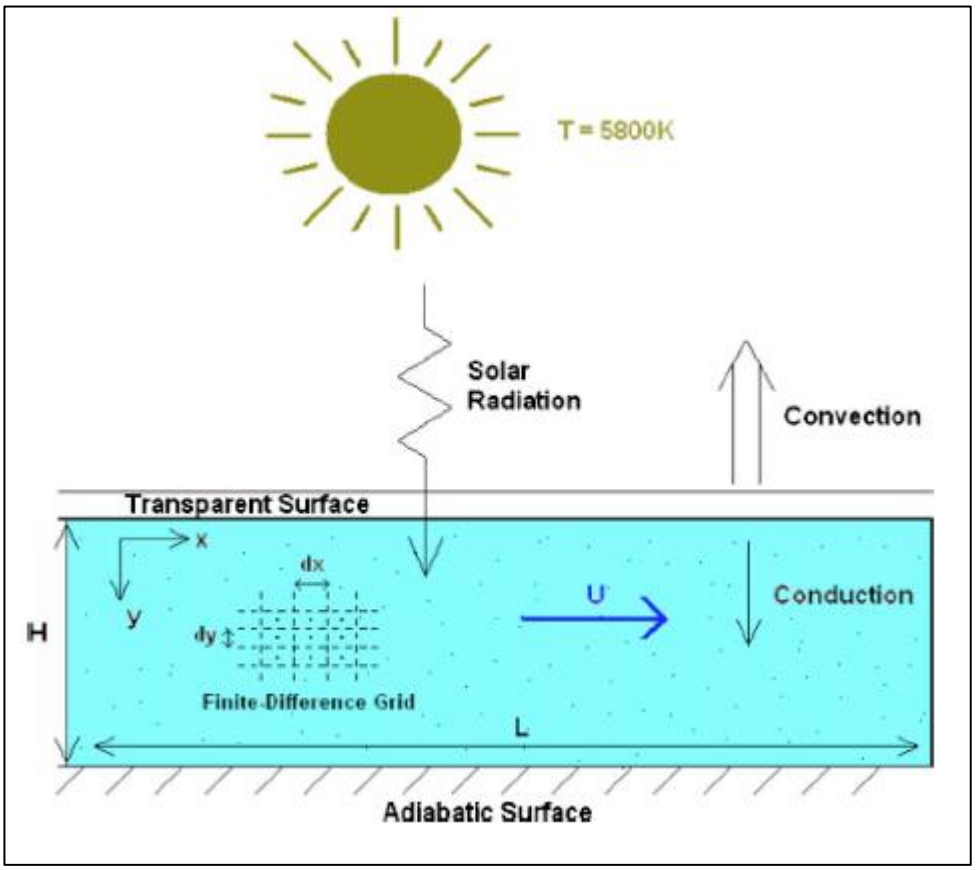

Figure 3.3 : Schematic of the nanofluid-based direct absorption solar collector (DAC)

$$I_{b\lambda}(\lambda, T_{solar}) = \frac{2hc_o^2}{\lambda^5\left[exp\left(\frac{hc_o}{\lambda k_B T_{solar}}\right)-1\right]} \quad (3.1)$$

In this equation:

h is the Plank's constant, equaled to 6.62606957 x 10^{-34} J.s or 4.135667516 x 10^{-15} eV.s (Mohr, et al., 2011),

$\mathbf{k_B}$ is the Boltzmann constant, equaled to 1.3 8 x 10^{-23} J/K (Tyagi, 2008),

$\mathbf{c_o}$ is the speed of light in vacuum, equaled to 2.9979 x 10^8 m/s and

λ is wavelength

Using this relation the spectral intensity incident upon the solar collector was evaluated. The radiation intensity within the fluid was assumed to vary only in one dimension (along the y - direction). Equation (3.2) is the radiative transport equation which was used in this model. The right side of the equation determines the attenuation in the intensity as the radiation travels through the fluid. Equation 3.2 is integrated and expressed as Equation 3.2a.

$$\frac{\delta I_\lambda}{\delta y} = -(K_{a\lambda} + K_{s\lambda})I_\lambda = -K_{e\lambda}I_\lambda \quad (3.2)$$

$$I = I_\lambda e^{-K_{e\lambda}y} \quad (3.2a)$$

$$\frac{I}{I_\lambda} = e^{-K_{e\lambda}y} = T \quad (3.2b)$$

where $\mathbf{K_{a\lambda}}$ is the spectral absorption coefficient, and $\mathbf{K_{s\lambda}}$ the spectral scattering coefficient. Taken together they can also be represented as $\mathbf{K_{e\lambda}}$, the spectral extinction coefficient where **I**, denotes the transmitted light intensity. Equation 3.2a confirmed that the intensity of light transmitted is inverse to the length of light path, **y** and is further rearrange to become equation 3.2b to obtain Transmissivity, **T**. This agrees with the Beer-Lambert Law. Since the temperatures in the solar collector are not expected to be very high, the emission term has not been included in Eq. (3.2). Also, in order to keep the model simple the effect of in-scattering has not been considered.

3.2 Radiative Properties of Nanofluid

The study of optical properties of nanofluid shows the need to study optical properties of the based fluid and nanoparticles separately. The brief theory and relation of light scattering and extinction for base fluid and nanoparticles are presented below.

3.2.1 Radiative Properties of Base Fluid

In order to fully understand the effects of suspending nanoparticles within a base fluid, the complete optical properties of the base fluid are needed. The bulk of the volumetric receiver is the fluid medium; therefore, the radiative properties of the fluid are critical to the efficiency of a volumetric design. An ideal fluid for a volumetric application would be completely transparent to the incoming solar radiation (Lenert, 2010). Base fluid normally used in direct solar collectors like water heater has to be non-toxic.

A study of solar-weighted absorption coefficient for fluid's baseline capacity for absorbing solar energy by Otanicar, et al. (2009) suggested that water is the best

absorber among the four tested liquids namely water, ethylene glycol, propylene glycol and therminol VP-1. However, it is still a weak absorber, only absorbing 13% of the energy. Another later study by Mercatelli et al. (2011) on absorption and scattering properties of carbon nanohorn-based nanofluids for DAC using glycol and water as base fluid also showed a more advantageous improvement from water-based nanofluid. Figure 3.4 below is extracted from Mercatelli et al.'s study to show the transmittance spectra of water and glycol-based nanofluids with the same Single Wall Carbon Nanohorn (SWCNH) concentrations. However, preliminary thermal stability tests performed showed that water-based suspensions are stable up to 120 ℃, while glycol-based suspensions are stable up to 150 ℃. An improvement of the thermal stability properties of the nanofluid should be expected by an optimization of SWCNH-surfactant concentration ratio. Despite the more superior performance of glycol-based nanofluid at high temperature, water is chosen to be the base fluid to study here as DAC is targeted to be used mainly in residential development and working temperature is estimated to be low.

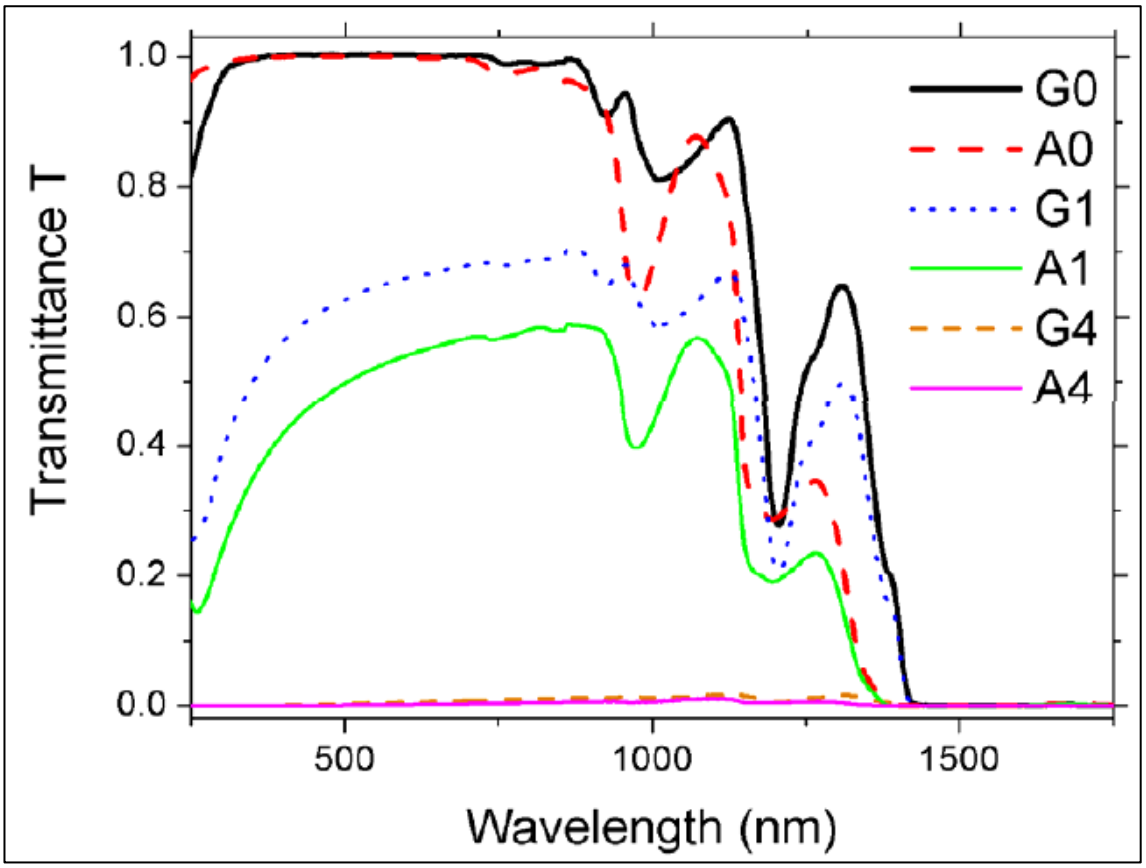

Figure 3.4 : Transmittance spectra of water and glycol-based nanofluids with the same SWCNH concentrations (0.005 g/L for G1 and A1 and 0.05 g/L for G4 and A4). Spectra of the pure base fluids are shown for comparison (G0 and A0) (Mercatelli, 2011).

For pure fluids, scattering can be neglected and only the attenuation caused by absorption may be considered. For that case, the spectral absorption coefficient can be calculated using Eq. (3.3),

$$K_{a\lambda} = \frac{4\pi k}{\lambda} \tag{3.3}$$

where $\boldsymbol{k}$ is the index of absorption and $\boldsymbol{\lambda}$ is the wavelength of incident light.

The definitive data on the absorption spectrum of pure water from 200 nm to 3500 nm had been obtained by Irvine and Pollack (1968, cited in Brewster, 1992).

These data is shown in Table A1 in Appendix 1. Figure 3.5 below demonstrates the absorption spectrum of pure water (Chaplin, 2011). From Figure 3.5, it can be seen that water has low absorption coefficient at shorter wavelength and increase over the visible light spectrum until near infrared region.

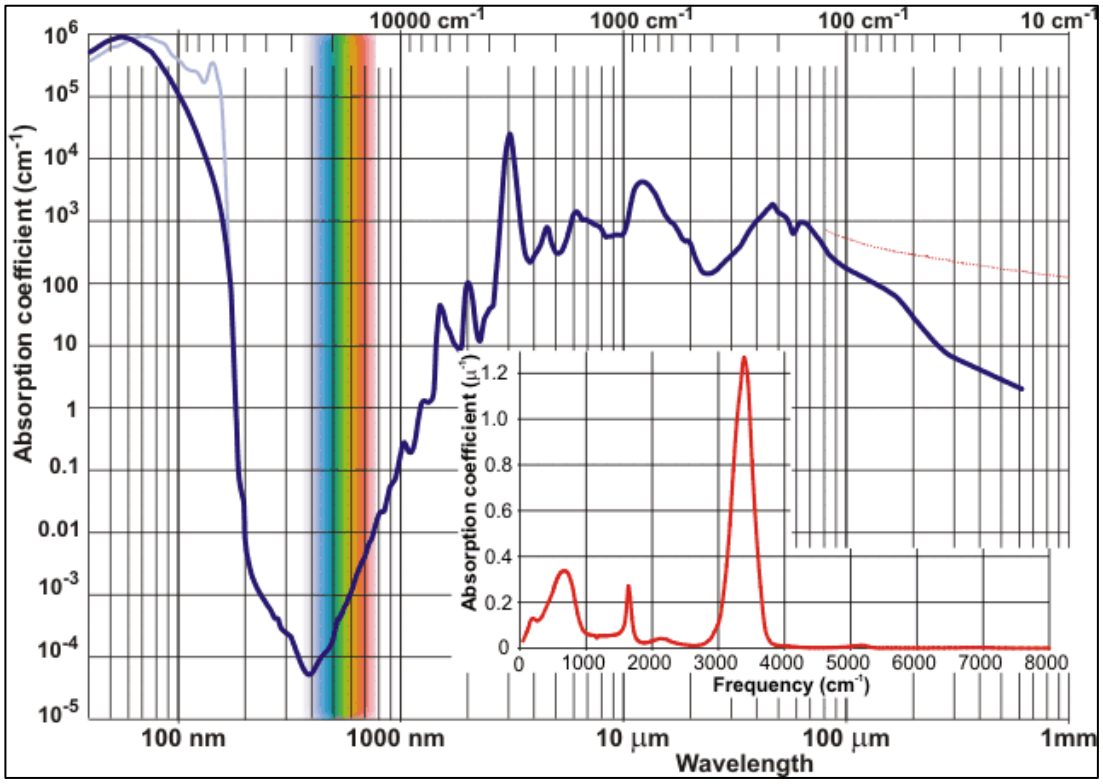

Figure 3.5 : Absorption Coefficient for water (Chaplin, 2011).

Figures 3.6 and 3.7 give further illustration to the absorption coefficient of pure water with refractive index and extinction/absorption index plotted versus wavelength (Otanicar et al., 2009). The graphs compare the data from previous work (Brewster, 1992 cited in Otanicar et al., 2009, p.972) and numerical calculations by the authors. The refractive index of pure water contributes almost constant values throughout the studied wavelength while the extinctive/absorptive index gives the major raise and is reflected in the absorption coefficient as shown in Figure 3.7.

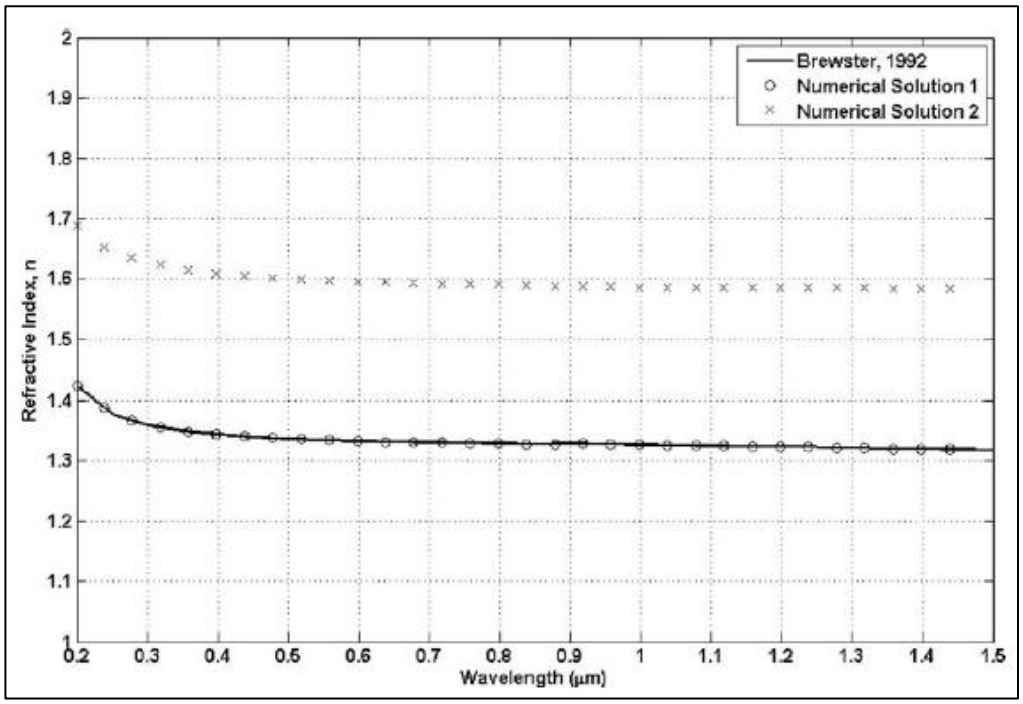

Figure 3.6 : Calculated and published values of Refractive Index, n of water (Otanicar et al., 2009)

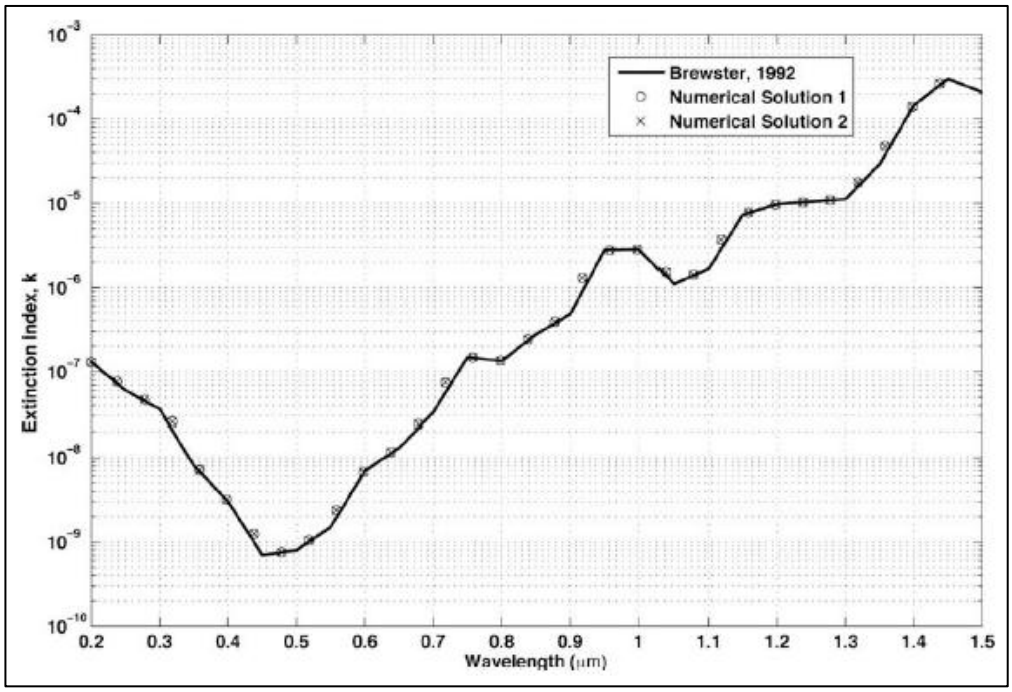

Figure 3.7 : Calculated and published values of Extinction Index, k of water (Otanicar et al., 2009)

Since the optical properties had long been study and data is verified by many researchers (Brewster, 1992; Kou, Labrie and Chylek, 1996; IAPWS, 1997; Pope and Fry, 1997; Otanicar et al., 2009; Chaplin, 2011), the spectrum of absorption coefficient used for calculation in this study will be based on the published data from previous work. The data used is by Brewster (1992) and Table A1 is referred.

3.2.2 Radiative Properties of Nanoparticles

When it comes to studying of optical properties of nanoparticles, there are a few assumptions to be made in order to simplify the complexity of equations involved.

Firstly, it is assumed that the nanoparticles are experiencing independent scattering. The inhomogeneous of nanoparticles in base fluid can see to be "alien" bodies immerse in a medium. It can be seen as dust or haze in the atmosphere or sand or mud in clear river water. However, if such particles are sufficiently far from each other, it is possible to study the scattering by one particle without reference to the other ones. This is called "independent scattering" (van de Hulst, 1981). But one may ask, what distance between the particles is sufficiently large to ensure independent scattering? Early estimates have shown that a mutual distance of 3 times the radius is a sufficient condition for independence (van de Hulst, 1981). In this study, the nanoparticles are provided in a very small size and the volume fraction is only a small portion of the base fluid. Thus, the scattering effect of nanoparticles in nanofluid can be considered to be independent.

Further to this, the scattering effect studied here is assumed to be of single scattering. Practical experiments most often employ a multitude of similar particles in a cloud or a solution, namely nanofluid. The obvious relations for a nanofluid containing

X scattering particles are that the intensity scattered by the fluid is X times that scattered by a single particle, and the energy removed from the original beam is also X times that removed by a single particle. This simple proportionality to the number of particles holds only if the radiation to which each particle is exposed is essentially the light of the original beam. In actuality, each particle is also exposed to light scattered by the other particles, whereas the light of the original beam may have suffered extinction by the other particles. If these effects are strong, we speak of multiple scattering and a simple proportionality does not exist. This situation may be illustrated by a white cloud in the sky. Such a cloud is like a dense fog; its droplets may be considered as independent scatter. Yet the total intensity scattered by the cloud is not proportional to the number of droplets contained in it, for not each droplet is illuminated by full sunlight. Drops within the cloud may receive no direct sunlight at all but only diffuse light which has been scattered by two or more droplets successively (van de Hulst, 1981). This multiple scattering effect is neglected in this study to abridge the calculations and relationships of light extinction.

In this study of nanofluids, where the presence of small particles influences the nature of absorption as well as scattering, Rayleigh scattering (Bohren & Huffman, 1983) can be applied. The particles are assumed to be spherical and the medium to be non-absorbing. This is merely for simplification of studying Rayleigh scattering effect while the effect of absorption of the base fluid, water, will be added into the main calculation later on.

In Rayleigh scattering $\alpha < 1$ and $|m|\ \alpha < 1$, where $\boldsymbol{\alpha}$ is defined as the size parameter and **m** is the normalized refractive index of the particles to the fluid. They are given by (Prasher, 2007; Tyagi, 2008; Tyagi, Phelan and Prasher, 2009; Otanicar et al., 2010):

$$\alpha = \frac{\pi D}{\lambda} \tag{3.4}$$

$$m = \frac{m_{particles}}{n_{fluid}} \tag{3.5}$$

$$m_{particles} = n + ik \tag{3.6}$$

where **D** is the diameter of the particles

λ is the wavelength of the incident solar radiant

$m_{particles}$ is the complex refractive index of the nanoparticles

n as the real part of the complex number, denote the refractive index of nanoparticles

k as the imaginary part of the complex number, denote the index of absorption of nanoparticles.

In physical terms, Rayleigh scattering can be understood as the regime in which the particle size is much smaller than the wavelength of the incident radiation. In general, the extinction coefficient can be given as:

$$K_{e\lambda} = \frac{3 f_v Q_{e\lambda}(\alpha, m)}{D} \tag{3.7}$$

where **f_v** is the particle volume fraction

$\mathbf{Q_{e\lambda}}$ is the extinction efficiency

The extinction efficiency in the Rayleigh regime is given by the following relation (Tyagi, 2008; Lenert, 2010):

$$Q_{e\lambda} = 4\alpha \ \mathrm{Im}\left\{\frac{m^2-1}{m^2+2}\left[1+\frac{\alpha^2}{15}\left(\frac{m^2-1}{m^2+2}\right)\frac{m^4+27m^2+38}{2m^2+3}\right]\right\} + \frac{8}{3}\alpha^4 \ Re\left|\left(\frac{m^2-1}{m^2+2}\right)\right|^2 \tag{3.8}$$

where the extinction efficiency, $\mathbf{Q_{e\lambda}}$, term shown above contains two terms, which are the absorption efficiency, $\mathbf{Q_{a\lambda}}$ and scattering efficiency $\mathbf{Q_{s\lambda}}$**,** are shown below:

$$Q_{a\lambda} = 4\alpha \ \mathrm{Im}\left\{\frac{m^2-1}{m^2+2}\left[1+\frac{\alpha^2}{15}\left(\frac{m^2-1}{m^2+2}\right)\frac{m^4+27m^2+38}{2m^2+3}\right]\right\} \tag{3.8a}$$

$$Q_{s\lambda} = \frac{8}{3}\alpha^4 \ Re\left|\left(\frac{m^2-1}{m^2+2}\right)\right|^2 \tag{3.8b}$$

By examining Eq. 3.8b, it is evident that the scattering efficiency, $\mathbf{Q_{s\lambda}}$ varies as the fourth power of particle size. In addition, it is found that absorption efficiency, $\mathbf{Q_{a\lambda}}$ predominantly varies almost linearly with particle size. This is true even though there is a $\boldsymbol{\alpha^2}$ term inside the imaginary term of Eq. 3.8a because $\boldsymbol{\alpha}$ is smaller than 1. Further, by substituting Eqs. 3.4 and 3.8 into Eq. 3.7, the following expression for $\mathbf{K_{e\lambda}}$ is obtained:

$$K_{e\lambda} = \frac{12\pi f_v}{\lambda}\ \mathrm{Im}\left\{\frac{m^2-1}{m^2+2}\left[1+\frac{\pi^2 D^2}{15\lambda^2}\left(\frac{m^2-1}{m^2+2}\right)\frac{m^4+27m^2+38}{2m^2+3}\right]\right\}$$

$$+\frac{8\pi^4 D^3 f_v}{\lambda^4}\ Re\left|\left(\frac{m^2-1}{m^2+2}\right)\right|^2$$

(3.9)

where the extinction coefficient, $\mathbf{K_{e\lambda}}$ term shown above contains two terms, which are the absorption coefficient $\mathbf{K_{a\lambda}}$ and scattering coefficient, $\mathbf{K_{s\lambda}}$. They are shown below.

$$K_{a\lambda} = \frac{12\pi f_v}{\lambda}\ \mathrm{Im}\left\{\frac{m^2-1}{m^2+2}\left[1+\frac{\pi^2 D^2}{15\lambda^2}\left(\frac{m^2-1}{m^2+2}\right)\frac{m^4+27m^2+38}{2m^2+3}\right]\right\} \quad (3.9a)$$

$$K_{s\lambda} = \frac{8\pi^4 D^3 f_v}{\lambda^4}\ Re\left|\left(\frac{m^2-1}{m^2+2}\right)\right|^2 \quad (3.9b)$$

Lenert (2010) suggested that the two complex expressions in Eq. 3.8 can be greatly simplified if the terms with a higher order of the size parameter, **α**, are neglected because this parameter is small in the case of nanoparticles. It was assumed that the amount of incident radiation absorbed by the nanoparticle is dominated over the amount of scattering by the particle. Since scattering is neglected, the attenuated light is assumed to be absorbed; thus the extinction coefficient is merely just absorption coefficient (Lenert, 2010). Equation 3.9 is greatly simplified to become as below:

$$K_{e\lambda} = \frac{6\pi f_v}{\lambda}\ \mathrm{Im}\left\{\frac{m^2-1}{m^2+2}\right\} \quad (3.10)$$

However, according to Tyagi (2008, 2009), the $\boldsymbol{\alpha^2}$ term does have a small influence in his studies and is illustrated in Figure 3.8 below. It was found that, with all other parameters such as particle volume fraction, collector height, and collector length being constant, the collector efficiency increased slightly with an increase in the particle size. Equation 3.9b shows that scattering coefficient, $\mathbf{K_{s\lambda}}$ varies as the third power of particle size. Since the particle size is extremely small in the present calculations, this term becomes negligible. However it can be seen that the expression for $\mathbf{K_{a\lambda}}$ has a fixed part and another part which varies as D^2. It was verified in Tyagi (2008, 2009) studies that the slightly increasing behavior of the curve seen in Figure 3.8 is due to the D^2 term.

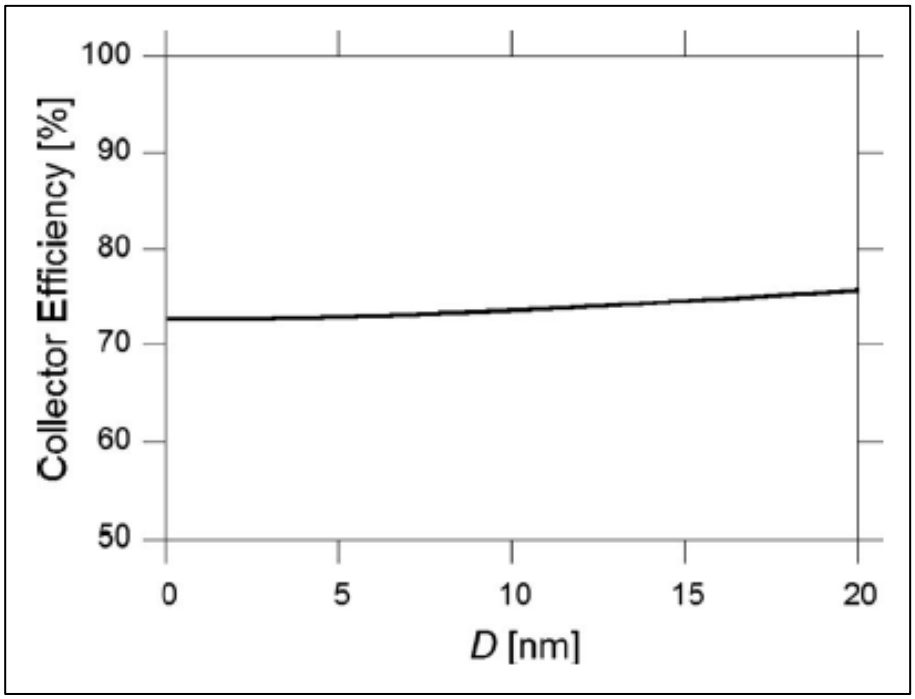

Figure 3.8 : Collector efficiency as a function of the particle size, D (f_v = 0.8%)

Taking into consideration with the effect of particle size towards the accuracy in determining the improvement of efficiency for collector, the calculation will be carried out with refer to Eq. 3.9.

Finally, by using Eqs. 3.5 and 3.8, the radiative properties of the nanofluid were evaluated. The net extinction caused by the nanofluid was obtained by adding the individual contributions from the nanoparticles as well as the base fluid. The intensity distribution within the solar collector was obtained using:

$$\frac{\delta I_\lambda}{\delta y} = -K_{e\lambda,nanofluid} I_\lambda = -\left(K_{\alpha\lambda,water} + K_{e\lambda,nanoparticles}\right) I_\lambda \tag{3.11}$$

where, $\mathbf{K_{a\lambda,water}}$ and $\mathbf{K_{e\lambda,nanoparticles}}$ are obtained from Eqs. 3.3 and 3.9 respectively.

When the volume fraction of nanoparticles is low the contributions of nanoparticles and base fluid could be added together as shown in Equation 3.11. This is because the present model assumes independent scattering, where the scattered radiations do not depend on one another and hence the intensities can be added. The equations above mentioned are used to learn the effect of nanofluid in direct solar collector.

Chapter 4: Results and Discussions

4.0 Introduction

With the aid of the equations set up and developed by researchers, the extinction coefficient of nanofluid with water as base fluid and aluminium as nanoparticles are studied.

Aluminium is chosen to be the nanoparticles for this study as it is one of the common and vastly available metals. Besides, the thermal properties of aluminium enhanced nanofluid have been studied extensively over the pass decades and had shown promising improvement to the thermal properties. The optical properties of aluminium are obtained from work by preceding researchers (Smith, Shiles and Inokuti, 1985) and are displayed with normalized value of Refractive index, **n'**, and Absorption index, **k'** calculated using equation 3.5 in Table A2 in Appendix 1.

The effects of nanoparticles in enhancing the optical properties of base fluid are explored with nanoparticle sizes and volume fraction as parameters. As mentioned in the previous chapter, nanoparticles proposed for this study should be of size lesser than 10% of the incident wavelength as Rayleigh scattering will not be valid anymore if the size of nanoparticles exceeded this size. This will limit the size of nanoparticles to 20 nm as incident solar intensity has most concentration starts from about 200 nm. The volume fraction of nanoparticles in the nanofluid is also to be a smaller percentage to allow possibility of applying the results to ETC and to avoid shifting of the maximum absorption coefficient of nanofluid to the longer wavelength which has lesser concentration. The maximum volume fraction, $\mathbf{f_v}$, is set to be 8% in this review.

4.1 Transmissivity of Base Fluid (Pure Water)

The Transmissivity, **T**, of the base fluid is first calculated to explore the effectiveness of light absorption for pure water. By using Equations 3.2b and 3.3, the transmissivity of pure water is tabulated in Table A3 and illustrated below.

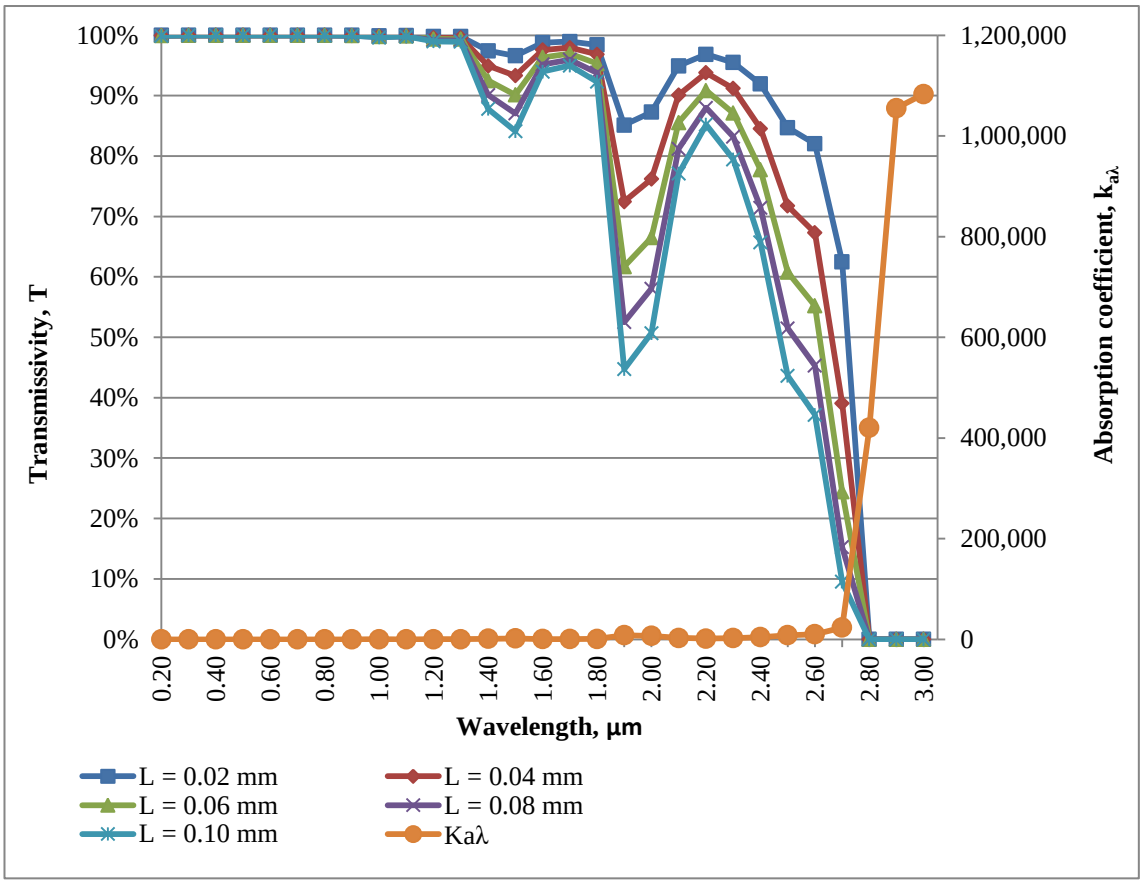

Figure 4.1 : Transmissivity and Absorption Coefficient, $k_{a\lambda}$ of Base Fluid (Pure Water) at Various Light Path Length

From Figure 4.1, pure water is almost transparent at the visible light region and does not absorb any of the light transmitted to it. The absorption of light only becomes noticeable when light wave goes into the near infrared region and reaches its maximum at 1.9 µm. After 1.9 µm, pure water again become non effective in absorbing light until the light wavelength exceeds 2.60 µm when then the absorption coefficient increase

sharply and transmissivity dropped abruptly. In general, pure water is not an effective light absorber especially in the visible light region.

4.2 Optical Properties of Nanoparticles

The study on the effect in enhancing optical properties of nanofluid by aluminium nanoparticles starts with choosing the suitable nanoparticle size. As mentioned earlier, the particle size is limited to below 20 nm. The absorption coefficient, $\mathbf{k_{a\lambda}}$, scattering coefficient, $\mathbf{k_{s\lambda}}$ and extinction coefficients, $\mathbf{k_{e\lambda}}$ of aluminium nanoparticle of few sizes namely 1 nm, 5 nm, 10 nm, 15 nm and 20 nm are calculated with Equations 3.9a, 3.9b and 3.9 with the volume fraction set to be 2%. The results are tabulated in Table A4, A5 and A6 and graphs are established to show the trend and pattern of increasing nanoparticle sizes.

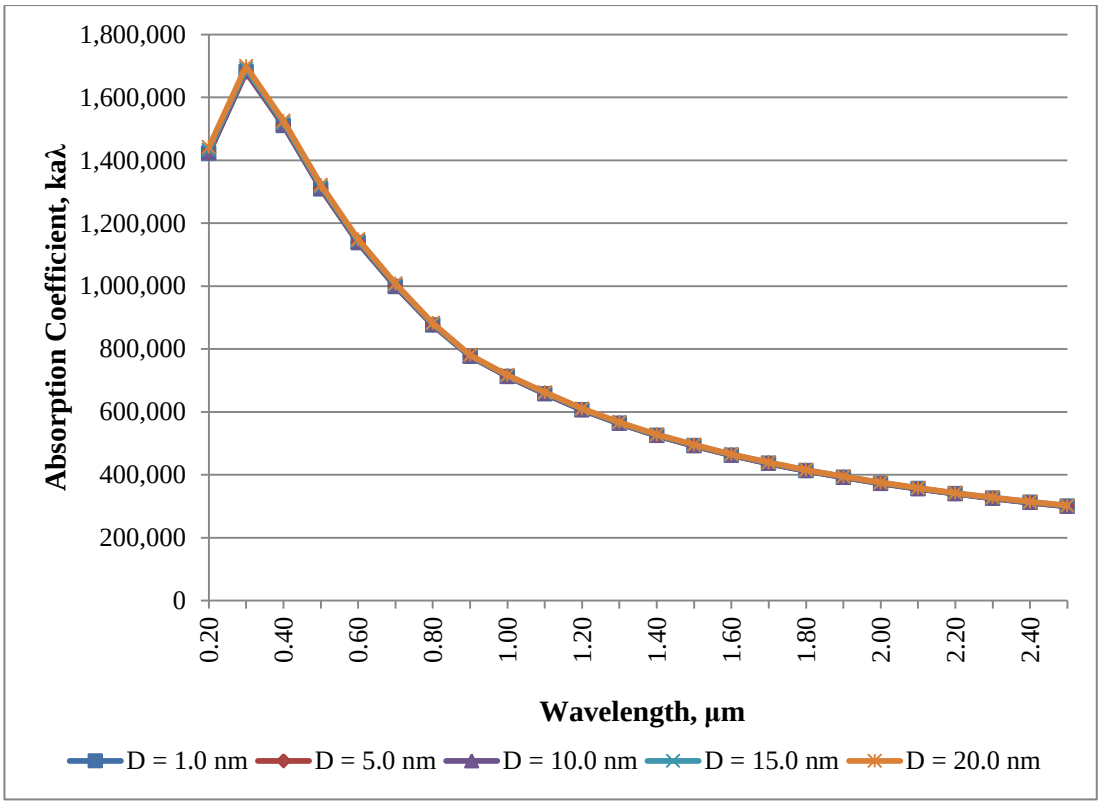

Figure 4.2 : The Effect of Nanoparticle Sizes towards Absorption Coefficient, $k_{a\lambda}$

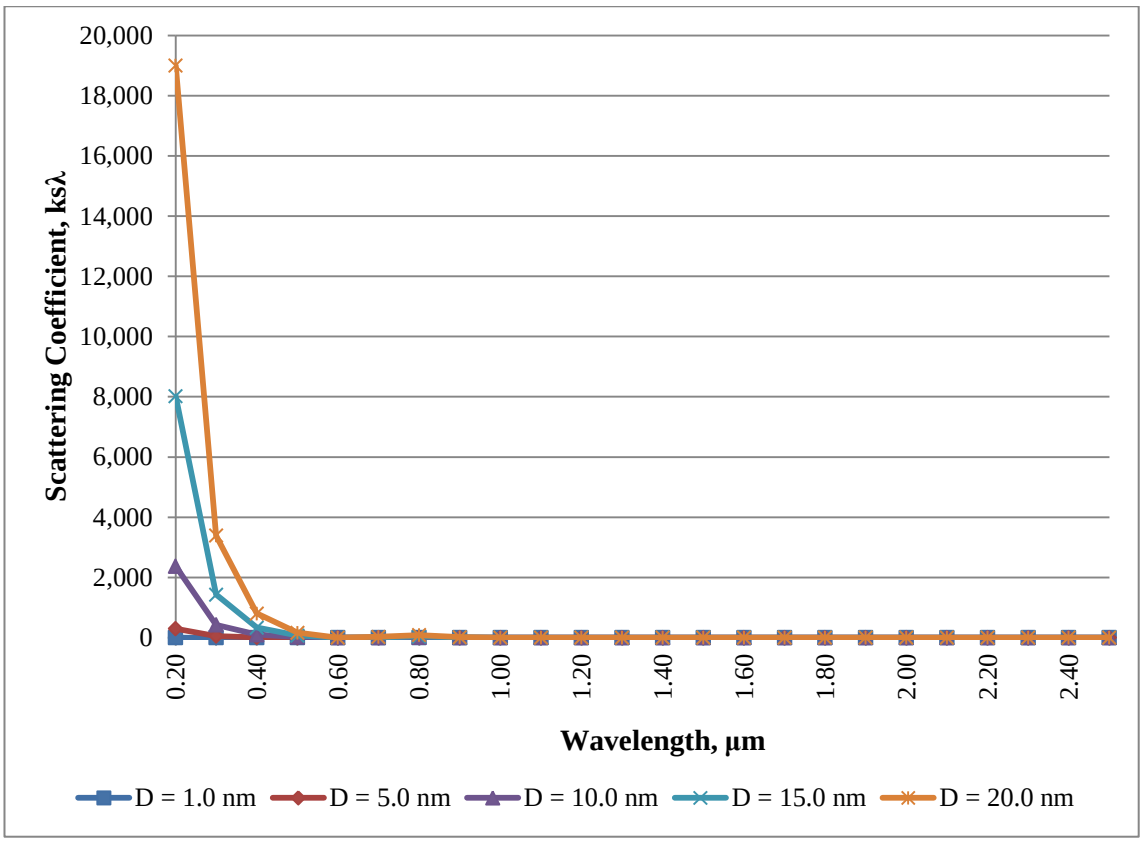

Figure 4.3 : The Effect of Nanoparticle Sizes towards Scattering Coefficient, $k_{s\lambda}$

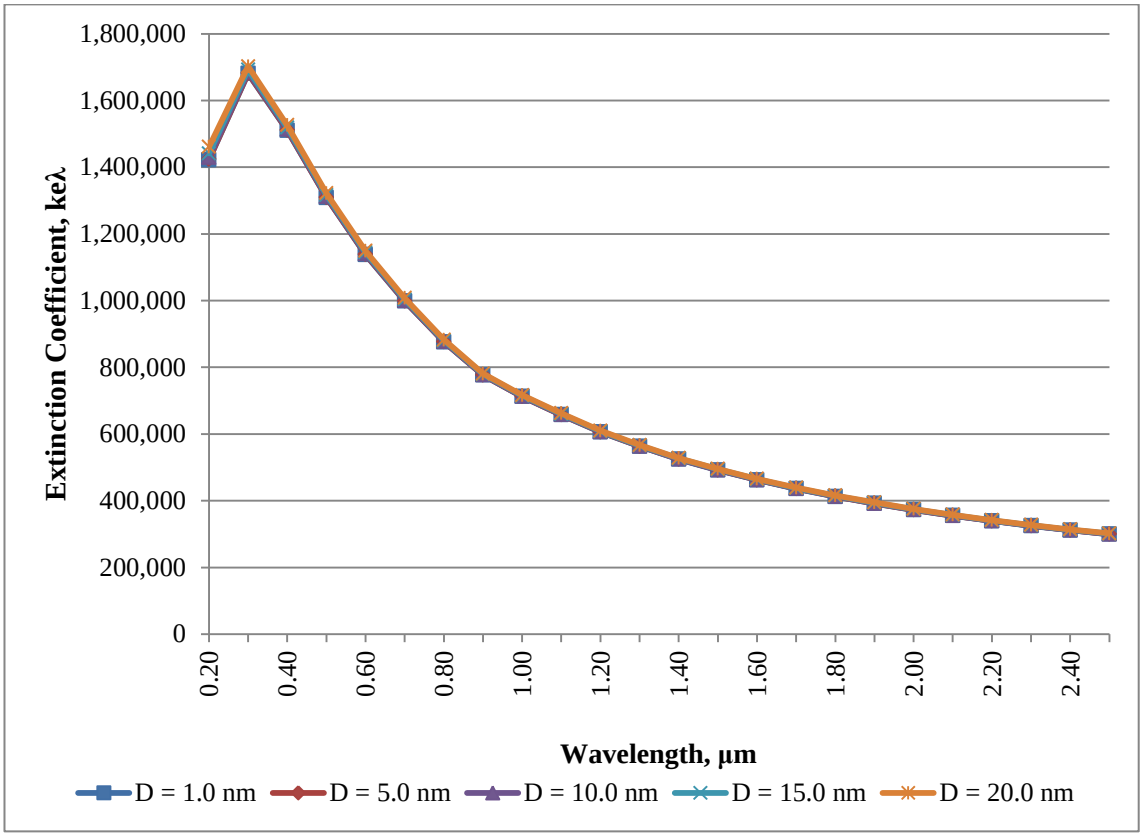

Figure 4.4 : The Effect of Nanoparticle Sizes towards Extinction Coefficient, $k_{e\lambda}$

Figure 4.2, 4.3 and 4.4 demonstrates the absorption coefficient, scattering coefficient and extinction coefficient of aluminium nanoparticles versus light wavelength with particle size as the parameter.

From Figure 4.2, it should be noted that there are five lines in the graph although the lines overlapped each other and only two very close lines (blue line and brown line which denote particle size of 1 nm and 20 nm respectively) are shown. The differences of absorption coefficient between particle sizes are tabulated in Table A4 in Appendix 1 and only very small differences are spotted at wavelength shorter than 0.6 μm. The differences are within 1.5% between the smallest and largest particle size calculated. The data shows identical absorption coefficient for the different sizes after 0.6 μm. This can be explained from equation 3.9a. The particle size in nanometer becomes very insignificant to the overall equation after being squared and also divided by the wavelength term in micrometer. The further increase in wavelength will overshadow the effect of particle size and eventually leads to near-constant absorption coefficient.

Figure 4.3 illustrated a similar trend as the absorption coefficient graph. The effect of different particle size become almost unnoticeable after wavelength is longer than 0.6 μm. This can be explained also by looking at the governing equation. The particle size is in power of three while wavelength is in power of four. In near UV region, where wavelength is shorter, the effect of having larger particles is still obvious. As wavelength becomes longer and the scattering coefficient is inversely proportional to the wavelength with power of four, the effect is minimized. Detail data is presented in Table A5 in Appendix 1.

Figure 4.4 is almost similar to figure 4.2. As described in Equation 2.4 and 3.9, the extinction coefficient is the sum of scattering coefficient and absorption

coefficient. The much smaller Scattering coefficient demonstrates no noteworthy influence to the overall extinction coefficient calculation. In short, particles used in nanofluid are extremely small and the terms D^2 and D^3 have very little impact to the Extinction coefficient equation. This is in common to the study by Lenert (2010) who suggested that the size of nanoparticle is not a deciding factor to the optical properties of nanofluid and the extinction coefficient is simply dependent on the optical properties in suspension and the total volume fraction. However, it is theoretically expected that the higher particle size should lead to higher extinction coefficient. However, as mentioned in the previous chapter, in order to apply Rayleigh scattering, the particle size has to be controlled within 20 nm. Since the particle size shows not much influence to the optical properties, particle size of 10 nm is simply picked for the following study in the effect of volume fraction to the optical properties.

Figure 4.5 and 4.6 illustrated the absorption coefficient spectrum for aluminium nanoparticles with particle size of 10 nm. The calculated data that served as the basis of these graphs are presented in Appendix 1 as Table A7 and A7a. Both the graph and data are divided into two sets, which the first set is with volume fraction increasing by 0.5% and the second set increasing by 1.0% at every interval, in order to study the sensitivity of volume fraction of nanoparticles towards its absorption coefficient.

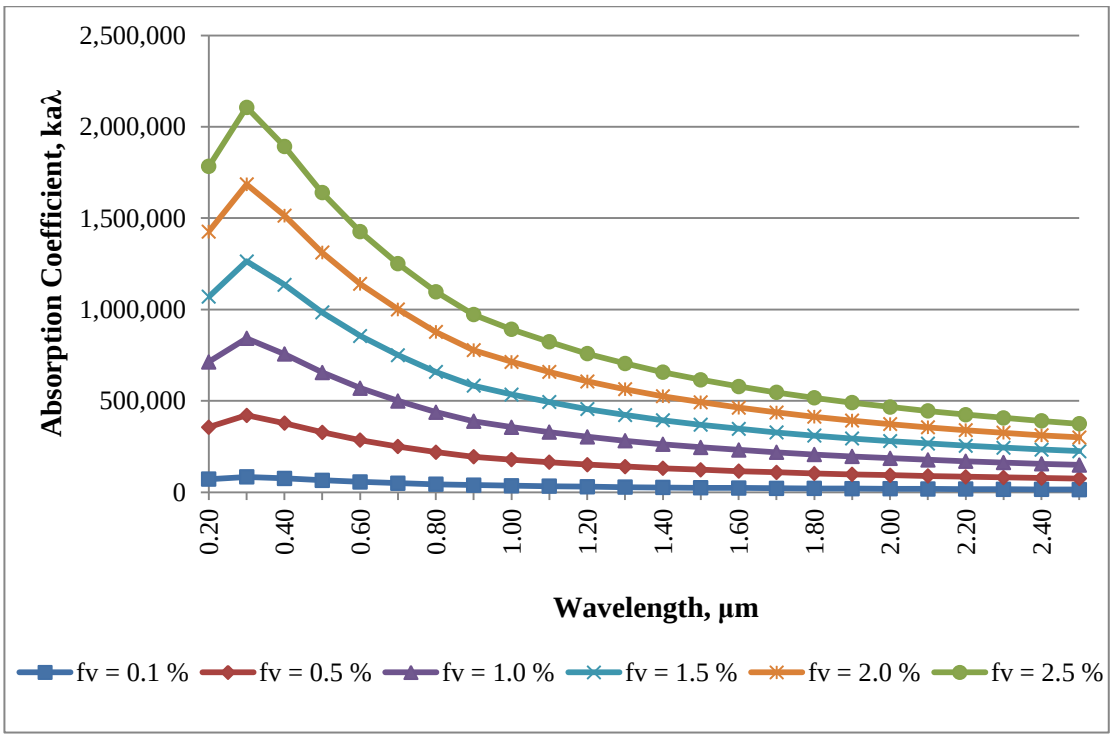

Figure 4.5 : The Effect of Nanoparticle Volume Fraction, f_v (0.1% - 2.5%) towards Absorption Coefficient, $k_{a\lambda}$

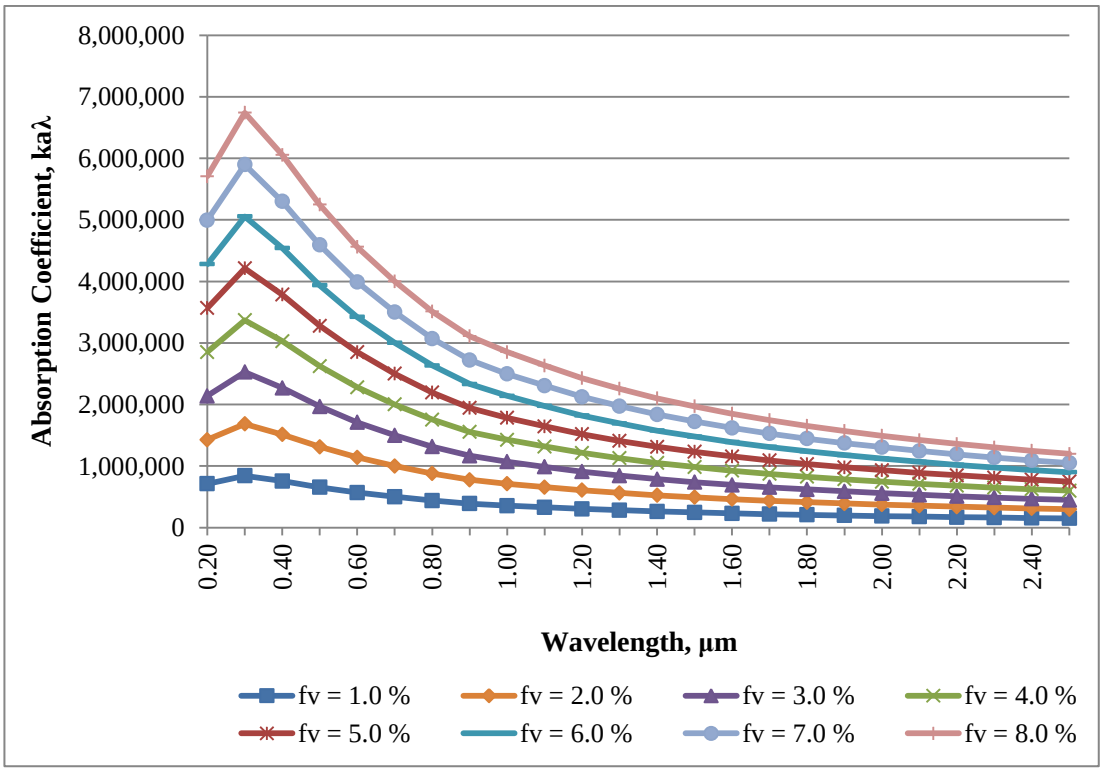

Figure 4.6 : The Effect of Nanoparticle Volume Fraction, f_v (1.0% - 8.0%) towards Absorption Coefficient, $k_{a\lambda}$

From Figures 4.5 and 4.6, we can see that the absorption coefficient gains it weight sharply from wavelength of 0.2 μm to slightly before 0.3 μm and ease with almost the same pace along the visible light region. The absorption coefficient slowly comes to a constant decreasing gradient after wavelength of 0.9 μm and continues all the way through the studied wavelengths. This phenomenon happens to every volume fraction calculated but however, larger volume fraction shows sharper rise and drop fashion. In general, absorption coefficient upsurges with the increase of volume fraction with the same rate. Absorption coefficient is linearly proportional to volume fraction and this can be confirmed from equation 3.9a.

Besides absorption coefficient, the scattering coefficient of aluminium nanoparticles is shown. Figures 4.7 and 4.8 display the trend of scattering coefficient along various light wavelengths while Table A8 and A8a give the developed data.

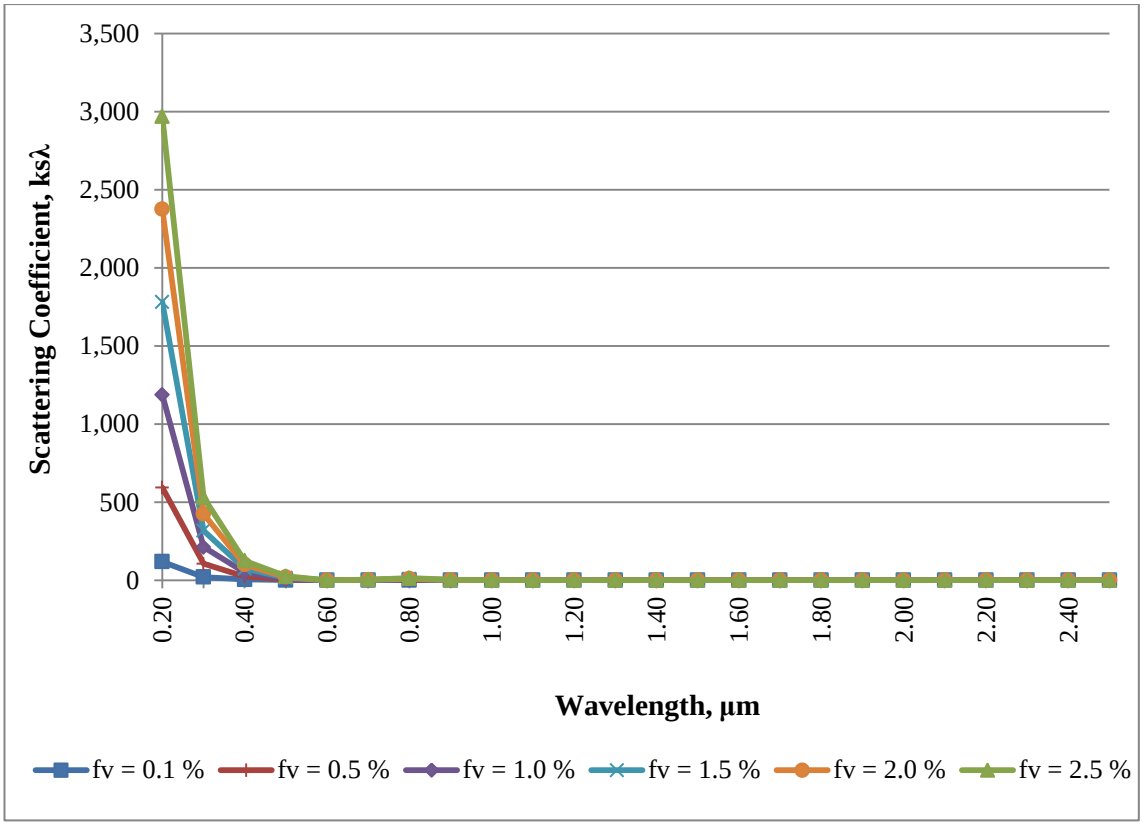

Figure 4.7 : The Effect of Nanoparticle Volume Fractions, f_v (0.1% - 2.5%) towards Scattering Coefficient, $k_{s\lambda}$

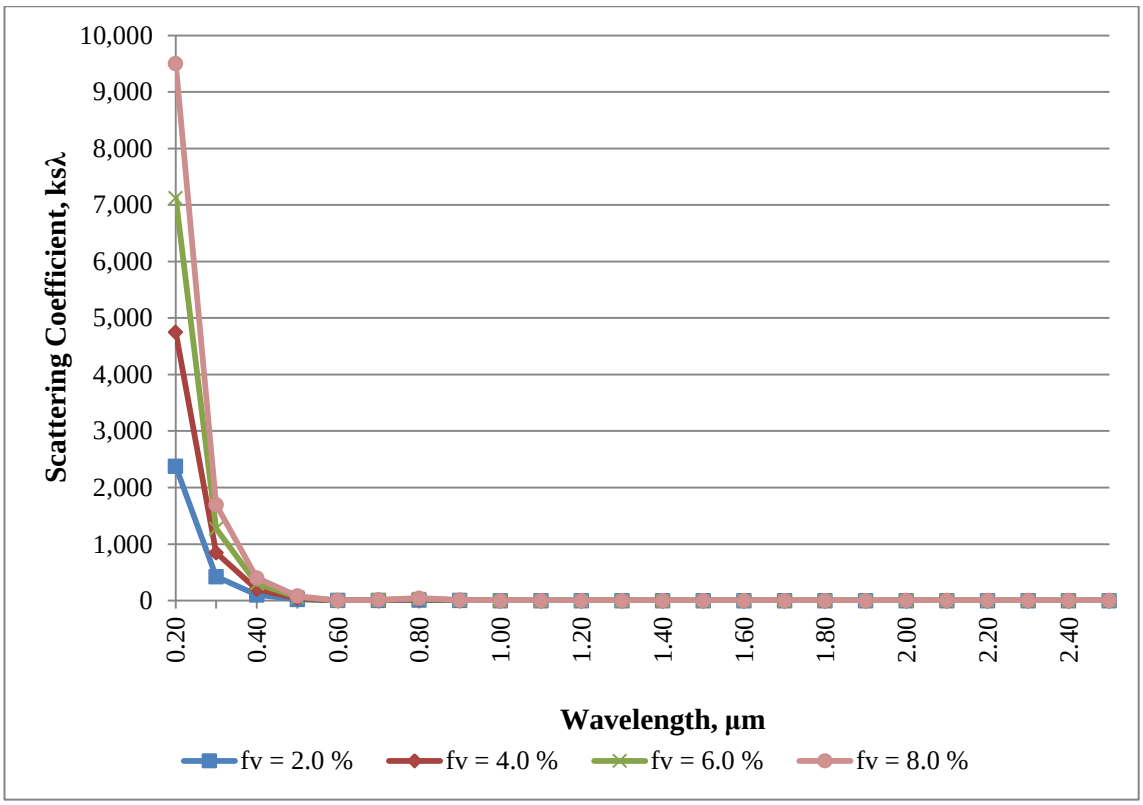

Figure 4.8 : The Effect of Nanoparticle Volume Fractions, f_v (2.0% - 8.0%) towards Scattering Coefficient, $k_{s\lambda}$

Similar to the graphs plotted for absorption coefficient, the trends are shown in two set of graphs to learn the sensitivity of scattering coefficient towards volume fraction. Figure 4.7 demonstrates the spectrum of scattering coefficient with interval of 0.5% increment of volume fraction while figure 4.8 gives 2.0% of increment. According to Figures 4.7 and 4.8, aluminium nanoparticles only contribute to scattering coefficient at a very small region. The scattering coefficients are large and significant at near UV section around 0.2 µm and it follows by an abrupt descent to close to nil when entering the visible light section. The scattering coefficient of nanoparticle decreases to below 100 at wavelength of 0.3 µm and reach zero after wavelength of 0.5 µm. The increment of volume fraction gives larger scattering coefficient but yet it turns out to be negligible after 0.3 µm of wavelength. This further proved that scattering coefficient can be

neglected in most wavelengths as its effect is not perceptible when combine with absorption coefficient. The combined absorption coefficient and scattering coefficient which gives the extinction coefficient of nanoparticles are shown in Figure 4.9 and tabulated in Table A9.

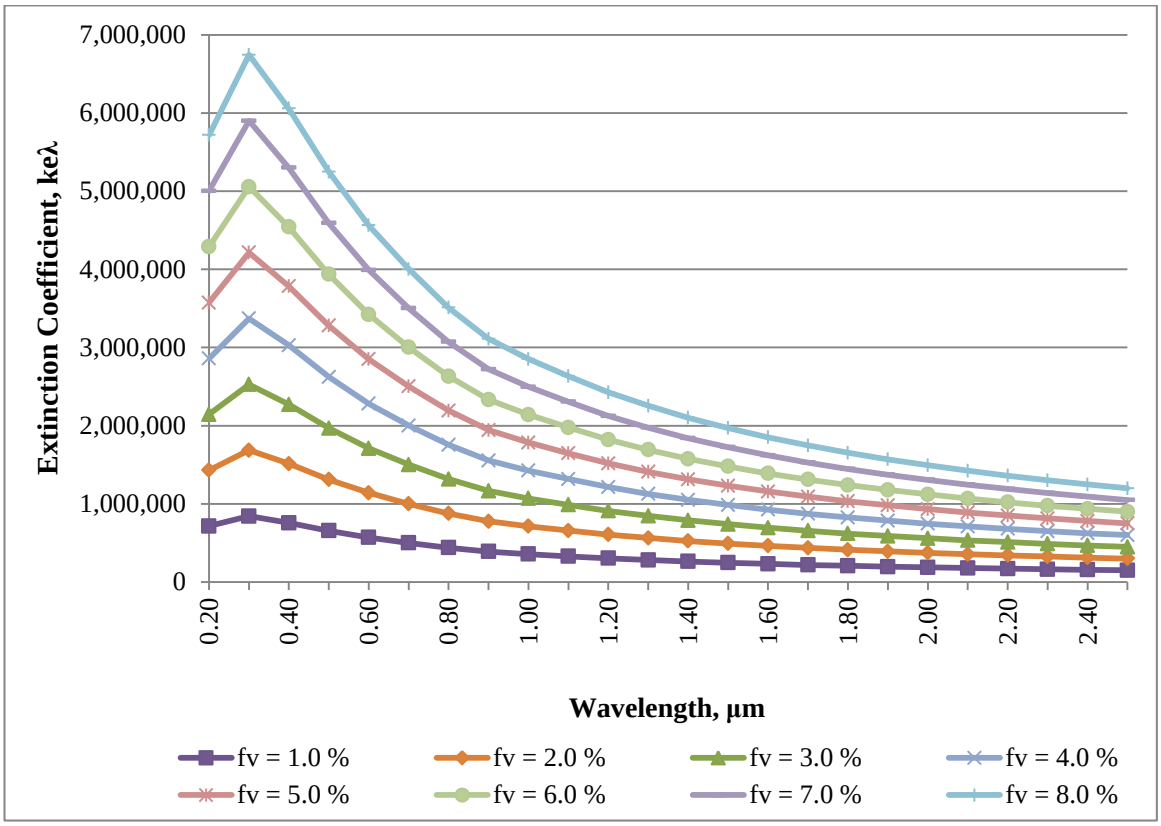

Figure 4.9 : The Effect of Nanoparticle Volume Fractions, f_v (1.0% - 8.0%) towards Extinction Coefficient, $k_{e\lambda}$

The spectrum of extinction coefficient is observed to be similar to the one in absorption coefficient. This is true as if we have a closer look; the value of scattering coefficient is of thousands while the absorption coefficient is in millions. Thus, the portion of scattering coefficient in the extinction coefficient is so minimal that the effect is inconspicuous. Besides, based on the trend in the extinction coefficient by increasing volume fraction of nanoparticles, we can conclude that the more concentrated the

nanoparticle is in the nanofluid, the higher extinction coefficient is expected. The pattern is of linear proportion as suggested from Equation 3.9.

After looking at the optical properties of nanoparticle with two parameters namely particle size and volume fraction considered, we can conclude two points:

1. The influence of particle size to the optical properties of nanoparticle can say to be very minimal or unimportant.

2. The extinction coefficient of nanoparticle is linearly proportional to the volume fraction. The more volume fraction is used, the larger the extinction coefficient will be.

Although the optical properties are in a more favourable trend when volume fraction is added, this parameter has a few controlling factors such as possible clogging effect, stability of suspended nanoparticles in the base fluid and the limitation to incorporate into heat pipes for Evacuated Tube Collector usage for determining the practical concentration of nanoparticles.

4.3 Transmissivity of Nanofluid

The influence to light transmissivity when aluminium nanoparticle is added to base fluid is studied. As mentioned above, the particle size is again simply chosen at 10 nm. Figures 54.10, 4.11 and 4.12 and Table A10, A11 and A12 are offered to explain this influence.

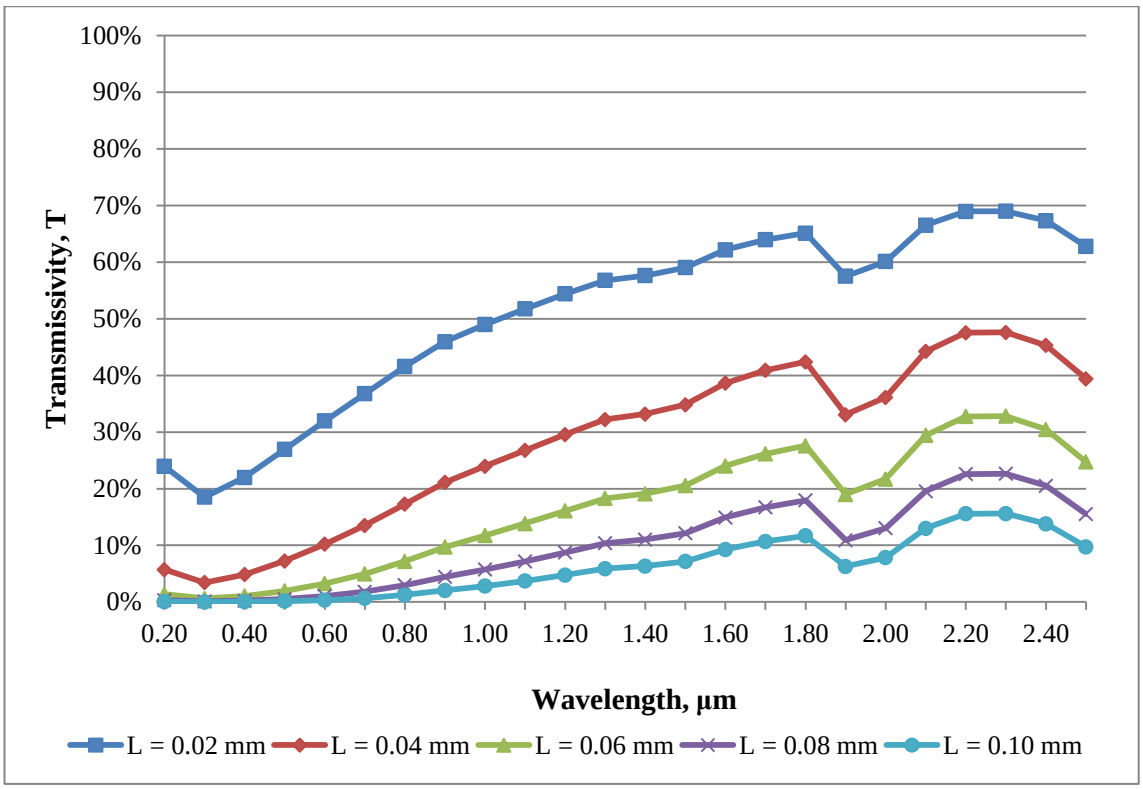

Figure 4.10 : The Transmissivity of Nanofluid (f_v = 0.1%)

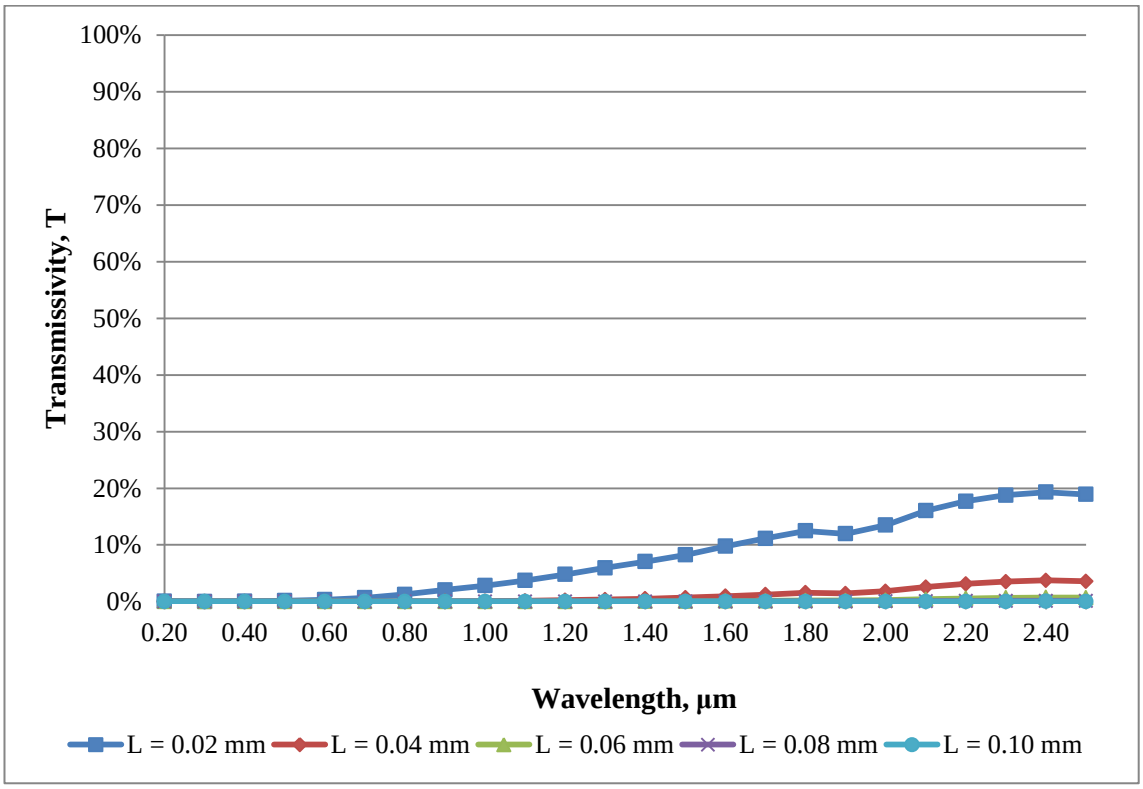

Figure 4.11 : The Transmissivity of Nanofluid (f_v = 0.5%)

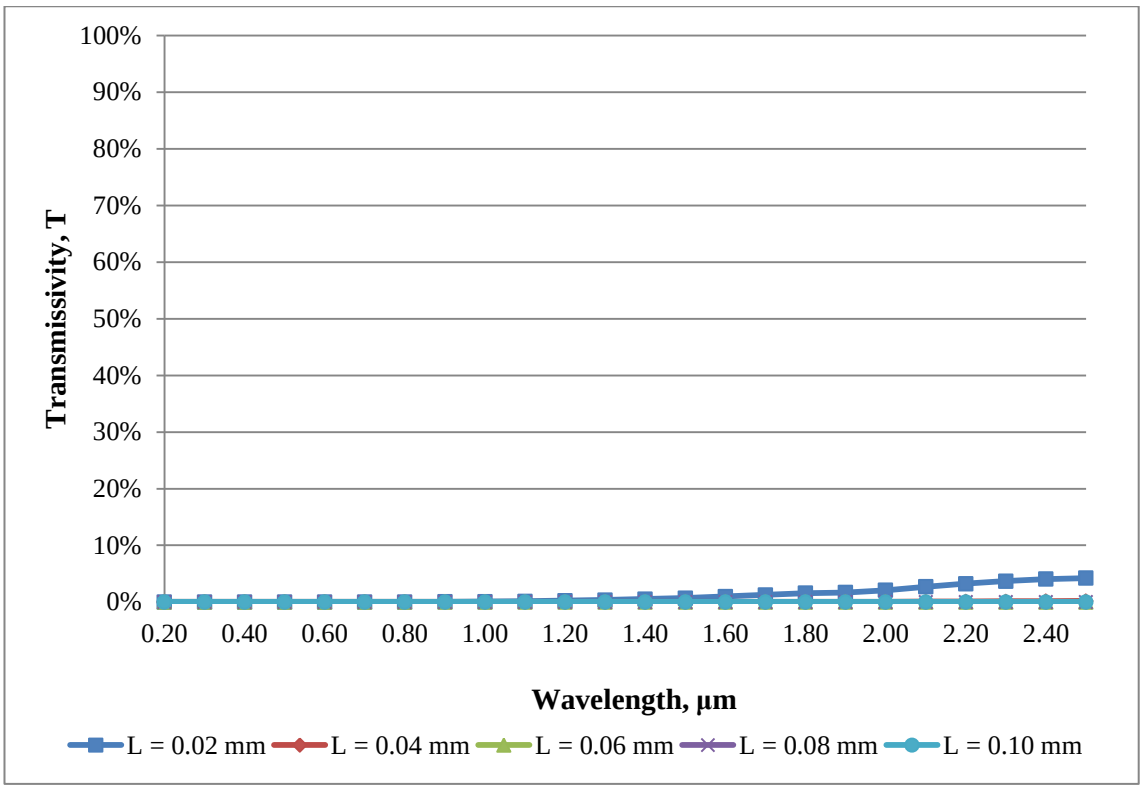

Figure 4.12 : The Transmissivity of Nanofluid (f_v = 1.0%)

We first compare Figure 4.10 and 4.1. The transmittance of light is greatly reduced by 60 % in average throughout the visible light region. This is the region where pure water is most transparent and visible light passes through freely. The transmissivity gradually increase after wavelength of 0.3 µm where the nanoparticle has the most extinction coefficient. As shown in Figure 4.9 also, the extinction coefficient of nanoparticles, regardless of volume fraction, decline slowly and continuously towards the near infrared region. This results in a greater transmissivity after visible light region and going towards the near infrared sector. Transmissivity touch zero percent or in other word, the nanofluid becomes opaque to light at near UV to about 0.5 µm wavelength when light travels 0.1 mm or 100 µm into the nanofluid.

The above enhancement in light absorption is just the result of having 0.1% of nanoparticle in the base fluid. When the concentration increases to 0.5%, the

improvement becomes even more distinguish. The nanofluid blocks or extinct almost all light when light path reaches 0.6 mm or 60 μm. It is only when wavelength exceeds 1.60 μm the light is able to transmit to a deeper layer of nanofluid. But light is totally prohibited from passing through when it reaches 0.8 mm light path and this is confirm by data developed in Table A11.

The transmissivity of light become impossible when 1.0% volume fraction of nanoparticle is used. Light can only barely pass through 0.02 mm or 20 μm of nanofluid and is being absorbed totally. This can be used to assume that the solar energy is completely harvested when light transmits about 0.03 mm into the nanofluid, which demonstrates a very promising improvement to utilizing solar energy. The detail data is presented in Table A12.

Unfortunately the optical properties of aluminium nanoparticles after wavelength of 2.5 μm is unable to be obtained and the actually enhancement after that wavelength of nanofluid cannot be determined. However, with the projection of graph in Figure 4.9 and the great absorption ability of pure water at that sector as illustrated in Figure 4.1, the nanofluid is predicted to be relatively opaque to light wave after wavelength of 2.5 μm.

Chapter 5: Conclusion and Future Recommendation

Solar energy, as the most vastly available energy and also supremely effective in terms of energy conversion has been the most sought after. The most common solar thermal collector utilizes black surface as radiant absorber but the efficiency is limited to the effectiveness of the black surface and the transfer of thermal energy from the black surface to the working fluid. After conducting this study, the thesis can bravely conclude the following:

1. Direct Solar Collector uses nanofluids as volumetric absorber and is expected to provide excellent optical properties and enhanced thermal transfer.

2. The extinction coefficient of nanofluid is evaluated with aluminium nanoparticle as additive material and pure water as base fluid and nanoparticle size and volume fraction as parameters. The particle sizes and volume fraction studied are 1 nm to 10 nm and 0.1% to 8.0% respectively. Pure water appears to be almost transparent to visible light but shows great absorption ability at longer wavelength of about 2.6 μm onwards. Aluminium nanoparticle shows very strong extinction coefficient at shorter wavelength and peak at 0.3 μm. The extinction coefficient demonstrates a descending trend after that. Despite a lower extinction coefficient at longer wavelength, aluminium nanoparticle is a good match to pure water as it enhanced the light absorption ability of water at the visible and shorter wavelength region.

3. The particle size shows minimal influence to the optical properties of nanofluid while the extinction coefficient is linearly proportionate to volume fraction. This is in common with the findings by Lenert (2010) and Tyagi (2008, 2009). It is suggested that although the extinction coefficient of nanofluid is disregard of the nanoparticle size, the nanoparticle size should be controlled to be below

20 nm in order for Rayleigh scattering to take place. On the other hand, the volume fraction should be minimal after obtaining the desired optical properties in order to avoid drawbacks like clogging and unstable suspension of nanoparticles when incorporating nanofluid technology to Solar Collector. The proposed nanoparticle size and volume fraction in this thesis is 10 nm and below 2.0% respectively.

4. The transmissivity of light is compared between pure water (base fluid) and nanofluid. The improvement is promising and with only 1.0% volume fraction, the nanofluid is already almost opaque to light wave. Since volume fraction of just 1.0% is already showing satisfactory improvement to solar absorption, nanofluid with aluminium as nanoparticles and pure water as base fluid can be concluded to be a good solution to Direct Solar Collector.

In the extension to this study, experiments to confirm the radiative properties of the nanofluid should be carried out. The radiative properties for this nanofluid to light wave exceeding wavelength of 2.5 μm can be determined by this way. Materials showing promising radiative properties such as Single Wall Carbon Nanohorn (SWCNH) (Mercatelli et al., 2011) can be integrated to future researches to investigate the probability to be functioned as nano-additive. Further to this, base fluid with better thermal properties and stability at high temperature can be studied to explore the possibility of using nanofluid in solar collector of concentrating type. Last of all, the researches in optical properties of nanofluid should take into consideration the manufacturing process and cost of integration to the existing systems. Direct Solar Collector has shown to be a very encouraging form of renewable energy and should be further exploit to give human beings a better and cleaner future.

Bibliography

Abdelrahman, M., Fumeaux, P. & Suter, P. (1979). *Study of Solid-Gas-Suspensions Used For Direct Absorption of Concentrated Solar-Radiation*. Solar Energy, **22(1)**, p. 45-48.

Anderson, B. (1977). *Solar energy: fundamentals in building design.* New York: McGraw-Hill.

ASTM (American Society for Testing and Materials) Terrestrial Reference Spectra. (2003). *Reference Solar Spectral Irradiance: Air Mass 1.5.* In ASTM G173-03.

Bar-Yosef, O. (2002). *The upper Paleolithic revolution*. Annual Review of Anthropology, **31**, 363-393.

Brewster, M.Q. (1992). *Thermal radiative transfer and properties*. Canada: John Wiley & Sons.

Buongiorno, J. (2006). *Convective transport in nanofluids*. Journal of Heat Transfer, **128(3)**, 240-251.

Chaplin, M. (2011). Water Absorption Spectrum. In *Water Structure and Science*. Retrieved 29 July 2011. From http://www.lsbu.ac.uk/water/vibrat.html#uv

Chen, C.W., Chiang, H.-P., Leung, P.T., & Tsai, D.P. (2008). *Temperature dependence of enhanced optical absorption and Raman Spectroscopy from Metallic Nanoparticles*. Solid State Communications, **148**, 413-416.

Choi, U.S. (1995). *Enhancing Thermal Conductivity of Fluids with Nanoparticles, Developments and Applications of Non-NewtonianFlows*, ASME FED 231/MD (66), 99-103.

EGRE (Expert Group on Renewable Energy). (2005). Renewables 2005 Background Report. In United Nations Department of Economic and Social Affairs (UNDESA), *Beijing International Renewable Energy Conference 2005 Background Report.* Beijing, People's Republic of China. 7-8th November 2005. New York: United Nations.

Everett, B. (2004). Solar Thermal Energy. In *Renewable Energy – Power for A Sustainable Future* (2nd ed.) (pp. 17-64). New York: Oxford University Press.

Fan, X., Tan, J., Zhang, G., & Zhang, F. (2007). *Isolation of carbon nanohorns assemblies and their potential for intracellular delivery*. Nanotechnology, **18**, 195103, 1-6.

Four Peaks Technologies Inc. (2010). Solar In-Depth. In *Solar Cell Central.* Retrieved 27 July 2011. From http://solarcellcentral.com/physics_page.html

Francia, G. (1961). *A new collector of solar radiant energy*. UN Conf. New Sources Energy, **4**, 572.

Gleiter, H. (1989). Nanocrystalline Materials, Progress in Materials Science, **33(4)**, 223–315.

Hollands, K.G.T. (1965). *Honeycomb devices in flat-plate solar collectors*. Solar Energy, **9(3)**, 159-164.

Hunt, A.J. (1978). *Small Particle Heat Exchangers*. Lawrence Berkeley Laboratory.

Horvath, H. (2009). *Gustav Mie and the scattering and absorption of light by particles: Historic developments and basics.* Journal of Quantitative Spectroscopy & Radiative Transfer, **110**, 787-799.

Iijima, S., Yudaseka, M., Yamada, R., Bandow, S., Suenaga, K., Kokai, F., et al. (1999). *Nano-aggregrates of single-walled graphite carbon nano-horns*. Chem Phys Lett, **309**, 165-170.

International Energy Agency Renewable Energy Working Party. (2002). *Renewable Energy... into the mainstream*, p. 9.

IAPWS (The International Association for the Properties of Water and Steam). (1997). *Release on the Refractive Index of Ordinary Water Substance as a Function of Wavelength, Temperature and Pressure.* Erlangen, Germany.

Kalogirou, S. (2003). *The potential of solar industrial process heat applications*. Applied Energy, **76(4)**, 337–361.

Kalogirou, S.A. (2004). *Solar Thermal Collectors and Applications*. Progress in Energy and Combustion Science, **30**, 231-295.

Kalogirou, S.A., Eleftheriou, P., Lloyd, S., & Ward, J. (1994). *Design and performance characteristics of a parabolic-trough solarcollector system*. Appl Energy, **47**, 341–354.

Kameya, Y. & Hanamura, K. (2011). *Enhancement of solar radiation absorption using nanoparticle suspension.* Solar Energy, **85**, 299-307.

Karkanas, P., Shahack-Gross, R., Ayalon, A., Bar-Matthews, M., Barkai, R., Frumkin, A., et al. (2007). *Evidence for habitual use of fire at the end of the Lower Paleolithic: Site-formation processes at Qesem Cave, Israel.* Journal of Human Evolution, **53 (2)**, 197-212.

Keblinski, P., Phillpot, S.R., Choi, S.U.S., & Eastman, J.A. (2002). *Mechanisms of heat flow in suspensions of nano-sized particles (nanofluids).* International Journal of Heat and Mass Transfer, **45**, 855–863.

Khlebtsov, N.G., Trachuk, L.A., & Mel'nikov, A.G. (2005). *The effect of the size, shape, and structure of metal nanoparticles on the dependence of their optical properties on the refractive index of a disperse medium.* Optics and Spectroscopy, **98(1)**, 77-85.

Koo, J., & Kleinstreuer, C. (2005). *Impact analysis of nanoparticle motion mechanisms on the thermal conductivity of nanofluids*. International Communication on Heat and Mass Transfer, **32(9)**, 1111–1118.

Kou, L., Labrie, D., & Chylek, P. (1993). *Refractive indices of water and ice in the 0.65 to 2.5 μm spectral range.* Applied Optics, **32(19)**, 3531-3540.

Kreider, J.F., Kreith, F. (1977). *Solar heating and cooling*. New York: McGraw-Hill.

Kreith, F., Kreider, J.F. (1978). *Principles of solar engineering*. New York: McGraw-Hill.

Kumar, N. (2008). *Comprehensive Physics* (7^{th} ed.). New Delhi: Laxmi Publications.

Lenert, A. (2010). *Nanofluid-based Receivers for High-Temperature, High-flux Direct Solar Collectors*. M. Sc. Massachusetts Institute of Technology.

Lilienfeld, P. (2004). *A Blue Sky History*. Optics and Photonics News, **June**, 32-39.

Masruroh, N. A., Li, B. & Klemes, J. (2006). *Life cycle analysis of solar thermal system with thermochemical storage process*, Renewable Energy, **31**, 537-548.

Meinel, A.B., Meinel, M.P. (1976). *Applied solar energy: an introduction.* Reading, MA: Addison-Wesley.

Mercatelli, L., Sani, E., Zaccanti, G., Martelli, F., Di Ninni, P., Barison, S., et al. (2011). *Absorption and scattering properties of carbon nanohorn-based nanofluid for direct sunlight absorbers*. Nanoscale Research Letters, **6**, 282.

Meteonorm. (2008). Global irradiance World. In *free meteonorm maps*. Retrieved 21st July 2011. From http://meteonorm.com/?id=32

Miller, F. J., and Koenigsdorff, R. W. (2000). *Thermal modeling of a small-particle solar central receiver*, J. Solar Energy Eng., **122,** 23-29.

Minardi, J. E., & Chunag, H. N. (1975). *Performance of a black liquid flat-plate solar collector*, Solar Energy, **17**, 179 -183.

Mishra, A., Srivastava, V.K., & Ram, S. (2008). *Nonlinear variation of optical absorption and rheological behavior with concentration in dispersed poly(vinyl pyrrolidone) of small molecules in water.* Journal of Molecular Liquids, **137**, 58-63.

Mishra, A., Ram, S., & Ghosh, G. (2009). *Dynamic Light Scattering and Optical Absorption in Biological Nanofluids of Gold Nanoparticles in Poly(vinyl pyrrolidone) Molecules.* J. Phys. Chem. C, **113**, 6976-6982.

Mohr, P.J., Taylor, B.N., & Newell, D.B. (2011). "The 2010 CODATA Recommended Values of the Fundamental Physical Constants" (Web Version 6.0). Retrieved 30 July 2011. From http://physics.nist.gov/constants

Molineaux, B., Lachal, B., & Gusian, O. (1994). *Thermal analysis of five outdoor swimming pools heated by unglazed solar collectors*. Solar Energy, **53(1)**, 21–26.

Okujagu, C. U., & Adjepong, S. K. (1989). *Performance of a simple flat-plate collector at an equatorial location*, Solar & Wind Tech., **6**, 283-289.

Otanicar, T.P., Phelan, P.E., & Golden, J.S. (2009) *Optical Properties of Liquids for Direct Absorption Solar Thermal Energy Systems*. Solar Energy, **83**, 969-977.

Otanicar, T.P., Phelan, P.E., Prasher, R.S., Rosengarten, G., & Taylor, R.A. (2010). *Nanofluid-based Direct Absorption Solar Collector*. Journal of Renewable and Sustainable Energy, **2**, 033102.

Pacheco, J.E. (2001). *Demonstration of solar-generated electricity on demand: The Solar Two project*. Journal of Solar Energy Engineering-Transactions of the ASME, **123(1)**, 5-5.

Pak, B.C., & Cho, I.Y. (1998). *Hydrodynamic and heat transfer study of dispersed fluids with sub-micron metallic oxide particles*. Experimental Heat Transfer, **11**, 151–170.

Pope, R.M., & Fry, E.S. (1997). *Absorption spectrum (380 – 700 nm) of pure water. II. Integrating cavity measurements.* Applied Optics, **36(33)**, 8710-8723.

REN21 (Renewable Energy Policy Network in the 21st Century). (2011). *Renewables 2011 – Global Status Report*, p.11.

Saidur, R., Leong, K.Y., & Mohammad, H.A. (2011). *A review on applications and challenges of nanofluids.* Renewable and Sustainable Energy Reviews, **15**, 1646-1668.

Sani, E., Barison, S., Pagura, C., Mercatelli, L., Sansoni, P., Fontani, D., et al. (2010). *Carbon nanohorns-based nanofluids as direct sunlight absorbers*. Optics Express, **18(5)**, 5179-5187.

Serrano, E., Rus, G., & Mart ńez, J.G. (2009). *Nanotechnology for sustainable energy*. Renewable and Sustainable Energy Reviews, **13**, 2373-2384.

Smith, D.Y., Shiles, E. & Inokuti, M. (1985). The Optical Properties of Metallic Aluminum. In E.D. Palik, ed. 1998. Handbook of optical constants of solids, Volume 5. London: Academic Press Limited.

Smith, G.H. (2006). *Camera Lenses: from Box Camera to Digital*. Washington: The International Society of Optical Engineering.

Soltau, H. (1992). *Testing the thermal performance of uncovered solar collectors*. Solar Energy, **49(4)**, 263–272.

Sørensen, B. (2011). *Renewable Energy* (4th ed.). Oxford: Academic Press.

Tester, J. W., Drake, E. M., Golay, M. W., Driscoll, M. J., & Peters, W. A. (2005). *Sustainable energy: Choosing among options*, MIT Press, MA, 64-74.

Twidell, J. & Weir, A.D. (2006). *Renewable Energy Resources* (2nd ed.). New York: Taylor & Francis.

Tyagi, H. (2008) *Radiative and Combustion Properties of Nanoparticles-Laden Liquid*, Ph. D. Arizona State University.

Tyagi, H., Phelan, P., & Prasher, R. (2009). *Predicted Efficiency of a Low-temperature Nanofluid-based Direct Absorption Solar Collector*. Journal of Solar Energy Engineering, **131**, 041004-1 - 041004-7.

US DOE (United States Department of Energy). (2010a). Overview. In *International Energy Outlook 2010*. Retrieved 17 July 2011. From http://www.eia.gov/oiaf/ieo/electricity.html

US DOE (United States Department of Energy). (2010b). Electricity Supply by Energy Source. In *International Energy Outlook 2010*. Retrieved 17 July 2011. From http://www.eia.gov/oiaf/ieo/electricity.html

US EPA (United States Environmental Protection Agency). (2011a). Nitrogen Dioxide. In *Six Common Pollutants*. Retrieved 17 July 2011. From http://www.epa.gov/air/nitrogenoxides/

US EPA (United States Environmental Protection Agency). (2011b). Health. In *Nitrogen Dioxide*. Retrieved 17 July 2011. From http://www.epa.gov/airquality/nitrogenoxides/health.html

Van de Hulst, H.C. (1981). *Light scattering by small particles*. New York: Dover Publications.

Weiss, W., & Mauthner, F. (2011). *Solar Heat Worldwide: Markets and Contribution to the Energy Supply 2009*, prepared for *IEA* Solar Heating and Cooling Programme.

Wikibooks. (2011). Energy from the Sun. In *High School Earth Science/Energy in the Atmosphere*. Retrieved 7 August 2011. From http://en.wikibooks.org/wiki/High_School_Earth_Science/Energy_in_the_Atmosphere

Wikipedia. (2011a). Objectives. In *Kyoto Protocol*. Retrieved 17 July, 2011. From http://en.wikipedia.org/wiki/Kyoto_protocol

Wikipedia, (2011b). Visible Spectrum. Retrieved 30 July, 2011. From http://en.wikipedia.org/wiki/Visible_spectrum#cite_ref-0.

Wikipedia. (2011c). Spectral colors. In *Visible Spectrum*. Retrieved 30 July, 2011. From http://en.wikipedia.org/wiki/Visible_spectrum#Spectral_colors.

Wikipedia. (2011e). *Light Scattering*. Retrieved 31 July, 2011. From http://en.wikipedia.org/wiki/Light_scattering

Winter, F. (1994). *Twenty-year progress report on the copper development association do-it-yourself solar swimming pool heating manual and on the associated prototype heater.* Solar Energy, **53(1)**, 33–36.

Wrangham, R. W., Jones, J. H., Laden, G., Pilbeam, D., Conklin-Brittain, N. (1999). *The raw and the stolen: Cooking and the ecology of human origins.* Current Anthropology, **40(5)**, 567-594.

Xuan, Y., & Li, Q. (2000). *Heat transfer enhancement of nanofluids. International Journal of Heat and Fluid Flow*, **21,** 58–64.

Appendix 1

Table A1 : Pure Water Refractive index, n and Absorption index, k, as Function of Wavelength, λ (Irvine and Pollack, 1968 cited in Brewster, 1992, p.507)

λ (μm)	n	k
0.20	1.4240	1.300E-07
0.30	1.3590	3.600E-08
0.40	1.3430	3.000E-09
0.50	1.3360	8.000E-10
0.60	1.3320	7.000E-09
0.70	1.3300	3.300E-08
0.80	1.3280	1.340E-07
0.90	1.3280	4.800E-07
1.00	1.3260	2.820E-06
1.10	1.3240	1.660E-06
1.20	1.3230	9.740E-06
1.30	1.3210	1.117E-05
1.40	1.3200	1.448E-04
1.50	1.3180	2.065E-04
1.60	1.3160	7.890E-05
1.70	1.3150	6.970E-05
1.80	1.3120	1.146E-04
1.90	1.3090	1.217E-03

λ (μm)	n	k
2.00	1.3040	1.082E-03
2.10	1.3000	4.345E-04
2.20	1.2930	2.800E-04
2.25	1.2920	3.040E-04
2.30	1.2860	4.210E-04
2.40	1.2760	8.020E-04
2.50	1.2460	1.651E-03
2.60	1.1800	2.048E-03
2.70	1.1340	5.049E-03
2.75	1.1330	2.401E-02
2.80	1.2320	9.361E-02
2.90	1.3100	2.435E-01
3.00	1.3510	2.586E-01
3.10	1.4260	1.828E-01
3.20	1.5090	9.422E-02
3.30	1.4700	4.333E-02
3.40	1.4490	1.888E-02
3.50	1.4230	9.300E-03

Table A2 : Optical Properties of Aluminium as a Function of Wavelength, λ

λ (μm)	n	k	n'	k'
0.20	0.130	2.39	0.091	1.678
0.30	0.276	3.61	0.203	2.656
0.40	0.490	4.86	0.365	3.619
0.50	0.769	6.08	0.576	4.551
0.60	1.200	7.26	0.901	5.450
0.70	1.830	8.31	1.376	6.248
0.80	2.800	8.45	2.108	6.363
0.90	2.060	8.30	1.551	6.250
1.00	1.350	9.58	1.018	7.225
1.10	1.200	11.20	0.906	8.459
1.20	1.210	12.00	0.915	9.070
1.30	1.230	13.20	0.931	9.992
1.40	1.260	14.00	0.955	10.606
1.50	1.380	15.40	1.047	11.684
1.60	1.500*	16.40*	1.138	12.443
1.70	1.620*	17.50*	1.229	13.278
1.80	1.770	18.30	1.349	13.948
1.90	1.990	19.80	1.520	15.126
2.00	2.150	20.70	1.649	15.874
2.10	2.350*	21.60*	1.802	16.564
2.20	2.540*	22.50*	1.948	17.255
2.30	2.730*	23.40*	2.094	17.945
2.40	2.920*	24.30*	2.239	18.635
2.50	3.070	25.60	2.354	19.632

Note: * Data obtained by linear interpolation.

Table A3 : Transmissivity of Pure Water at Various Light Path Length

λ (μm)	$K_{a\lambda}$	T				
		L = 0.02 mm	L = 0.04 mm	L = 0.06 mm	L = 0.08 mm	L = 0.10 mm
0.20	8.17	99.98%	99.97%	99.95%	99.93%	99.92%
0.30	1.51	100.00%	99.99%	99.99%	99.99%	99.98%
0.40	0.09	100.00%	100.00%	100.00%	100.00%	100.00%
0.50	0.02	100.00%	100.00%	100.00%	100.00%	100.00%
0.60	0.15	100.00%	100.00%	100.00%	100.00%	100.00%
0.70	0.59	100.00%	100.00%	100.00%	100.00%	99.99%
0.80	2.10	100.00%	99.99%	99.99%	99.98%	99.98%
0.90	6.70	99.99%	99.97%	99.96%	99.95%	99.93%
1.00	35.44	99.93%	99.86%	99.79%	99.72%	99.65%
1.10	18.96	99.96%	99.92%	99.89%	99.85%	99.81%
1.20	102.00	99.80%	99.59%	99.39%	99.19%	98.99%
1.30	107.97	99.78%	99.57%	99.35%	99.14%	98.93%
1.40	1299.72	97.43%	94.93%	92.50%	90.12%	87.81%
1.50	1729.97	96.60%	93.31%	90.14%	87.08%	84.11%
1.60	619.68	98.77%	97.55%	96.35%	95.16%	93.99%
1.70	515.22	98.97%	97.96%	96.96%	95.96%	94.98%
1.80	800.06	98.41%	96.85%	95.31%	93.80%	92.31%
1.90	8049.09	85.13%	72.47%	61.70%	52.52%	44.71%
2.00	6798.41	87.29%	76.19%	66.50%	58.05%	50.67%
2.10	2600.04	94.93%	90.12%	85.56%	81.22%	77.10%
2.20	1599.36	96.85%	93.80%	90.85%	87.99%	85.22%
2.30	2300.19	95.50%	91.21%	87.11%	83.19%	79.45%
2.40	4199.26	91.94%	84.54%	77.73%	71.47%	65.71%
2.50	8298.83	84.71%	71.75%	60.78%	51.48%	43.61%
2.60	9898.43	82.04%	67.30%	55.22%	45.30%	37.16%
2.70	23499.11	62.50%	39.06%	24.42%	15.26%	9.54%
2.80	420120.70	0.02%	0.00%	0.00%	0.00%	0.00%
2.90	1055141.81	0.00%	0.00%	0.00%	0.00%	0.00%
3.00	1083221.15	0.00%	0.00%	0.00%	0.00%	0.00%

Table A4 : The Effect of Nanoparticle Sizes towards Absorption Coefficient, $k_{a\lambda}$

λ (μm)	D				
	D = 1.0 nm	D = 5.0 nm	D = 10.0 nm	D = 15.0 nm	D = 20.0 nm
0.20	1,422,047.07	1,423,242.74	1,426,979.23	1,433,206.72	1,441,925.20
0.30	1,680,767.38	1,681,860.43	1,685,276.20	1,690,969.16	1,698,939.30
0.40	1,510,386.24	1,511,297.00	1,514,143.12	1,518,886.66	1,525,527.62
0.50	1,308,800.50	1,309,588.14	1,312,049.49	1,316,151.74	1,321,894.90
0.60	1,137,768.87	1,138,456.79	1,140,606.55	1,144,189.46	1,149,205.55
0.70	998,403.46	998,992.39	1,000,832.78	1,003,900.12	1,008,194.38
0.80	875,946.96	876,357.83	877,641.81	879,781.77	882,777.72
0.90	776,563.53	776,840.81	777,707.31	779,151.48	781,173.32
1.00	712,258.05	712,536.52	713,406.73	714,857.07	716,887.56
1.10	657,495.77	657,790.38	658,711.05	660,245.48	662,393.69
1.20	605,961.53	606,225.02	607,048.43	608,420.78	610,342.07
1.30	562,913.17	563,167.73	563,963.21	565,289.02	567,145.15
1.40	524,456.25	524,687.34	525,409.52	526,613.14	528,298.22
1.50	491,778.51	492,008.64	492,727.79	493,926.38	495,604.41
1.60	462,233.61	462,449.77	463,125.25	464,251.05	465,827.18
1.70	436,064.97	436,271.14	436,915.40	437,989.18	439,492.46
1.80	412,493.61	412,685.89	413,286.76	414,288.21	415,690.25
1.90	391,682.61	391,875.78	392,479.45	393,485.56	394,894.11
2.00	372,545.93	372,728.80	373,300.25	374,252.66	375,586.04
2.10	355,149.11	355,321.45	355,860.03	356,757.65	358,014.32
2.20	339,295.61	339,458.54	339,967.71	340,816.33	342,004.40
2.30	324,789.59	324,944.06	325,426.79	326,231.33	327,357.69
2.40	311,466.90	311,613.72	312,072.55	312,837.25	313,907.84
2.50	299,466.23	299,624.64	300,119.68	300,944.74	302,099.83

Table 5 : The Effect of Nanoparticle Sizes towards Scattering Coefficient, $k_{s\lambda}$

λ (μm)	D				
	D = 1.0 nm	D = 5.0 nm	D = 10.0 nm	D = 15.0 nm	D = 20.0 nm
0.20	2.37	296.87	2,374.97	8,015.52	18,999.76
0.30	0.42	53.06	424.48	1,432.62	3,395.85
0.40	0.10	12.57	100.55	339.35	804.37
0.50	0.02	2.56	20.52	69.24	164.12
0.60	0.00	0.07	0.54	1.82	4.32
0.70	0.00	0.43	3.42	11.53	27.33
0.80	0.01	1.36	10.87	36.70	86.98
0.90	0.00	0.30	2.42	8.17	19.36
1.00	0.00	0.00	0.00	0.01	0.02
1.10	0.00	0.01	0.04	0.14	0.34
1.20	0.00	0.00	0.02	0.08	0.20
1.30	0.00	0.00	0.01	0.04	0.09
1.40	0.00	0.00	0.00	0.01	0.03
1.50	0.00	0.00	0.00	0.01	0.02
1.60	0.00	0.00	0.02	0.06	0.15
1.70	0.00	0.00	0.04	0.13	0.32
1.80	0.00	0.01	0.07	0.23	0.55
1.90	0.00	0.01	0.11	0.37	0.88
2.00	0.00	0.02	0.13	0.44	1.03
2.10	0.00	0.02	0.15	0.50	1.18
2.20	0.00	0.02	0.15	0.52	1.24
2.30	0.00	0.02	0.16	0.53	1.25
2.40	0.00	0.02	0.15	0.52	1.23
2.50	0.00	0.02	0.14	0.49	1.16

Table A6 : The Effect of Nanoparticle Sizes towards Extinction Coefficient, $k_{e\lambda}$

λ (μm)	$k_{e\lambda}$				
	D = 1.0 nm	D = 5.0 nm	D = 10.0 nm	D = 15.0 nm	D = 20.0 nm
0.20	1,422,049.44	1,423,539.62	1,429,354.20	1,441,222.24	1,460,924.96
0.30	1,680,767.80	1,681,913.49	1,685,700.68	1,692,401.78	1,702,335.15
0.40	1,510,386.34	1,511,309.57	1,514,243.67	1,519,226.01	1,526,331.99
0.50	1,308,800.52	1,309,590.70	1,312,070.00	1,316,220.98	1,322,059.02
0.60	1,137,768.88	1,138,456.86	1,140,607.09	1,144,191.29	1,149,209.87
0.70	998,403.46	998,992.81	1,000,836.20	1,003,911.65	1,008,221.72
0.80	875,946.97	876,359.19	877,652.68	879,818.47	882,864.70
0.90	776,563.53	776,841.11	777,709.73	779,159.65	781,192.68
1.00	712,258.05	712,536.52	713,406.73	714,857.08	716,887.58
1.10	657,495.77	657,790.39	658,711.09	660,245.63	662,394.04
1.20	605,961.53	606,225.02	607,048.45	608,420.87	610,342.27
1.30	562,913.17	563,167.73	563,963.22	565,289.06	567,145.25
1.40	524,456.25	524,687.34	525,409.52	526,613.16	528,298.25
1.50	491,778.51	492,008.64	492,727.80	493,926.39	495,604.43
1.60	462,233.61	462,449.77	463,125.27	464,251.12	465,827.33
1.70	436,064.97	436,271.14	436,915.44	437,989.31	439,492.78
1.80	412,493.61	412,685.90	413,286.83	414,288.45	415,690.80
1.90	391,682.61	391,875.80	392,479.56	393,485.93	394,895.00
2.00	372,545.93	372,728.81	373,300.38	374,253.10	375,587.08
2.10	355,149.11	355,321.47	355,860.17	356,758.15	358,015.50
2.20	339,295.61	339,458.56	339,967.87	340,816.86	342,005.64
2.30	324,789.59	324,944.08	325,426.94	326,231.86	327,358.95
2.40	311,466.90	311,613.74	312,072.70	312,837.77	313,909.07
2.50	299,466.23	299,624.66	300,119.82	300,945.23	302,100.99

Table A7 : The Effect of Nanoparticle Volume Fraction (0.1% - 2.5%) towards Absorption Coefficient, $k_{a\lambda}$

λ	$k_{a\lambda}$					
(μm)	f_v = 0.1 %	f_v = 0.5 %	f_v = 1.0 %	f_v = 1.5 %	f_v = 2.0 %	f_v = 2.5 %
0.20	71,348.96	356,744.81	713,489.62	1,070,234.43	1,426,979.23	1,783,724.04
0.30	84,263.81	421,319.05	842,638.10	1,263,957.15	1,685,276.20	2,106,595.25
0.40	75,707.16	378,535.78	757,071.56	1,135,607.34	1,514,143.12	1,892,678.90
0.50	65,602.47	328,012.37	656,024.74	984,037.12	1,312,049.49	1,640,061.86
0.60	57,030.33	285,151.64	570,303.27	855,454.91	1,140,606.55	1,425,758.18
0.70	50,041.64	250,208.20	500,416.39	750,624.59	1,000,832.78	1,251,040.98
0.80	43,882.09	219,410.45	438,820.90	658,231.36	877,641.81	1,097,052.26
0.90	38,885.37	194,426.83	388,853.66	583,280.48	777,707.31	972,134.14
1.00	35,670.34	178,351.68	356,703.36	535,055.04	713,406.73	891,758.41
1.10	32,935.55	164,677.76	329,355.52	494,033.28	658,711.05	823,388.81
1.20	30,352.42	151,762.11	303,524.21	455,286.32	607,048.43	758,810.54
1.30	28,198.16	140,990.80	281,981.61	422,972.41	563,963.21	704,954.02
1.40	26,270.48	131,352.38	262,704.76	394,057.14	525,409.52	656,761.90
1.50	24,636.39	123,181.95	246,363.90	369,545.84	492,727.79	615,909.74
1.60	23,156.26	115,781.31	231,562.63	347,343.94	463,125.25	578,906.56
1.70	21,845.77	109,228.85	218,457.70	327,686.55	436,915.40	546,144.25
1.80	20,664.34	103,321.69	206,643.38	309,965.07	413,286.76	516,608.45
1.90	19,623.97	98,119.86	196,239.72	294,359.59	392,479.45	490,599.31
2.00	18,665.01	93,325.06	186,650.12	279,975.18	373,300.25	466,625.31
2.10	17,793.00	88,965.01	177,930.01	266,895.02	355,860.03	444,825.03
2.20	16,998.39	84,991.93	169,983.86	254,975.79	339,967.71	424,959.64
2.30	16,271.34	81,356.70	162,713.39	244,070.09	325,426.79	406,783.48
2.40	15,603.63	78,018.14	156,036.27	234,054.41	312,072.55	390,090.68
2.50	14,992.96	74,964.81	149,929.62	224,894.43	299,859.23	374,824.04

Table A7a : The Effect of Nanoparticle Volume Fraction (1.0% - 8.0%) towards Absorption Coefficient, $k_{a\lambda}$

λ (μm)	$k_{a\lambda}$							
	f_v = 1.0 %	f_v = 2.0 %	f_v = 3.0 %	f_v = 4.0 %	f_v = 5.0 %	f_v = 6.0 %	f_v = 7.0 %	f_v = 8.0 %
0.20	713,489.62	1,426,979.23	2,140,468.85	2,853,958.47	3,567,448.09	4,280,937.70	4,994,427.32	5,707,916.94
0.30	842,638.10	1,685,276.20	2,527,914.30	3,370,552.40	4,213,190.50	5,055,828.61	5,898,466.71	6,741,104.81
0.40	757,071.56	1,514,143.12	2,271,214.68	3,028,286.24	3,785,357.80	4,542,429.37	5,299,500.93	6,056,572.49
0.50	656,024.74	1,312,049.49	1,968,074.23	2,624,098.98	3,280,123.72	3,936,148.46	4,592,173.21	5,248,197.95
0.60	570,303.27	1,140,606.55	1,710,909.82	2,281,213.09	2,851,516.36	3,421,819.64	3,992,122.91	4,562,426.18
0.70	500,416.39	1,000,832.78	1,501,249.18	2,001,665.57	2,502,081.96	3,002,498.35	3,502,914.75	4,003,331.14
0.80	438,820.90	877,641.81	1,316,462.71	1,755,283.62	2,194,104.52	2,632,925.43	3,071,746.33	3,510,567.24
0.90	388,853.66	777,707.31	1,166,560.97	1,555,414.62	1,944,268.28	2,333,121.93	2,721,975.59	3,110,829.25
1.00	356,703.36	713,406.73	1,070,110.09	1,426,813.45	1,783,516.81	2,140,220.18	2,496,923.54	2,853,626.90
1.10	329,355.52	658,711.05	988,066.57	1,317,422.09	1,646,777.62	1,976,133.14	2,305,488.66	2,634,844.19
1.20	303,524.21	607,048.43	910,572.64	1,214,096.86	1,517,621.07	1,821,145.28	2,124,669.50	2,428,193.71
1.30	281,981.61	563,963.21	845,944.82	1,127,926.43	1,409,908.03	1,691,889.64	1,973,871.24	2,255,852.85
1.40	262,704.76	525,409.52	788,114.28	1,050,819.04	1,313,523.79	1,576,228.55	1,838,933.31	2,101,638.07
1.50	246,363.90	492,727.79	739,091.69	985,455.59	1,231,819.48	1,478,183.38	1,724,547.28	1,970,911.17
1.60	231,562.63	463,125.25	694,687.88	926,250.50	1,157,813.13	1,389,375.75	1,620,938.38	1,852,501.01
1.70	218,457.70	436,915.40	655,373.10	873,830.81	1,092,288.51	1,310,746.21	1,529,203.91	1,747,661.61
1.80	206,643.38	413,286.76	619,930.14	826,573.52	1,033,216.90	1,239,860.28	1,446,503.66	1,653,147.04
1.90	196,239.72	392,479.45	588,719.17	784,958.90	981,198.62	1,177,438.34	1,373,678.07	1,569,917.79
2.00	186,650.12	373,300.25	559,950.37	746,600.49	933,250.62	1,119,900.74	1,306,550.86	1,493,200.99
2.10	177,930.01	355,860.03	533,790.04	711,720.05	889,650.06	1,067,580.08	1,245,510.09	1,423,440.10
2.20	169,983.86	339,967.71	509,951.57	679,935.43	849,919.29	1,019,903.14	1,189,887.00	1,359,870.86
2.30	162,713.39	325,426.79	488,140.18	650,853.58	813,566.97	976,280.36	1,138,993.76	1,301,707.15
2.40	156,036.27	312,072.55	468,108.82	624,145.09	780,181.36	936,217.64	1,092,253.91	1,248,290.18
2.50	149,929.62	299,859.23	449,788.85	599,718.47	749,648.08	899,577.70	1,049,507.32	1,199,436.94

Table 4.8 : The Effect of Nanoparticle Volume Fraction (0.1% - 2.5%) towards Scattering Coefficient, $k_{s\lambda}$

λ (μm)	$k_{s\lambda}$					
	f_v = 0.1 %	f_v = 0.5 %	f_v = 1.0 %	f_v = 1.5 %	f_v = 2.0 %	f_v = 2.5 %
0.20	118.75	593.74	1,187.48	1,781.23	2,374.97	2,968.71
0.30	21.22	106.12	212.24	318.36	424.48	530.60
0.40	5.03	25.14	50.27	75.41	100.55	125.68
0.50	1.03	5.13	10.26	15.39	20.52	25.64
0.60	0.03	0.13	0.27	0.40	0.54	0.67
0.70	0.17	0.85	1.71	2.56	3.42	4.27
0.80	0.54	2.72	5.44	8.15	10.87	13.59
0.90	0.12	0.60	1.21	1.81	2.42	3.02
1.00	0.00	0.00	0.00	0.00	0.00	0.00
1.10	0.00	0.01	0.02	0.03	0.04	0.05
1.20	0.00	0.01	0.01	0.02	0.02	0.03
1.30	0.00	0.00	0.01	0.01	0.01	0.01
1.40	0.00	0.00	0.00	0.00	0.00	0.00
1.50	0.00	0.00	0.00	0.00	0.00	0.00
1.60	0.00	0.00	0.01	0.01	0.02	0.02
1.70	0.00	0.01	0.02	0.03	0.04	0.05
1.80	0.00	0.02	0.03	0.05	0.07	0.09
1.90	0.01	0.03	0.06	0.08	0.11	0.14
2.00	0.01	0.03	0.06	0.10	0.13	0.16
2.10	0.01	0.04	0.07	0.11	0.15	0.18
2.20	0.01	0.04	0.08	0.12	0.15	0.19
2.30	0.01	0.04	0.08	0.12	0.16	0.20
2.40	0.01	0.04	0.08	0.12	0.15	0.19
2.50	0.01	0.04	0.07	0.11	0.14	0.18

Table 4.8a : The Effect of Nanoparticle Volume Fraction (2.0% - 8.0%) towards Scattering Coefficient, $k_{s\lambda}$

λ (μm)	$k_{s\lambda}$						
	f_v = 2.0 %	f_v = 3.0 %	f_v = 4.0 %	f_v = 5.0 %	f_v = 6.0 %	f_v = 7.0 %	f_v = 8.0 %
0.20	2,374.97	3,562.45	4,749.94	5,937.42	7,124.91	8,312.39	9,499.88
0.30	424.48	636.72	848.96	1,061.20	1,273.44	1,485.68	1,697.92
0.40	100.55	150.82	201.09	251.37	301.64	351.91	402.19
0.50	20.52	30.77	41.03	51.29	61.55	71.80	82.06
0.60	0.54	0.81	1.08	1.35	1.62	1.89	2.16
0.70	3.42	5.13	6.83	8.54	10.25	11.96	13.67
0.80	10.87	16.31	21.75	27.18	32.62	38.06	43.49
0.90	2.42	3.63	4.84	6.05	7.26	8.47	9.68
1.00	0.00	0.00	0.00	0.01	0.01	0.01	0.01
1.10	0.04	0.06	0.09	0.11	0.13	0.15	0.17
1.20	0.02	0.04	0.05	0.06	0.07	0.09	0.10
1.30	0.01	0.02	0.02	0.03	0.04	0.04	0.05
1.40	0.00	0.01	0.01	0.01	0.01	0.01	0.02
1.50	0.00	0.00	0.01	0.01	0.01	0.01	0.01
1.60	0.02	0.03	0.04	0.05	0.06	0.07	0.08
1.70	0.04	0.06	0.08	0.10	0.12	0.14	0.16
1.80	0.07	0.10	0.14	0.17	0.21	0.24	0.27
1.90	0.11	0.17	0.22	0.28	0.33	0.39	0.44
2.00	0.13	0.19	0.26	0.32	0.39	0.45	0.52
2.10	0.15	0.22	0.29	0.37	0.44	0.51	0.59
2.20	0.15	0.23	0.31	0.39	0.46	0.54	0.62
2.30	0.16	0.23	0.31	0.39	0.47	0.55	0.63
2.40	0.15	0.23	0.31	0.38	0.46	0.54	0.62
2.50	0.14	0.22	0.29	0.36	0.43	0.51	0.58

Table A9 : The Effect of Nanoparticle Volume Fractions towards Extinction Coefficient, $k_{e\lambda}$

λ (μm)	$k_{s\lambda}$								
	f_v = 1.0 %	f_v = 2.0 %	f_v = 2.5 %	f_v = 3.0 %	f_v = 4.0 %	f_v = 5.0 %	f_v = 6.0 %	f_v = 7.0 %	f_v = 8.0 %
0.20	714,677.10	1,429,354.20	1,786,692.76	2,144,031.31	2,858,708.41	3,573,385.51	4,288,062.61	5,002,739.71	5,717,416.82
0.30	842,850.34	1,685,700.68	2,107,125.85	2,528,551.02	3,371,401.37	4,214,251.71	5,057,102.05	5,899,952.39	6,742,802.73
0.40	757,121.83	1,514,243.67	1,892,804.59	2,271,365.50	3,028,487.34	3,785,609.17	4,542,731.01	5,299,852.84	6,056,974.67
0.50	656,035.00	1,312,070.00	1,640,087.50	1,968,105.01	2,624,140.01	3,280,175.01	3,936,210.01	4,592,245.01	5,248,280.01
0.60	570,303.54	1,140,607.09	1,425,758.86	1,710,910.63	2,281,214.17	2,851,517.71	3,421,821.26	3,992,124.80	4,562,428.34
0.70	500,418.10	1,000,836.20	1,251,045.25	1,501,254.30	2,001,672.40	2,502,090.50	3,002,508.61	3,502,926.71	4,003,344.81
0.80	438,826.34	877,652.68	1,097,065.85	1,316,479.02	1,755,305.36	2,194,131.71	2,632,958.05	3,071,784.39	3,510,610.73
0.90	388,854.87	777,709.73	972,137.16	1,166,564.60	1,555,419.46	1,944,274.33	2,333,129.19	2,721,984.06	3,110,838.92
1.00	356,703.36	713,406.73	891,758.41	1,070,110.09	1,426,813.46	1,783,516.82	2,140,220.18	2,496,923.55	2,853,626.91
1.10	329,355.54	658,711.09	823,388.86	988,066.63	1,317,422.18	1,646,777.72	1,976,133.27	2,305,488.81	2,634,844.36
1.20	303,524.23	607,048.45	758,810.57	910,572.68	1,214,096.91	1,517,621.13	1,821,145.36	2,124,669.59	2,428,193.81
1.30	281,981.61	563,963.22	704,954.03	845,944.84	1,127,926.45	1,409,908.06	1,691,889.67	1,973,871.29	2,255,852.90
1.40	262,704.76	525,409.52	656,761.90	788,114.28	1,050,819.04	1,313,523.80	1,576,228.56	1,838,933.33	2,101,638.09
1.50	246,363.90	492,727.80	615,909.75	739,091.69	985,455.59	1,231,819.49	1,478,183.39	1,724,547.29	1,970,911.19
1.60	231,562.64	463,125.27	578,906.59	694,687.91	926,250.54	1,157,813.18	1,389,375.81	1,620,938.45	1,852,501.08
1.70	218,457.72	436,915.44	546,144.30	655,373.16	873,830.88	1,092,288.61	1,310,746.33	1,529,204.05	1,747,661.77
1.80	206,643.41	413,286.83	516,608.54	619,930.24	826,573.66	1,033,217.07	1,239,860.48	1,446,503.90	1,653,147.31
1.90	196,239.78	392,479.56	490,599.45	588,719.34	784,959.12	981,198.90	1,177,438.68	1,373,678.46	1,569,918.23
2.00	186,650.19	373,300.38	466,625.47	559,950.56	746,600.75	933,250.94	1,119,901.13	1,306,551.31	1,493,201.50
2.10	177,930.09	355,860.17	444,825.22	533,790.26	711,720.34	889,650.43	1,067,580.52	1,245,510.60	1,423,440.69
2.20	169,983.93	339,967.87	424,959.84	509,951.80	679,935.74	849,919.67	1,019,903.61	1,189,887.54	1,359,871.48
2.30	162,713.47	325,426.94	406,783.68	488,140.42	650,853.89	813,567.36	976,280.83	1,138,994.30	1,301,707.78
2.40	156,036.35	312,072.70	390,090.87	468,109.05	624,145.40	780,181.75	936,218.10	1,092,254.45	1,248,290.80
2.50	149,929.69	299,859.38	374,824.22	449,789.07	599,718.76	749,648.45	899,578.14	1,049,507.83	1,199,437.51

Table A10 : The Extinction Coefficient and Transmissivity of Nanofluid (f_v = 0.1%)

λ (μm)	$K_{e\lambda}$ (D=10nm, f_v=0.1%)	T				
		L = 0.02 mm	L = 0.04 mm	L = 0.06 mm	L = 0.08 mm	L = 0.10 mm
0.20	71475.88	23.94%	5.73%	1.37%	0.33%	0.08%
0.30	84286.54	18.53%	3.43%	0.64%	0.12%	0.02%
0.40	75712.28	22.00%	4.84%	1.06%	0.23%	0.05%
0.50	65603.52	26.93%	7.25%	1.95%	0.53%	0.14%
0.60	57030.50	31.96%	10.22%	3.27%	1.04%	0.33%
0.70	50042.40	36.76%	13.51%	4.97%	1.83%	0.67%
0.80	43884.74	41.57%	17.28%	7.19%	2.99%	1.24%
0.90	38892.19	45.94%	21.10%	9.70%	4.45%	2.05%
1.00	35705.77	48.96%	23.97%	11.74%	5.75%	2.81%
1.10	32954.52	51.73%	26.76%	13.84%	7.16%	3.71%
1.20	30454.42	54.38%	29.58%	16.09%	8.75%	4.76%
1.30	28306.14	56.77%	32.23%	18.30%	10.39%	5.90%
1.40	27570.20	57.61%	33.19%	19.12%	11.02%	6.35%
1.50	26366.36	59.02%	34.83%	20.56%	12.13%	7.16%
1.60	23775.94	62.16%	38.63%	24.01%	14.93%	9.28%
1.70	22360.99	63.94%	40.88%	26.14%	16.71%	10.69%
1.80	21464.40	65.10%	42.38%	27.59%	17.96%	11.69%
1.90	27673.07	57.50%	33.06%	19.01%	10.93%	6.28%
2.00	25463.43	60.09%	36.11%	21.70%	13.04%	7.84%
2.10	20393.05	66.51%	44.23%	29.42%	19.56%	13.01%
2.20	18597.75	68.94%	47.53%	32.76%	22.59%	15.57%
2.30	18571.54	68.97%	47.58%	32.81%	22.63%	15.61%
2.40	19802.90	67.30%	45.29%	30.48%	20.51%	13.80%
2.50	23291.80	62.76%	39.39%	24.72%	15.52%	9.74%

Table A11 : The Extinction Coefficient and Transmissivity of Nanofluid (f_v = 0.5%)

λ (μm)	$K_{e\lambda}$ (D=10nm, f_v=0.5%)	T				
		L = 0.02 mm	L = 0.04 mm	L = 0.06 mm	L = 0.08 mm	L = 0.10 mm
0.20	357346.72	0.08%	0.00%	0.00%	0.00%	0.00%
0.30	421426.68	0.02%	0.00%	0.00%	0.00%	0.00%
0.40	378561.01	0.05%	0.00%	0.00%	0.00%	0.00%
0.50	328017.52	0.14%	0.00%	0.00%	0.00%	0.00%
0.60	285151.92	0.33%	0.00%	0.00%	0.00%	0.00%
0.70	250209.64	0.67%	0.00%	0.00%	0.00%	0.00%
0.80	219415.28	1.24%	0.02%	0.00%	0.00%	0.00%
0.90	194434.13	2.05%	0.04%	0.00%	0.00%	0.00%
1.00	178387.12	2.82%	0.08%	0.00%	0.00%	0.00%
1.10	164696.74	3.71%	0.14%	0.01%	0.00%	0.00%
1.20	151864.11	4.80%	0.23%	0.01%	0.00%	0.00%
1.30	141098.78	5.95%	0.35%	0.02%	0.00%	0.00%
1.40	132652.10	7.04%	0.50%	0.03%	0.00%	0.00%
1.50	124911.92	8.22%	0.68%	0.06%	0.00%	0.00%
1.60	116401.00	9.75%	0.95%	0.09%	0.01%	0.00%
1.70	109744.08	11.14%	1.24%	0.14%	0.02%	0.00%
1.80	104121.77	12.46%	1.55%	0.19%	0.02%	0.00%
1.90	106168.98	11.96%	1.43%	0.17%	0.02%	0.00%
2.00	100123.50	13.50%	1.82%	0.25%	0.03%	0.00%
2.10	91565.08	16.02%	2.57%	0.41%	0.07%	0.01%
2.20	86591.32	17.70%	3.13%	0.55%	0.10%	0.02%
2.30	83656.93	18.77%	3.52%	0.66%	0.12%	0.02%
2.40	82217.44	19.31%	3.73%	0.72%	0.14%	0.03%
2.50	83263.68	18.91%	3.58%	0.68%	0.13%	0.02%

Table A12 : The Extinction Coefficient and Transmissivity of Nanofluid (f_v = 1.0%)

λ (μm)	$K_{e\lambda}$ (D=10nm, f_v=1.0%)	T				
		L = 0.02 mm	L = 0.04 mm	L = 0.06 mm	L = 0.08 mm	L = 0.10 mm
0.20	714685.27	0.00%	0.00%	0.00%	0.00%	0.00%
0.30	842851.85	0.00%	0.00%	0.00%	0.00%	0.00%
0.40	757121.93	0.00%	0.00%	0.00%	0.00%	0.00%
0.50	656035.02	0.00%	0.00%	0.00%	0.00%	0.00%
0.60	570303.69	0.00%	0.00%	0.00%	0.00%	0.00%
0.70	500418.69	0.00%	0.00%	0.00%	0.00%	0.00%
0.80	438828.45	0.02%	0.00%	0.00%	0.00%	0.00%
0.90	388861.57	0.04%	0.00%	0.00%	0.00%	0.00%
1.00	356738.80	0.08%	0.00%	0.00%	0.00%	0.00%
1.10	329374.51	0.14%	0.00%	0.00%	0.00%	0.00%
1.20	303626.22	0.23%	0.00%	0.00%	0.00%	0.00%
1.30	282089.59	0.35%	0.00%	0.00%	0.00%	0.00%
1.40	264004.48	0.51%	0.00%	0.00%	0.00%	0.00%
1.50	248093.87	0.70%	0.00%	0.00%	0.00%	0.00%
1.60	232182.31	0.96%	0.01%	0.00%	0.00%	0.00%
1.70	218972.94	1.25%	0.02%	0.00%	0.00%	0.00%
1.80	207443.47	1.58%	0.02%	0.00%	0.00%	0.00%
1.90	204288.87	1.68%	0.03%	0.00%	0.00%	0.00%
2.00	193448.59	2.09%	0.04%	0.00%	0.00%	0.00%
2.10	180530.13	2.70%	0.07%	0.00%	0.00%	0.00%
2.20	171583.29	3.23%	0.10%	0.00%	0.00%	0.00%
2.30	165013.66	3.69%	0.14%	0.01%	0.00%	0.00%
2.40	160235.61	4.06%	0.16%	0.01%	0.00%	0.00%
2.50	158228.52	4.22%	0.18%	0.01%	0.00%	0.00%